Theoretical Study of Performance Characteristics of Semiconductor Quantum Dot Lasers

Li Jiang

Dissertation submitted to the faculty of the
Virginia Polytechnic Institute and State University
in partial fulfillment of the requirements for the degree of

Doctor of Philosophy
In
Materials Science and Engineering

Approved:

Professor Levon V. Asryan, Chair / Advisor
Professor Louis J. Guido
Professor Robert W. Hendricks
Professor Guo-Quan Lu

September 2, 2008
Blacksburg, Virginia

Keywords: quantum dot lasers, semiconductor lasers

Theoretical Study of Performance Characteristics of Semiconductor Quantum Dot Lasers

Li Jiang

Abstract

The effect of different factors on the operating characteristics of a semiconductor quantum dot (QD) laser is studied. Specifically, the following topics are included in the dissertation:

1) Effect of carrier-density-dependent internal loss in the optical confinement layer (OCL) on the characteristic temperature.

Internal optical loss in a QD laser couples the confined-carrier level occupancy in QDs to the free-carrier density in the OCL. Due to this coupling, which is controlled by the threshold condition, the free-carrier density is increased and more temperature-sensitive, and also the confined-carrier level occupancy becomes temperature-dependent. As a result, the characteristic temperature of a laser is considerably reduced. Carrier-density-dependent internal loss also sets an upper limit for operating temperatures of a QD laser and constrains the shallowest potential well depth and the smallest tolerable size of a QD at which the lasing can be attained. The dependences of the characteristic temperature, maximum operating temperature, and shallowest potential well depth on the parameters of the structure are obtained. At the maximum operating temperature or when any parameter of the structure is equal to its critical tolerable value, the characteristic temperature reduces to zero.

2) Effect of excited-states in QDs on the light-current characteristic (LCC).

The carrier capture from the three-dimensional reservoir (optical confinement layer – OCL) into the QD ground-state and escape from the ground-state to the OCL are assumed to occur via the QD excited-state. Such a two-step capture places a fundamental limitation on ground-state lasing—the output power saturates at high injection currents. The saturation power is controlled by the transition time between the excited- and ground-state in a QD. The longest, cut-off transition time exists, beyond which no ground-state lasing is possible. The following characteristics are analyzed versus the injection current density and the transition time:

occupancies of the ground- and excited-state, free carrier density in the OCL, threshold current density, number of stimulated photons emitted, output power, internal and external differential quantum efficiencies.

3) Effect of longitudinal spatial hole burning (SHB) and multimode lasing on the LCC.

The number of modes is shown to remain limited with increasing injection current. The maximum number of modes that can oscillate in a QD laser is analytically estimated. While this number increases with increasing surface density of QDs or cavity length, it remains limited (first increases and then decreases) with increasing scatter in the QD-size. The critical tolerable values of the structure parameters are derived beyond which higher-order longitudinal modes can not oscillate. It is notable that, in addition to the maximum tolerable scatter, there also exists the minimum scatter in the QD-size for each higher-order mode to start lasing. The threshold currents and output powers of modes are computed numerically. The power of the main mode is reduced due to lasing of higher-order modes and spatially nonuniform carrier distribution. As a new mode turns on, kinks appear in the LCCs of existing modes. SHB reduces the total optical power of a laser and contributes to nonlinearity of the overall LCC. The effect is more significant when any of the structure parameters is close to its critical tolerable value. The LCC becomes more linear with improving QD-size uniformity or increasing surface density of QDs or cavity length.

Acknowledgments

I would like to take this opportunity to express my sincere thanks to my advisor, Professor Levon Asryan, for his guidance and support throughout the course of my Ph.D. study. From his profound knowledge and attitude toward research I have learned a lot.

I also thank the members of my committee, Professor Louis Guido, Professor Robert Hendricks, and Professor Guo-Quan Lu, for their help to oversee the completion of my study.

I would like to thank my graduate student colleague, Dae-Seob Han, for his encouragement and discussions. I also thank all the persons at the MSE department, with whose help I could make my study successful.

I would like to acknowledge the U.S. Army Research Office for funding of this work.

I would like to thank all the friends I have come to know in Blacksburg, who made my life here more colorful.

I owe my sincere appreciation to my parents, whose support and encouragement have helped me get this far. I understand I am your pride, and I will always be.

Last but not least, my special thank you goes to my dear wife, Jing Zhou, for her love, company, understanding, and persistent support.

Table of Contents

List of Figures

List of Tables

Chapter 1

Introduction

1.1. Semiconductor lasers

Semiconductor lasers are one of the most important inventions of the 20th century. Since their invention in the early 1960s, semiconductor lasers have been among the most extensively used lasers. Nowadays, semiconductor lasers appear in various areas of our daily life. They present a critical component in optical communication systems [1] and in many commercial products, such as compact disk players [2], laser printers [2, 3], and pointers.

Unlike other types of lasers, a semiconductor laser is pumped by electric current and its basic structure is a p-n junction. For this reason, semiconductor laser is also called injection laser or diode laser. Fig. 1.1 shows as an example a separate confinement double heterostructure semiconductor laser. Different layers in such a laser are made of semiconductor materials with different band gaps. Electrons and holes are injected from the n- and p-cladding layers, respectively. In the active region, electrons and holes recombine via spontaneous and stimulated recombination thus generating photons. The generated emission is confined within the waveguide layer (optical confinement layer). Photons leaving the cavity from its facet(s) form the output of a laser.

A key characteristic of a semiconductor laser is the light current curve. It presents the output optical power versus the pump current (Fig. 1.2). The more linear is this curve, or the larger is its slope, or the closer is the starting point of the curve to the origin, the better is the laser diode. The current density at which lasing starts is defined as the threshold current density j_{th}. The lower j_{th}, the higher is the output optical power at a given injection current density. The temperature dependence of j_{th} can be empirically described by an exponential function (Fig. 1.2), where T_0 is a figure of merit called the characteristic temperature. The higher T_0, the higher is the temperature stability of j_{th}. Lowering j_{th} and improving its temperature stability have been important objectives in the development of semiconductor lasers [4].

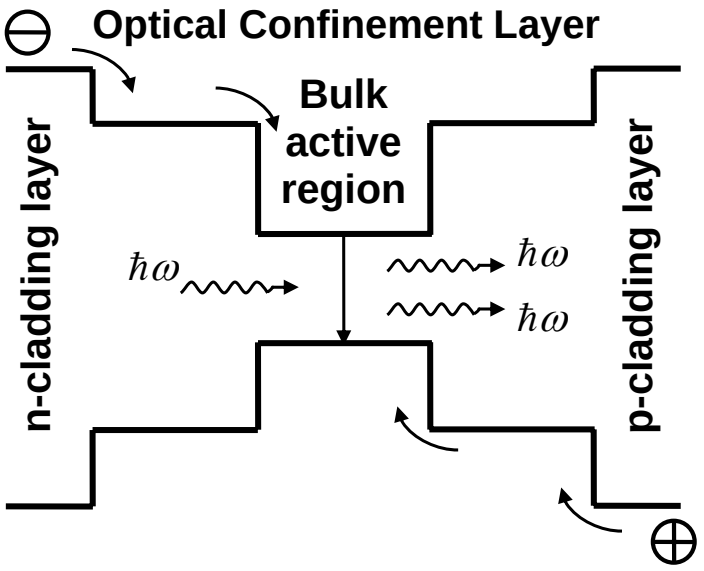

Fig. 1.1. Schematic view of a separate confinement double heterostructure laser.

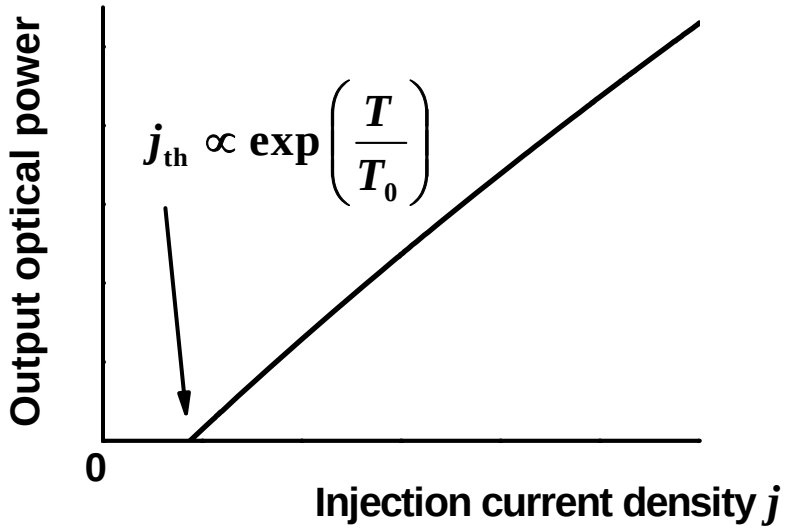

Fig. 1.2. Illustrative light-current curve of a semiconductor laser.

1.1.1. Evolution of semiconductor lasers

Laser is the acronym for "Light Amplification by Stimulated Emission of Radiation" [5]. Early study of feasibility of lasing in semiconductors was published by several researchers [6, 7].

The year of 1962 should be marked as an important milestone in the history of semiconductor lasers. It was in this year that several groups independently demonstrated lasing action in semiconductors, both in the infrared [8–10] (using GaAs) and visible light range [11] (using $GaAs_{1-x}P_x$). However, since these earliest semiconductor lasers utilized bulk materials and homostructures, they suffered from high threshold current density ($10^4 \sim 10^5$ A/cm^2) and were only able to operate at cryogenic temperature.

In 1963, a double heterostructure laser, wherein the active layer of a semiconductor material of one type is sandwiched between the layers of a different semiconductor material having a wider band gap, was suggested by Alferov and Kazarinov [12] and Kroemer [13] to achieve high efficiency radiative recombination in the narrow band gap semiconductor. A single heterostructure laser was first demonstrated in 1969 [14] with a room temperature threshold current density (pulsed operation) of about 8.6 kA/cm^2.

The practical use of semiconductor lasers was made possible only after the room temperature continuous-wave operation was realized in 1970 by Alferov *et al*. [15] and Panish *et al*. [16, 17] using a double heterostructure. A room temperature continuous-wave threshold current density as low as 1.6 kA/cm^2 [17] was achieved. A significant reduction of j_{th} in a double heterostructure laser is mainly due to two reasons: 1) a wider band gap of the cladding layers effectively confines the carriers in the active region, and 2) a higher refractive index of the active layer compared to that of the cladding layers forms a waveguide and effectively confines the emitted light within the active layer.

Advanced performance of heterostructure lasers (compared to homostructure lasers) made them capable for the use in many areas, such as the optical communication systems (since 1978). The use of bulk materials for the active region however blocked a further improvement of heterostructure lasers. A new hope appeared when quantum wells (QWs) attracted the attention of laser scientists. The use of QW lasers was motivated by the strong modification of properties of a semiconductor crystal in low-dimensional heterostructures. It has been predicted in the middle 1970s that reducing the dimensionality of the active region can significantly improve the performance of semiconductor lasers [18]: restriction of the carrier motion in the direction perpendicular to the QW plane produces a stair-like density of states [Fig. 1.3(b)] and leads to more efficient devices operating at lower threshold currents compared to bulk active-region lasers.

Although the optically [19] and electrically pumped [20] QW lasers had been demonstrated in 1975 and 1977, respectively, it was not until the crystal growth techniques were developed well enough to achieve thin films of good quality that the full potential of QW lasers could be realized. During the years following the first demonstration of QW lasers, much effort has been put to improve the QW laser design. By reducing the doping of the layers around the active region and using a graded index separate confinement heterostructure, Tsang achieved j_{th} as low as 160 A/cm^2 [21], which was much lower compared to bulk heterostructure lasers (> 500 A/cm^2) [22–24]. This result clearly demonstrated the advantage of QW lasers over bulk active-region lasers and can be viewed as another milestone in the history of semiconductor lasers. A new technique – the use of strain – has enabled QW lasers to lase with j_{th} below 50 A/cm^2 [25]. The use of new material systems largely expanded the range of the emission wavelength (from red [26] to far-infrared). The use of GaN based materials further shortened the wavelength range to blue/green region [27] and the use of antimonide semiconductors to the wavelength range beyond 2 μm [28]. Nowadays, QW lasers almost completely took the place of bulk heterostructure lasers and dominate over the semiconductor laser market [29].

Hence, the quantum confinement effect has already led to high performance QW lasers. To achieve even better performance, a natural approach was to further restrict the motion of carriers in the remaining two directions. This led to the concept of quantum dot (QD) lasers. In a QD laser, the active region consists of a layer (or layers) with a large number of QDs (with a typical QD size on the order of 10 nanometers). Due to the complete confinement of carriers in all three directions, the transitions between the electron and hole levels in QDs are analogous to those between the discrete levels in individual atoms.

Fig. 1.3 shows the density of states in semiconductor materials of different dimensionality. The density of states describes the number of states per unit volume per unit energy. With reducing dimensionality of the active region, the density of states profile becomes narrower and hence a smaller number of states should be filled by carriers to achieve the population inversion required for lasing. As a result, the threshold current is reduced [30]. As seen from Fig. 1.3, with the transition from a bulk (3D) to a quantum well (2D) medium, the density of states remains continuous. A qualitative change to a discrete, delta-function density of states [Fig. 1.3(c)] occurs only when a QD (0D) medium is used. Radically reduced j_{th} would thus be expected in QD lasers.

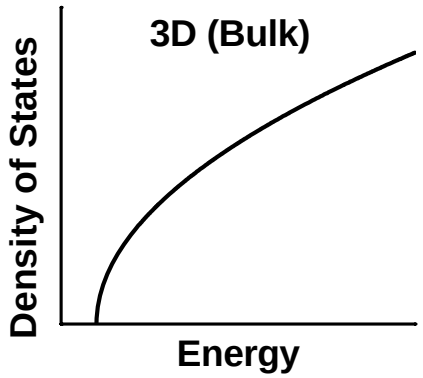

(a)

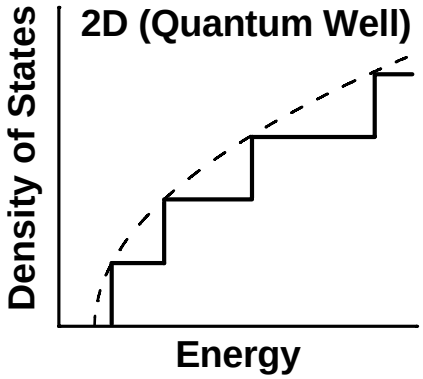

(b)

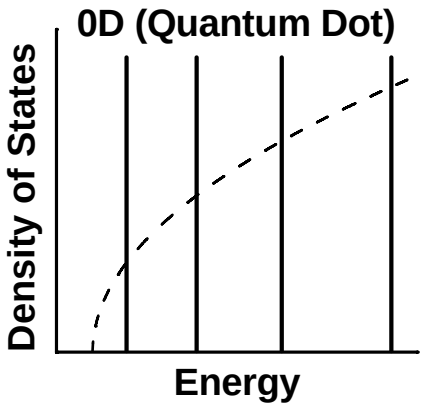

(c)

Fig. 1.3. Density of states in materials of different dimensionality: (a) 3D (bulk), (b) 2D (QW), and (c) 0D (QD).

Another important advantage of QD lasers is high temperature stability of operation. In an ideal QD laser, the injection current should go entirely into the recombination in QDs and the charge neutrality in QDs should hold [31, 32]. In such a case, the threshold current would not depend on temperature and hence the characteristic temperature would be infinitely high [33].

1.2. Progress in fabricating QD lasers

1.2.1. Early work

Although low threshold current [34] and high temperature stability [33] have been predicted for QD lasers in the 1980s, the realization of lasing was lagged due to the lack of an appropriate technology at that time. Lasing properties of three-dimensionally quantized carriers were first investigated indirectly by placing QW lasers in strong magnetic fields [33, 35], which demonstrated an increase in the characteristic temperature.

There have been several approaches to the realization of QD structures. A traditional way was to selectively etch QW structures. In 1987, Miyamoto *et al.* demonstrated electrically pumped light emission from a QD structure, which was realized from an MOCVD-grown GaInAsP/InP QW by applying the holographic process, etching, and overgrowing [36]. The authors reported a Fabry-Perot-mode-like spectrum, which suggested a possible stimulated emission. Later efforts yielded a laser operation, but the devices exhibited high j_{th} (7.6 kA/cm^2 at 77 K under pulsed operation in [37]), most probably due to a high density of surface states created during etching.

1.2.2. Self-organization growth of QD structures and improving the laser characteristics

A real breakthrough occurred when the approach of self-organized growth was developed to an extent allowing for the realization of dense and relatively uniform QD ensembles with significantly reduced density of defects. Fig. 1.4 shows typical plan-view and cross-sectional TEM images of a QD structure. The high resolution TEM image in Fig. 1.5 illustrates a single self-organized QD, which is of pyramidal shape.

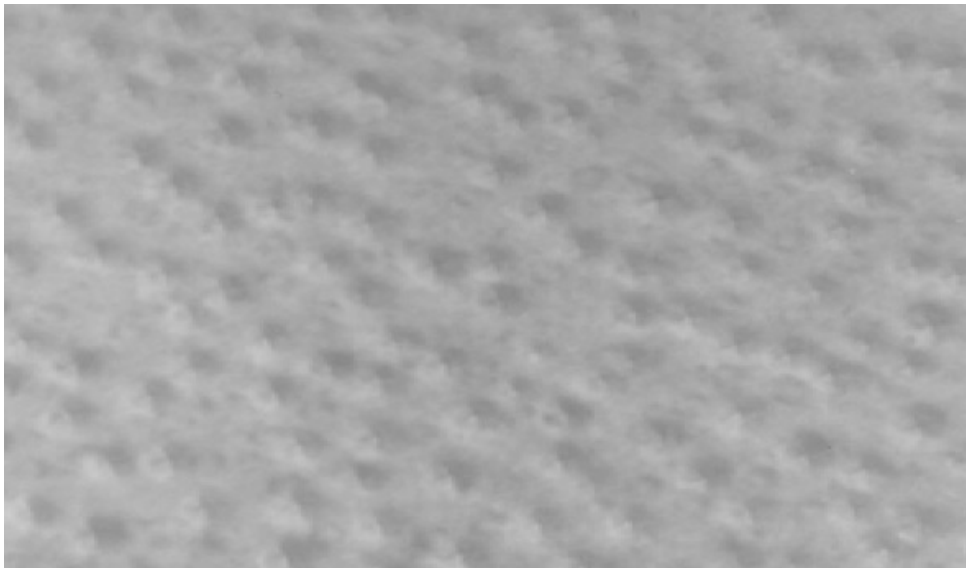

(a)

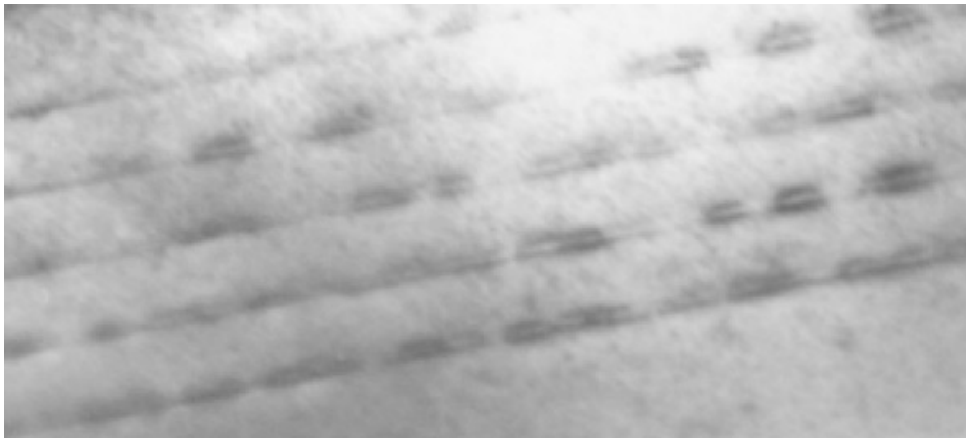

(b)

Fig. 1.4. Plan-view (a) and cross-sectional (b) TEM images of a QD structure. (Reprinted from Fig. 2 of ref. [38], Copyright (2003), with permission from Elsevier.)

In 1994, Ledentsov *et al*. [40] demonstrated optically pumped lasing in an InGaAs-GaAs structure with high density of QDs and low density of defects. Electrically pumped lasing from self-organized InGaAs QDs was also reported in the same year [41, 42]. The lasing was observed both at low and room temperature. In [42], a low threshold current density (120 A/cm^2) was reported at 77 K and a high T_0 = 350 K for the temperature range from 50 to 120 K.

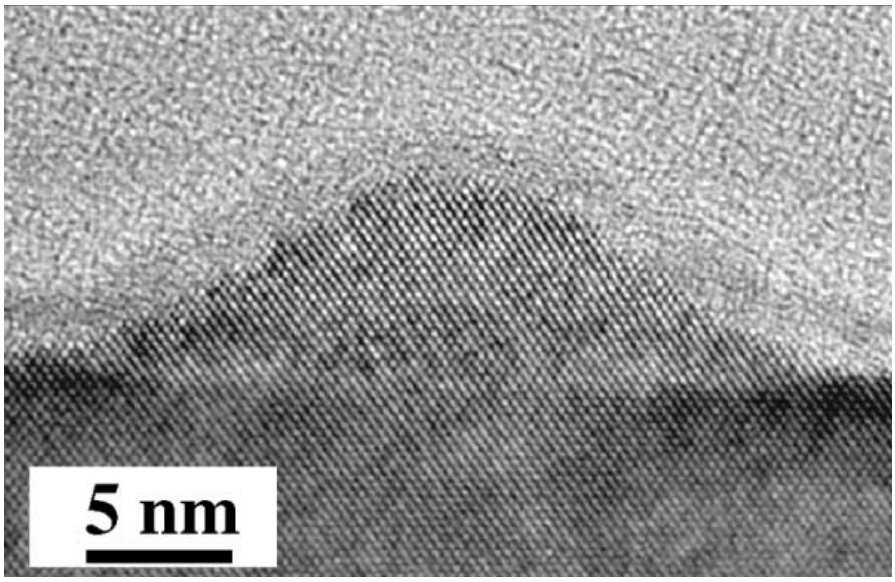

Fig. 1.5. High resolution TEM image of a single self-organized QD grown by deposition of 16 periods of 0.25ML InAs / 0.25ML GaAs separated by 5 s pauses. (Reprinted from Fig. 1 of ref. [39], Copyright (2001), with permission from Elsevier.)

Since then, a rapid progress has been made in fabricating QD lasers [43, 44]. Although the early stage QD lasers did not show a superior performance over QW lasers [thus, in [44], j_{th} of the QD laser was about twice of that of a reference QW laser having a similar structure to that of the QD laser (except for the active region)], a successful fabrication of QD lasers has been reported continuously in succeeding years [45–60]. By now, low j_{th} [54–56, 58–60] and high T_0 values [46, 58] have been achieved in QD lasers, which surpass the corresponding characteristics of commercial QW lasers.

The self-organization technique allowed for a control over the size, density, and composition of dots, which is realized via controlling the growth conditions and/or materials used. Variation of parameters of a QD laser structure can strongly affect its operating characteristics. Thus, j_{th} depends strongly on the surface density of QDs [see the experimental Figs. 1.6 and 1.7, where the surface density of QDs is varied by changing the number of QD layers (number of stacks); compare these figures to the theoretical Fig. 1.8, which shows the decrease and then increase of j_{th} with increasing surface density of QDs], root mean square (RMS) of QD size fluctuations

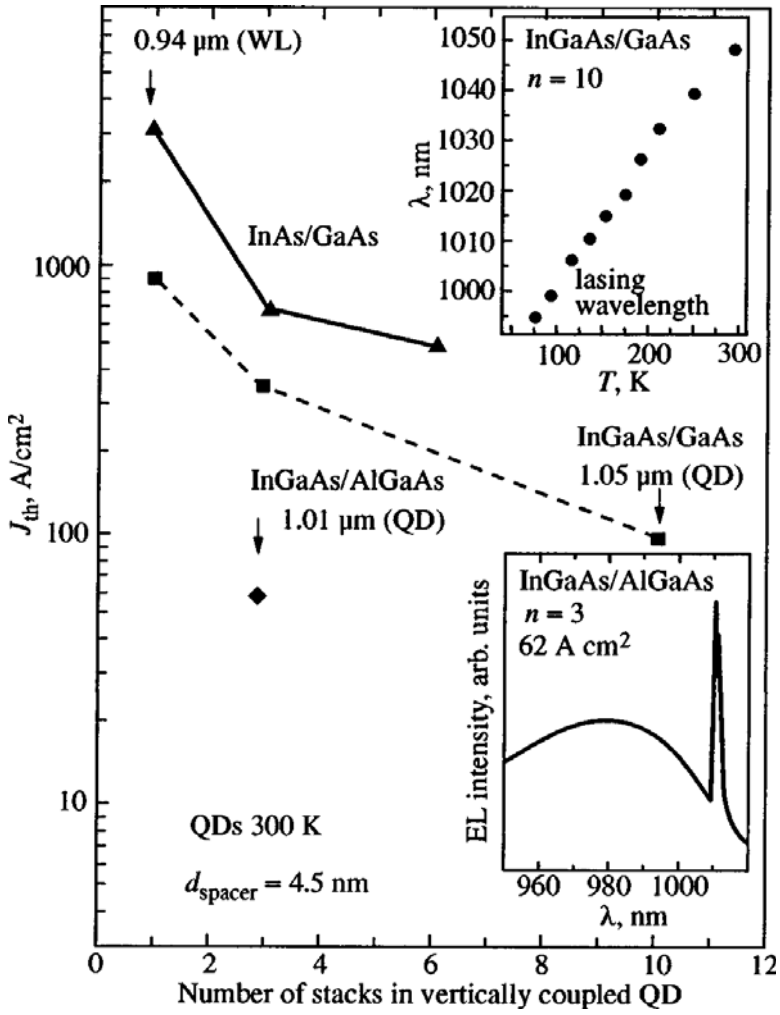

Fig. 1.6. Threshold current density as a function of the number of QD layers: experiment. (Fig. 16 of ref. [47], reprinted with kind permission of Springer Science and Business Media.)

[see the experimental Fig. 1.9; the FWHM of the spontaneous electroluminescence (EL) spectra corresponds to the RMS of QD size fluctuations; compare this figure to the theoretical Fig. 1.10], and cavity length (Fig. 1.11; compare this figure to the theoretical Fig. 1.12). In Figs. 1.9 and 1.13, the FWHM of the EL spectra and the surface density of QDs are changed through changing the misorientation angle.

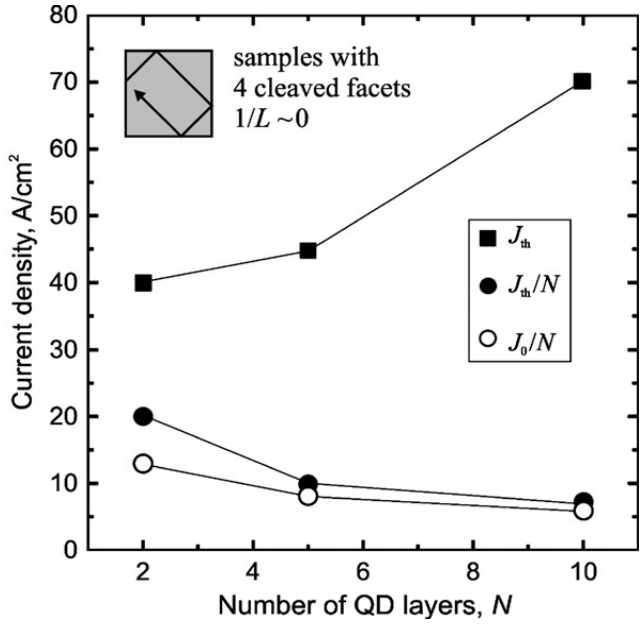

Fig. 1.7. Threshold current density (solid squares), threshold current density per QD layer (solid circles), and transparency current density per QD layer (open circles) versus the number of QD layers: experiment. (Reprinted from Fig. 3 of ref. [57], Copyright (2003), with permission from Elsevier.)

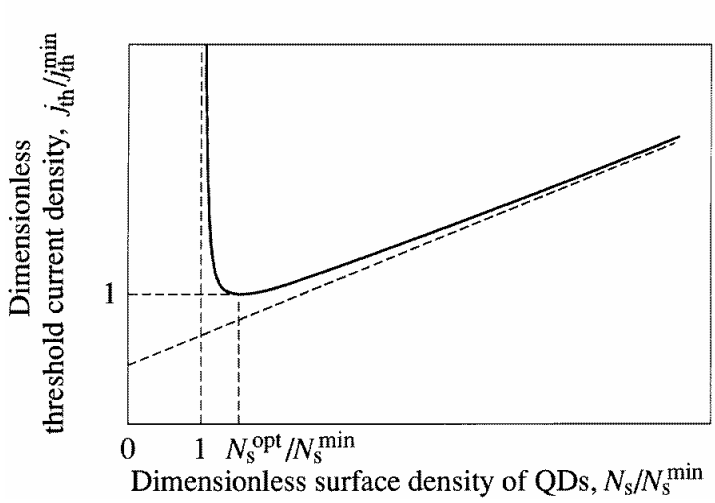

Fig. 1.8. Dimensionless threshold current density versus the dimensionless surface density of QDs: theory. The inclined straight line shows the transparency current density. (Fig. 4(b) of ref. [61], reprinted with permission of IOP Publishing Ltd.)

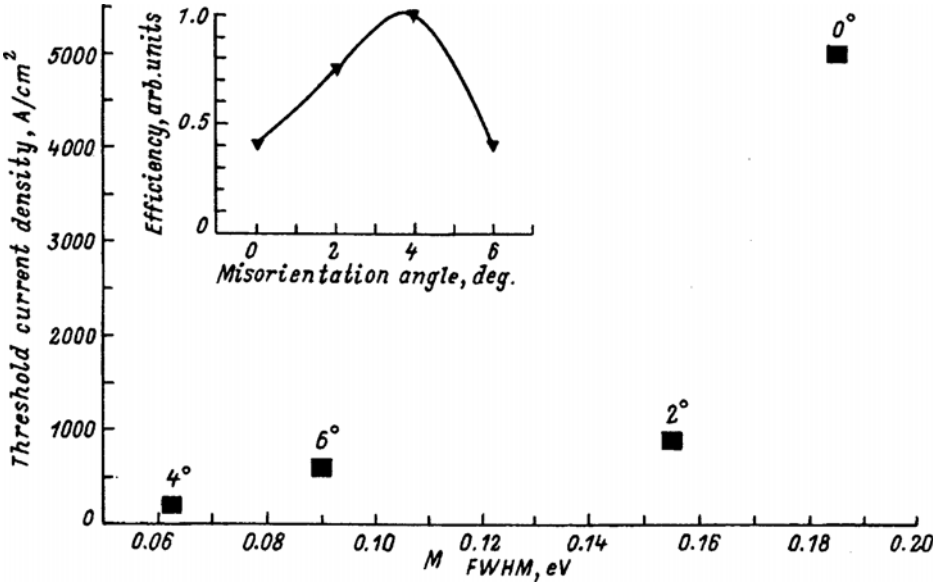

Fig. 1.9. Threshold current density versus the FWHM of the spontaneous EL spectra for samples with various substrate misorientation angles (0, 2, 4, and 6°): experiment. (Fig. 4 of ref. [49], reprinted with kind permission of Springer Science and Business Media.)

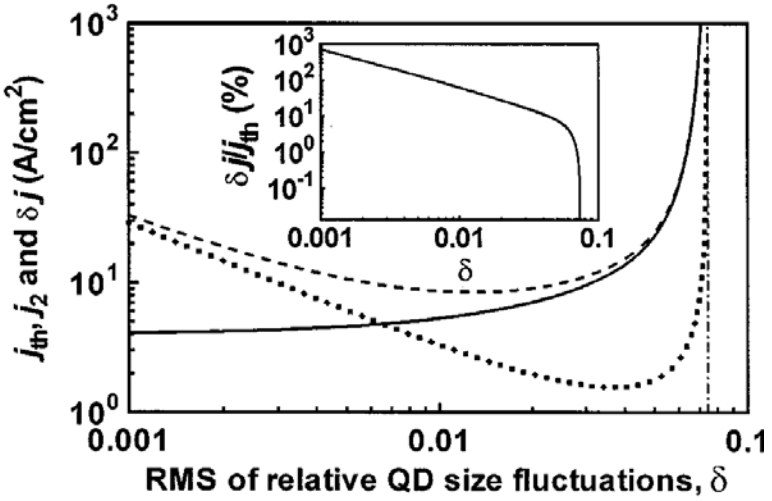

Fig. 1.10. Threshold current density (solid curve) versus the RMS of QD size fluctuations: theory. (Fig. 6(b) of ref. [62], © [2000] IEEE.)

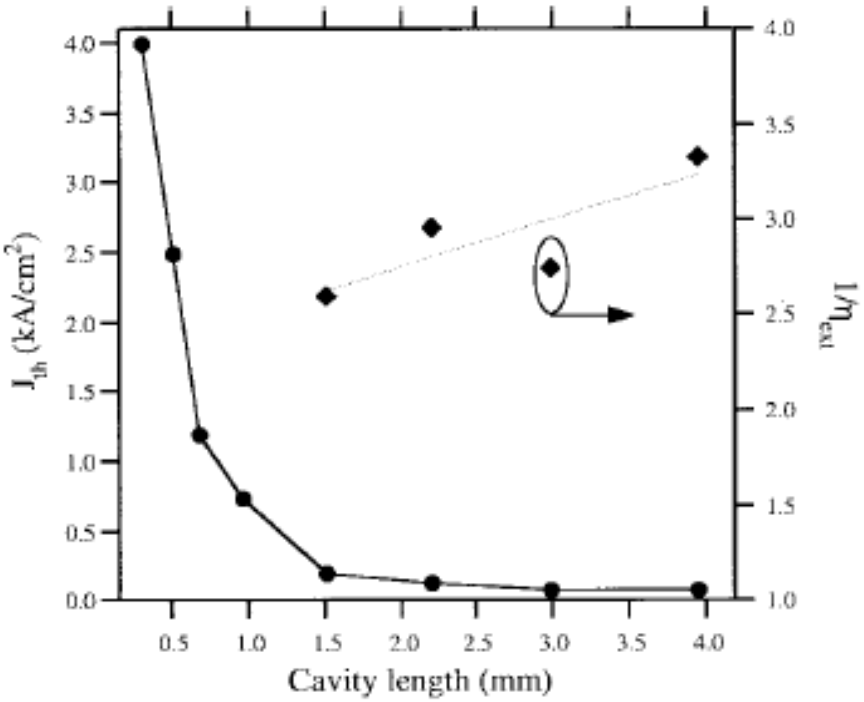

Fig. 1.11. Threshold current density (left axis) versus the cavity length: experiment. (Fig. 3 of ref. [53], © [1999] IEEE.)

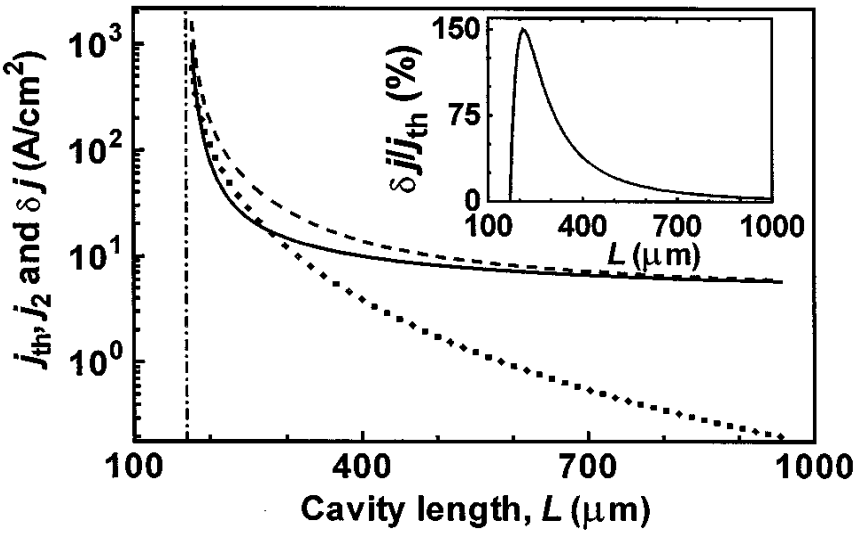

Fig. 1.12. Threshold current density (solid curve) versus the cavity length: theory. (Fig. 6(c) of ref. [62], © [2000] IEEE.)

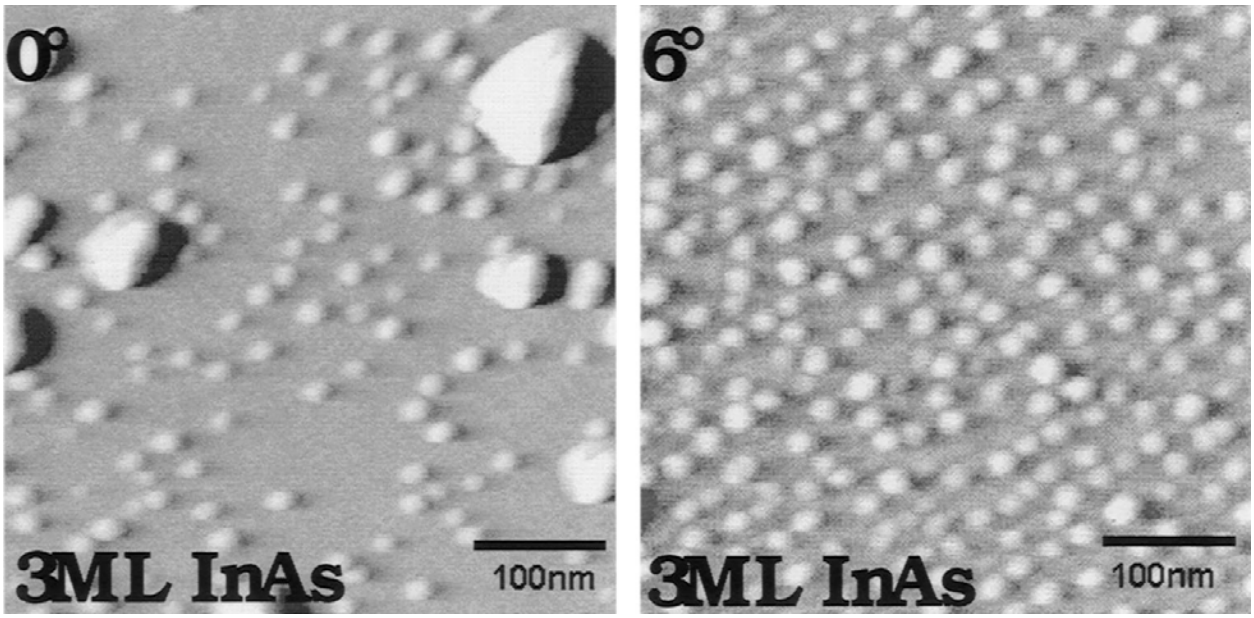

Fig. 1.13. AFM image of 3 ML InAs grown on the GaAs (0 0 1) surfaces exactly oriented and misoriented by 6°. (Reprinted from Fig. 2 of ref. [51], Copyright (1999), with permission from Elsevier.)

Special techniques, such as p-type doping [63, 64] and tunneling injection [65], have been proposed to further enhance T_0. Recently, a QD laser with temperature insensitive threshold current ($T_0 \approx \infty$) at room temperature has been reported [66]. The reasons behind this temperature-insensitivity are yet to be clarified.

Till now, the most extensively studied QD lasers are those grown on GaAs substrates. Using different combinations of heterosystems, the lasing wavelength can be varied in the wide spectral range from visible to infrared (see, e.g., [67–69]), including the telecommunication wavelengths 1.3 and 1.55 μm. The most superior performance on GaAs substrates is achieved around 1.3 μm. There have been encouraging results at 1.55 μm using other material systems (see, e.g., [70] for an InAs/InP QD laser).

In the family of lasers, even in the family of semiconductor lasers, QD lasers are relatively young. Although they have already demonstrated a superior performance over existing semiconductor lasers, their full potential is yet to be realized, and hence much effort should be devoted to the experimental and theoretical study of the characteristics of these novel devices.

1.3. Previous theoretical work on QD lasers and motivation for this work

There have been theoretical works on QD lasers. Some of them, which are related to the topic of this research, are summarized here.

In an ideal QD laser, the density of states should be a delta-function (see Fig. 1.3). The advantages of QD lasers stem from this property. However, in actual situation, self-organized QDs are not identical. They vary in different aspects, primarily in size and shape (see, e.g., [71]). The fluctuations in QD parameters lead to an inhomogeneously broadened gain spectrum. In the early work of Asryan and Suris [61], inhomogeneous line broadening and its effect on the threshold current of a QD laser were analyzed; the dependence of the threshold current density on the RMS of QD size fluctuations, as well as on the other parameters, was calculated.

In an ideal scenario, there should be one electron and one hole energy level in a QD. In actual QD structures, there are also excited-states [72]. In [73, 74], the effect of excited-states on the threshold current density of a QD laser was studied; a small overlap integral for transitions in QDs (and hence a long spontaneous radiative lifetime) was shown to be a possible reason for a low single-layer modal gain limiting the ground-state lasing in short-cavity devices. The presence of excited states in QDs can strongly affect the ground-state lasing [53, 75, 76]. A study of this effect presents one of the objectives of this dissertation.

Charge neutrality violation in QDs and its effect on the laser characteristics were studied in [31, 32, 77]. It was shown that the electron and hole level occupancies in a QD can differ from each other, and the difference can be comparable to the occupancies themselves. Charge neutrality violation can strongly affect the gain and the threshold current [32]. It also introduces the temperature dependence of the electron and hole level occupancies, and hence an extra temperature dependence of the threshold current [31, 77]. Therefore, even if the parasitic recombination outside QDs (which is the main source of temperature dependence of j_{th} at high T) is fully suppressed, j_{th} will still be temperature dependent and T_0 will remain finite. At low T, the thermal escape of carriers from QDs is essentially suppressed, and very high T_0 could be expected. However, T_0 remains limited [42], and it is the charge neutrality violation that is responsible for this.

The internal optical loss can strongly affect the characteristics of a semiconductor laser. In [78, 79], the effect of internal loss on j_{th} of a QD laser was studied assuming that the internal

loss coefficient is linear with the carrier density in the optical confinement layer (OCL). The internal loss was shown to considerably narrow the region of tolerable structure parameters in which the lasing is attainable. The calculations suggested that the internal loss is likely to be another major limiting factor for lasing in short-cavity QD structures. The carrier-density-dependent internal loss acts as an additional source of the temperature-dependence of the threshold current. In this dissertation, the characteristic temperature of a QD laser is studied in the presence of such a loss.

Another problem of primary importance is the multimode generation. Multiple mode generation can be due to longitudinal spatial hole burning (SHB), which is caused by nonuniformity of the stimulated recombination along the cavity. Nonuniformity of stimulated recombination can lead to nonuniform carrier distributions. In QW or bulk-active-region lasers, nonuniform carrier distributions are effectively smoothed out by the diffusion. In a QD laser, smoothing out nonuniform carrier distribution requires also the thermal escape of carriers from QDs to the OCL. It is the thermal escape, which was shown in [62, 80] to be the limiting factor. Therefore, SHB is more strongly pronounced in QD lasers as compared to bulk or QW lasers. Using a linear approximation, Asryan and Suris [62, 80] calculated the multimode generation threshold (the difference between the threshold current densities of the first and second longitudinal modes) and studied the dependence of this threshold on the structure parameters. It was found that a decrease in the QD size dispersion considerably increases the relative multimode generation threshold. With increasing injection current and hence intensity of light, SHB becomes more strongly pronounced. A study of the effect of SHB and multimode emission on high-power operation of a QD laser is one more objective of this dissertation.

1.4. Objectives, structure, and main findings of the dissertation

The main objective of this research is a comprehensive study of the effect of different factors on the operating characteristics of a semiconductor QD laser. Specifically, the following topics are included in the dissertation:

1) Effect of carrier-density-dependent internal optical loss on the characteristic temperature (Chapter 2).

It is shown that [A5–A7] [*)] internal optical loss in a semiconductor QD laser couples the confined-carrier level occupancy in QDs to the free-carrier density in the waveguide. Due to this coupling, which is controlled by the threshold condition, the free-carrier density is increased and more temperature-sensitive, and also the confined-carrier level occupancy becomes temperature-dependent. As a result, the characteristic temperature of a laser is considerably reduced. Carrier-density-dependent internal loss also sets an upper limit for operating temperatures of a QD laser and constrains the shallowest potential well depth and the smallest tolerable size of a QD at which the lasing can be attained. The dependences of the characteristic temperature, maximum operating temperature, and shallowest potential well depth on the parameters of the structure are obtained. At the maximum operating temperature or when any parameter of the structure is equal to its critical tolerable value, the characteristic temperature reduces to zero.

2) Effect of excited-states in QDs on the light-current characteristic (Chapter 3).

We develop a comprehensive theory of the output power of a QD laser in the presence of excited states in QDs [A4, A8, A9]. The carrier capture from the three-dimensional reservoir (optical confinement layer – OCL) into the QD ground-state and escape from the ground-state to the OCL are assumed to occur via the QD excited-state. Such a two-step capture places a fundamental limitation on ground-state lasing—the output power saturates at high injection currents. The saturation power is controlled by the transition time between the excited- and ground-state in a QD. The longest, cut-off transition time exists, beyond which no ground-state lasing is possible. The following characteristics are analyzed versus the injection current density and the transition time: occupancies of the ground- and excited-state, free carrier density in the OCL, threshold current density, number of stimulated photons emitted, output power, internal and external differential quantum efficiencies.

[*)] "A" in the reference number indicates the publications of the author of this dissertation.

3) Effect of longitudinal SHB and multimode lasing on the light-current characteristic (Chapter 4).

We use a set of rate equations for confined carriers in QDs, free carriers in the optical confinement layer, and photons to study the multi longitudinal mode oscillation in a QD laser. The number of modes is shown to remain limited with increasing injection current [A2, A3]. The maximum number of modes that can oscillate in a QD laser is analytically estimated. While this number increases with increasing surface density of QDs or cavity length, it remains limited (first increases and then decreases) with increasing scatter in the QD-size. The critical tolerable values of the structure parameters are derived beyond which higher-order longitudinal modes can not oscillate. It is notable that, in addition to the maximum tolerable scatter, there also exists the minimum scatter in the QD-size for each higher-order mode to start lasing. The threshold currents and output powers of modes are computed numerically [A1]. The power of the main mode is reduced due to lasing of higher-order modes and spatially nonuniform carrier distribution. As a new mode turns on, kinks appear in the LCCs of existing modes. SHB reduces the total optical power of a laser and contributes to nonlinearity of the overall LCC. The effect is more significant when any of the structure parameters is close to its critical tolerable value. The LCC becomes more linear with improving QD-size uniformity or increasing surface density of QDs or cavity length.

List of publications of the author of this dissertation

[A1] L. Jiang and L. V. Asryan, "Multimode emission and optical power in a semiconductor quantum dot laser," *Nanotechnology*, vol. 19, no. 41, art. no. 415204 (8 pages), Oct. 2008.

[A2] L. Jiang and L. V. Asryan, "How many longitudinal modes can oscillate in a quantum dot laser: an analytical estimate," accepted for publication in *IEEE Photon. Technol. Lett.*, vol. 20, 2008.

[A3] L. Jiang and L. V. Asryan, "Maximum number of longitudinal modes oscillating in a quantum dot laser due to spatial hole burning," *International Semiconductor Device Research Symposium*. College Park, Maryland, Dec. 12–14, 2007. Paper no. WP9-18-07, 2 pages.

[A4] L. Jiang and L.V. Asryan, "Indirect capture and ground-state lasing in quantum dot structures," *Proceedings of 15th International Symposium "Nanostructures: Physics and Technology"*. Novosibirsk, Russia, June 25–29, 2007. pp. 38–39.

[A5] L. Jiang and L.V. Asryan, "Internal-loss-limited maximum operating temperature and characteristic temperature of quantum dot laser," *Laser Phys. Lett.*, vol. 4, no. 4, pp. 265–269, Apr. 2007.

[A6] L. Jiang and L. V. Asryan, "Maximum operating temperature of quantum dot laser," *Abstracts of International Symposium and Spring School "Nano and Giga Challenges in Electronics and Photonics"*. Phoenix, Arizona, Mar. 12–16, 2007. p. 37.

[A7] L. Jiang and L.V. Asryan, "Maximum operating temperature and characteristic temperature of a quantum dot laser in the presence of internal loss," *Proceedings of SPIE's International Symposium Photonics West*. San Jose, California, Jan. 20–25, 2007. vol. 6481, pp. 648107-1–648107-6.

[A8] L. Jiang and L.V. Asryan, "Effect of excited states on light-current characteristic of a quantum dot laser," *Proceedings of SPIE's International Symposium Photonics West*. San Jose, California, Jan. 20–25, 2007. vol. 6481, pp. 648108-1–648108-7.

[A9] L. Jiang and L. V. Asryan, "Excited-state-mediated capture of carriers into the ground state and the saturation of optical power in quantum-dot lasers," *IEEE Photon. Technol. Lett.*, vol. 18, no. 24, pp. 2611–2613, Dec. 2006.

Presentations at the MSE seminar

1) "Effect of internal loss on temperature dependence of threshold current of semiconductor quantum dot laser," Oct. 6, 2006.

2) "Indirect capture of carriers into the ground state and the saturation of optical power in quantum dot lasers," Feb. 9, 2007.

3) "Spatial hole burning and high power operation of a semiconductor quantum dot laser," Feb. 15, 2008.

REFERENCES

[1] T. Ikegami, "Survey of telecommunications applications of quantum-electronics – progress with optical fiber communications," *Proc. IEEE*, vol. 80, no. 3, pp. 411–419, March 1992.

[2] R. A. Bartolini, A. E. Bell, and F. W. Spong, "Diode-laser optical-recording using trilayer structures," *IEEE J. Quantum Electron.*, vol. 17, no. 1, pp. 69–77, Jan. 1981.

[3] D. B. Carlin and Y. Tsunoda, "Diode-lasers for mass-market applications - optical-recording and printing," *Proc. IEEE*, vol. 82, no. 4, pp. 469–481, Apr. 1994.

[4] Zh. I. Alferov, "Double heterostructure lasers: early days and future perspectives," *IEEE J. Sel. Top. Quantum Electron.*, vol. 6, no. 6, pp. 832–840, Nov./Dec. 2000.

[5] G. P. Agrawal and N. K. Dutta, *Long-Wavelength Semiconductor Lasers*. New York: Van Nostrand Reinhold, 1986, p. 473.

[6] N. G. Basov, O. N. Krokhin, and Yu. M. Popov, "Production of negative-temperature states in P-N junctions of degenerate semiconductors," *Zh. Eskp. Theor. Fiz.*, vol. 40, pp. 1879–1880, 1961 (*Sov. Phys. JETP*, vol. 13, pp. 1320–1321, 1961).

[7] M. G. A. Bernard and G. Duraffourg, "Laser conditions in semiconductors," *Phys. Status Solidi*, vol. 1, no. 7, pp. 699–703, 1961.

[8] R. N. Hall, G. E. Fenner, J. D. Kingsley, T. J. Soltys, R. O. and Carlson, "Coherent light emission from GaAs junctions," *Phys. Rev. Lett.*, vol. 9, no. 9, pp. 366–368, Nov. 1962.

[9] M. I. Nathan, W. P. Dumke, G. Burns, F. H. Dill, and G. Lasher, "Stimulated emission of radiation from GaAs *p-n* junctions," *Appl. Phys. Lett.*, vol. 1, no. 3, pp. 62–64, Nov. 1962.

[10] T. M. Quist, R. H. Rediker, R. J. Keyes, W. E. Krag, B. Lax, A. L. McWhorter, and H. J. Zeiger, "Semiconductor maser of GaAs," *Appl. Phys. Lett.*, vol. 1, no. 4, pp. 91–92, Dec. 1962.

[11] N. Holonyak, Jr. and S. F. Bevacqua, "Coherent (visible) light emission from $Ga(As_{1-x}P_x)$ junctions," *Appl. Phys. Lett.*, vol. 1, no. 4, pp. 82–83, Dec. 1962.

[12] Zh. I. Alferov and R. F. Kazarinov, *Semiconductor laser with electrical pumping*. Inventor's Certificate 181737, 1963.

[13] H. Kroemer, "A proposed class of heterojunction injection lasers," *Proc. IEEE*, vol. 51, no. 12, pp. 1782–1783, Dec. 1963.

[14] I. Hayashi, M. B. Panish, and P. W. Foy, "A low-threshold room-temperature injection

laser," *IEEE J. Quantum Electron.*, vol. QE-5, no. 4, pp. 211–212, Apr. 1969.

[15] Zh. I. Alferov, V. M. Andreev, D. Z. Garbuzov, Y. V Zhilyaev, E. P. Morozov, E. L. Portnoi, and V. G. Trofim, "Investigation of the influence of the AlGaAs-GaAs heterostructure parameters on the laser threshold current and the realization of continuous emission at the room temperature," *Fiz. Tekh. Poluprovodn.*, vol. 4, no. 9, pp. 1826–1829, 1970 (*Sov. Phys. Semicond.*, vol. 4, no. 9, pp. 1573–1575, 1971).

[16] M. B. Panish, I. Hayashi, and S. Sumski, "Double-heterostructure injection lasers with room-temperature thresholds as low as 2300 A/cm^2," *Appl. Phys. Lett.*, vol. 16, no. 8, pp. 326–327, Apr. 1970.

[17] I. Hayashi, M. B. Panish, P. W. Foy, and S. Sumski, "Junction lasers which operate continuously at room temperature," *Appl. Phys. Lett.*, vol. 17, no. 3, pp. 109–111, Aug. 1970.

[18] R. Dingle and C. H. Henry, *Quantum effects in heterostructure lasers*. U.S. Patent 3982207, Sept. 1976.

[19] J. P. van der Ziel, R. Dingle, R. C. Miller, W. Wiegmann, and W. A. Nordland, "Laser oscillation from quantum states in very thin GaAs-$Al_{0.2}Ga_{0.8}As$ multilayer structures," *Appl. Phys. Lett.*, vol. 26, no. 8, pp. 463–465, Apr. 1975.

[20] R. D. Dupuis, P. D. Dapkus, N. Holonyak, E. A. Rezek, and R. Chin, "Room-temperature laser operation of quantum-well $Ga_{(1-x)}Al_xAs$-GaAs laser-diodes grown by metalorganic chemical vapor deposition," *Appl. Phys. Lett.*, vol. 32, no. 5, pp. 295–297, Mar. 1978.

[21] W. T. Tsang, "Extremely low threshold (AlGa)As graded-index waveguide separate confinement heterostructure lasers grown by molecular beam epitaxy," *Appl. Phys. Lett.*, vol. 40, no. 3, pp. 217–219, Feb. 1982.

[22] R. D. Dupuis and P. D. Dapkus, "Very low threshold $Ga_{(1-x)}Al_xAs$-GaAs double-heterostructure lasers grown by metalorganic chemical vapor deposition," *Appl. Phys. Lett.*, vol. 32, no. 8, pp. 473–475, Apr. 1978.

[23] E. J. Thrush, P. R. Selway, and G. D. Henshall, "Metalorganic C.V.D. growth of GaAs-GaAlAs double heterojunction lasers having low interfacial recombination and low threshold current," *Electron. Lett.*, vol. 15, no. 5, pp. 156–158, Mar. 1979.

[24] W. T. Tsang, "A graded-index wave-guide separate-confinement laser with very low threshold and a narrow Gaussian beam," *Appl. Phys. Lett.*, vol. 39, no. 2, pp. 134–137, July

1981.

[25] N. Chand, E. E. Becker, J. P. van der Ziel, S. N. G. Chu, and N. K. Dutta, "Excellent uniformity and very low (<50 A/cm^2) threshold current density strained InGaAs quantum well diode lasers on GaAs substrate," *Appl. Phys. Lett.*, vol. 58, no. 16, pp. 1704–1706, Apr. 1991.

[26] R. Hiroyama, D. Inoue, S. Kameyama, A. Tajiri, M. Shono, M. Sawada, and A. Ibaraki, "High-power 200 mW 660 nm AlGaInP laser diodes with low operating current," *Jpn. J. Appl. Phys.*, vol. 43, no. 4B, pp. 1951–1955, Apr. 2004.

[27] S. Nakamura, "GaN-based blue/green semiconductor laser," *IEEE J. Select. Topics Quantum Electron.*, vol. 3, no. 2, pp. 435–442, Apr. 1997.

[28] G. W. Turner, H. K. Choi, and M. J. Manfra, "Ultralow-threshold (50 A/cm^2) strained single-quantum-well GaInAsSb/AlGaAsSb lasers emitting at 2.05 μm," *Appl. Phys. Lett.*, vol. 72, no. 8, pp. 876–878, Feb. 1998.

[29] P. S. Zory Jr., Ed., *Quantum Well Lasers*. Boston, MA: Academic, 1993, p. 504.

[30] L. V. Asryan and S. Luryi, "Quantum dot lasers: theoretical overview," Chapter 4 in T. Steiner, Ed., *Semiconductor nanostructures for optoelectronic applications*. Boston: Artech House, 2004, p. 424.

[31] L. V. Asryan and R. A. Suris, "Characteristic temperature of quantum dot laser," *Electron. Lett.*, vol. 33, no. 22, pp. 1871–1872, Oct. 1997.

[32] L. V. Asryan and R. A. Suris, "Charge neutrality violation in quantum dot lasers," *IEEE J. Select. Topics Quantum Electron.*, vol. 3, no. 2, pp. 148–157, Apr. 1997.

[33] Y. Arakawa and H. Sakaki, "Multidimensional quantum well laser and temperature dependence of its threshold current," *Appl. Phys. Lett.*, vol. 40, no. 11, pp. 939–941, June 1982.

[34] M. Asada, Y. Miyamoto, and Y. Suematsu, "Gain and the threshold of three-dimensional quantum-box lasers," *IEEE J. Quantum Electron.*, vol. QE-22, no. 9, pp. 1915–1921, Sept. 1986.

[35] K. Vahala, Y. Arakawa, and A. Yariv, "Reduction of the field spectrum linewidth of a multiple quantum-well laser in a high magnetic-field - spectral properties of quantum dot lasers," *Appl. Phys. Lett.*, vol. 50, no. 7, pp. 365–367, Feb. 1987.

[36] Y. Miyamoto, M. Cao, Y. Shingai, K. Furuya, Y. Suematsu, K. G. Ravikumar, and, S. Arai,

"Light-emission from quantum-box structure by current injection," *Jpn. J. Appl. Phys.*, vol. 26, no. 4, pp. L225–L227, Apr. 1987.

[37] H. Hirayama, K. Matsunaga, M. Asada, and Y. Suematsu, "Lasing action of $Ga_{0.67}In_{0.33}As$/GaInAsP/InP tensile-strained quantum-box laser," *Electron. Lett.*, vol. 30, no. 2, pp. 142–143, Jan. 1994.

[38] J. S. Kim, J. H. Lee, S. U. Hong, W. S. Han, H. S. Kwack, and D. K. Oh, "Influence of InGaAs overgrowth layer on structural and optical properties of InAs quantum dots," *J. Cryst. Growth*, vol. 255, no. 1–2, pp. 57–62, July 2003.

[39] P. Bhattacharya, S. Krishna, J. Phillips, P. J. McCann, and K. Namjou, "Carrier dynamics in self-organized quantum dots and their application to long-wavelength sources and detectors," *J. Cryst. Growth*, vol. 227–228, pp. 27–35, July, 2001.

[40] N. N. Ledentsov, V. M. Ustinov, A. Y. Egorov, A. E. Zhukov, M. V. Maksimov, I. G. Tabatadze, and P. S. Kopev, "Optical-properties of heterostructures with InGaAs-GaAs quantum clusters," *Semiconductors*, vol. 28, no. 8, pp. 832–834, Aug. 1994.

[41] A. Y. Egorov, A. E. Zhukov, P. S. Kopev, N. N. Ledentsov, M. V. Maksimov, and V. M. Ustinov, "Effect of deposition conditions on the formation of (In,Ga)As quantum clusters in a GaAs matrix," *Semiconductors*, vol. 28, no. 8, pp. 809–811, Aug. 1994.

[42] N. Kirstädter, N. N. Ledentsov, M. Grundmann, D. Bimberg, V. M. Ustinov, S. S. Ruvimov, M. V. Maximov, P. S. Kop'ev, Zh. I. Alferov, U. Richter, P. Werner, U. Gösele, and J. Heydenreich, "Low threshold, large T_0 injection laser emission from (InGa)As quantum dots," *Electron. Lett.*, vol. 30, no. 17, pp. 1416–1417, Aug. 1994.

[43] K. Kamath, P. Bhattacharya, T. Sosnowski, T. Norris, and J. Phillips, "Room-temperature operation of $In_{0.4}Ga_{0.6}As$/GaAs self-organised quantum dot lasers," *Electron. Lett.*, vol. 32, no. 15, pp. 1374–1415, July 1996.

[44] R. Mirin, A. Gossard, and J. Bowers, "Room temperature lasing from InGaAs quantum dots," *Electron. Lett.*, vol. 32, no. 18, pp. 1732–1734, Aug. 1996.

[45] N. N. Ledentsov, V. A. Shchukin, M. Grundmann, N. Kirstaedter, J. Bo¨hrer, O. Schmidt, D. Bimberg, V. M. Ustinov, A. Yu. Egorov, A. E. Zhukov, P. S. Kop'ev, S. V. Zaitsev, N. Yu. Gordeev, Zh. I. Alferov, A. I. Borovkov, A. O. Kosogov, S. S. Ruvimov, P. Werner, U. Gosele, and J. Heydenreich, "Direct formation of vertically coupled quantum dots in Stranski-Krastanow growth," *Phys. Rev. B*, vol. 54, no. 12, pp. 8743–8750, Sept. 1996.

[46] M. V. Maximov, I. V. Kochnev, Y. M. Shernyakov, S. V. Zaitsev, N. Y. Gordeev, A. F. Tsatsul'nikov, A. V. Sakharov, I. L. Krestnikov, P. S. Kop'ev, Zh. I. Alferov, N. N. Ledentsov, D. Bimberg, A. O. Kosogov, P. Werner, and U. Gosele, "InGaAs/GaAs quantum dot lasers with ultrahigh characteristic temperature (T_0 = 385 K) grown by metal organic chemical vapour deposition," *Jpn. J. Appl. Phys.*, vol. 36, no. 6B, pp. 4221–4223, June 1997.

[47] N. N. Ledentsov, V. M. Ustinov, V. A. Shchukin, P. S. Kop'ev, Zh. I. Alferov, and D. Bimberg, "Quantum dot heterostructures: Fabrication, properties, lasers," *Semiconductors*, vol. 32, no. 4, pp. 343–365, Apr. 1998.

[48] L. Harris, D. J. Mowbray, M. S. Skolnick, M. Hopkinson, and G. Hill, "Emission spectra and mode structure of InAs/GaAs self-organized quantum dot lasers," *Appl. Phys. Lett.*, vol. 73, no. 7, pp. 969–971, Aug. 1998.

[49] V. P. Evtikhiev, I. V. Kudryashov, E. Yu. Kotel'nikov, V. E. Tokranov, A. N. Titkov, I. S. Tarasov, and Zh. I. Alferov, "Continuous stimulated emission at T = 293 K from separate-confinement heterostructure diode lasers with one layer of InAs quantum dots grown on vicinal GaAs(001) surfaces misoriented in the (010) direction in the active region," *Semiconductors*, vol. 32, no. 12, pp. 1323–1327, Dec. 1998.

[50] M. Sugawara, K. Mukai, and Y. Nakata, "Light emission spectra of columnar-shaped self-assembled InGaAs/GaAs quantum-dot lasers: Effect of homogeneous broadening of the optical gain on lasing characteristics," *Appl. Phys. Lett.*, vol. 74, no. 11, pp. 1561–1563, Mar. 1999.

[51] V.P. Evtikhiev, V.E. Tokranov, A.K. Kryganovskii, A.M. Boiko, R.A. Suris, and A.N. Titkov, "Characteristics of the InAs quantum dots MBE grown on the vicinal GaAs(0 0 1) surfaces misoriented to the [0 1 0] direction," *J. Cryst. Growth*, vol. 201–202, pp. 1154–1157, May, 1999.

[52] A. R. Kovsh, A. E. Zhukov, D. A. Lifshits, A. Y. Egorov, V. M. Ustinov, M. V. Maximov, Y. G. Musikhin, N. N. Ledentsov, P. S. Kop'ev, Zh. I. Alferov, and D. Bimberg, "3.5 W CW operation of quantum dot laser," *Electron. Lett.*, vol. 35, no. 14, pp. 1161–1163, July 1999.

[53] L. F. Lester, A. Stintz, H. Li, T. C. Newell, E. A. Pease, B. A. Fuchs, and K. J. Malloy, "Optical characteristics of 1.24-μm InAs quantum-dot laser diodes," *IEEE Photon. Technol. Lett.*, vol. 11, no. 8, pp. 931–933, Aug. 1999.

[54] G. Park, O. B. Shchekin, D. L. huffaker, and D. G. Deppe, "Low-threshold oxide-confined 1.3-μm quantum-dot laser," *IEEE Photon. Technol. Lett.*, vol. 13, no. 3, pp. 230–232, Mar. 2000.

[55] P. G. Eliseev, H. Li, A. Stintz, G. T. Liu, T. C. Newell, K. J. Malloy and L. F. Lester, "Transition dipole moment of InAs/InGaAs quantum dots from experiments on ultralow-threshold laser diodes," *Appl. Phys. Lett.*, vol. 77, no. 2, pp. 262–264, July 2000.

[56] P. G. Eliseev, H. Li, G. T. Liu, A. Stintz, T. C. Newell, L. F. Lester, and K. J. Malloy, "Ground-state emission and gain in ultralow-threshold InAs-InGaAs quantum-dot lasers," *IEEE J. Select. Topics Quantum Electron.*, vol. 7, no. 2, pp. 135–142, Mar./Apr. 2001.

[57] A. R. Kovsh, N. A. Maleev, A. E. Zhukov, S. S. Mikhrin, A. P. Vasil'ev, E. A. Semenova, Yu. M. Shernyakov, M. V. Maximov, D. A. Livshits, V. M. Ustinov, N. N. Ledentsov, D. Bimberg, and Zh. I. Alferov, "InAs/InGaAs/GaAs quantum dot lasers of 1.3 μm range with enhanced optical gain," *J. Cryst. Growth*, vol. 251, no. 1–4, pp. 729–736, Apr. 2003.

[58] V. Tokranov, M. Yakimov, A. Katsnelson, M. Lamberti, S. Oktyabrsky, "Enhanced thermal stability of laser diodes with shape-engineered quantum dot medium," *Appl. Phys. Lett.*, vol. 83, no. 5, pp. 833–835, Aug. 2003.

[59] I. R. Sellers, H. Y. Liu, K. M. Groom, D. T. Childs, D. Robbins, T. J. Badcock, M. Hopkinson, D. J. Mowbray, A. S. Skolnick, "1.3 μm InAs/GaAs multilayer quantum-dot laser with extremely low room-temperature threshold current density," *Electron. Lett.*, vol. 40, no. 22, pp. 1412–1413, Oct. 2004.

[60] H. Y. Liu, D. T. Childs, T. J. Badcock, K. M. Groom, I. R. Sellers, M. Hopkinson, R. A. Hogg, D. J. Robbins, D. J. Mowbray, and M. S. Skolnick, "High-performance three-layer 1.3-μu m InAs-GaAs quantum-dot lasers with very low continuous-wave room-temperature threshold currents," *IEEE Photon. Technol. Lett.*, vol. 17, no. 6, pp. 1139–1141, June 2005.

[61] L. V. Asryan and R. A. Suris, "Inhomogeneous line broadening and the threshold current density of a semiconductor quantum dot laser," *Semicond. Sci. Technol.*, vol. 11, no. 4, pp. 554–567, Apr. 1996.

[62] L. V. Asryan and R. A. Suris, "Longitudinal spatial hole burning in a quantum-dot laser," *IEEE J. Quantum Electron.*, vol. 36, no. 10, pp. 1151–1160, Oct. 2000.

[63] O. B. Shchekin, D. G. Deppe, "The role of p-type doping and the density of states on the

modulation response of quantum dot lasers," *Appl. Phys. Lett.*, vol. 80, no. 15, pp. 2758–2760, Apr. 2002.

[64] O. B. Shchekin and D. G. Deppe, "Low-threshold high-T_0 1.3-μm InAs quantum-dot lasers due to p-type modulation doping of the active region," *IEEE Photon. Technol. Lett.*, vol. 14, no. 9, pp. 1231–1233, Sept. 2002.

[65] L. V. Asryan and S. Luryi, "Tunneling-injection quantum-dot laser: Ultrahigh temperature stability," *IEEE J. Quantum Electron.*, vol. 37, no. 7, pp. 905–910, July 2001.

[66] S. Fathpour, Z. Mi, P. Bhattacharya, A. R. Kovsh, S. S. Mikhrin, I. L. Krestnikov, A. V. Kozhukhov, and N. N. Ledentsov, "The role of Auger recombination in the temperature-dependent output characteristics ($T_0 = \infty$) of p-doped 1.3 μm quantum dot lasers," *Appl. Phys. Lett.*, vol. 85, no. 22, pp. 5164–5166, Nov. 2004.

[67] S. Fafard, K. Hinzer, S. Raymond, M. Dion, J. McCaffrey, Y. Feng, and S. Charbonneau, "Red-emitting semiconductor quantum dot lasers," *Science*, vol. 274, no. 5291, pp. 1350–1353, Nov. 1996.

[68] T. W. Schlereth, S. Gerhard, W. Kaiser, and S. Hofling, "High-performance short-wavelength (~760 nm) AlGaInAs quantum-dot lasers," *IEEE Photon. Technol. Lett.*, vol. 19, no. 17–20, pp. 1380–1382, Sept.–Oct. 2007.

[69] N. N. Ledentsov, A. R. Kovsh, A. E. Zhukov, N. A. Maleev, S. S. Mikhrin, A. P. Vasil'ev, E. S. Sernenova, M. V. Maximov, Y. M. Shernyakov, N. Kryzhanovskaya, V. Ustinov, and D. Bimberg, "High performance quantum dot lasers on GaAs substrates operating in 1.5 μm range," *Electron. Lett.*, vol. 39, no. 25, pp. 1126–1128, July 2003.

[70] E. Homeyer, R. Piron, F. Grillot, O. Dehaese, K. Tavernier, E. Mace, J. Even, A. Le Corre, and S. Loualiche, "Demonstration of a low threshold current in 1.54 μm InAs/InP(311)B quantum dot laser with reduced quantum dot stacks," *Jpn. J. Appl. Phys.*, vol. 46, no. 10A, pp. 6903–6905, Oct. 2007.

[71] D. Leonard, S. Fafard, K. Pond, Y. H. Zhang, J. L. Merz, and P. M. Petroff, "Structural and optical properties of self-assembled InGaAs quantum dots," *J. Vac. Sci. Technol. B*, vol. 12, no. 4, pp. 2516–2520, July/Aug. 1994.

[72] O. Stier, M. Grundmann, and D. Bimberg, "Electronic and optical properties of strained quantum dots modeled by 8-band $\mathbf{k} \cdot \mathbf{p}$ theory," *Phys. Rev. B*, vol. 59, no. 8, pp. 5688–5701, Feb. 1999.

[73] L. V. Asryan, M. Grundmann, N. N. Ledentsov, O. Stier, R. A. Suris and D. Bimberg, "Effect of excited-state transition on the threshold characteristics of a quantum dot laser," *IEEE J. Quantum Electron.*, vol. 37, no. 3, pp. 418–425, Mar. 2001.

[74] L. V. Asryan, M. Grundmann, N. N. Ledentsov, O. Stier, R. A. Suris, and D. Bimberg, "Maximum modal gain of a self-assembled InAs/GaAs quantum-dot laser," *J. Appl. Phys.*, vol. 90, no. 3, pp. 1666–1668, Aug. 2001.

[75] M. V. Maximov, M. V. Y. M. Shernyakov, I. N. Kaiander, D, A. Bedarev, E. Y. Kondrat'eva, P. S. Kop'ev, A. R. Kovsh, N. A. Maleev, S. S. Mikhrin, A. F. Tsatsul'nikov, V. M. Ustinov, B. V. Volovik, A. E. Zhukov, Zh. J. Alferov, N. N. Ledentsov, and D. Bimberg, "Single transverse mode operation of long wavelength (similar to 1.3 μm) InAsGaAs quantum dot laser," *Electron. Lett.*, vol. 35, no. 23, pp. 2038–2039, Nov. 1999.

[76] G. Park, O. B. Shchekin, S. Csutak, D. L. Huffaker, and D. G. Deppe, "Room-temperature continuous-wave operation of a single-layered 1.3 μm quantum dot laser," *Appl. Phys. Lett.*, vol. 75, no. 21, pp. 3267–3269, Nov. 1999.

[77] L. V. Asryan and R. A. Suris, "Temperature dependence of the threshold current density of a quantum dot laser," *IEEE J. Quantum Electron.*, vol. 34, no. 5, pp. 841–850, May 1998.

[78] L. V. Asryan and S. Luryi, "Two lasing thresholds in semiconductor lasers with a quantum-confined active region," *Appl. Phys. Lett.*, vol. 83, no. 26, pp. 5368–5370, Dec. 2003.

[79] L. V. Asryan and S. Luryi, "Effect of internal optical loss on threshold characteristics of semiconductor lasers with a quantum-confined active region," *IEEE J. Quantum Electron.*, vol. 40, no. 7, pp. 833–843, July 2004.

[80] L. V. Asryan and R. A. Suris, "Spatial hole burning and multimode generation threshold in quantum-dot lasers," *Appl. Phys. Lett.*, vol. 74, no. 9, pp. 1215–1217, Mar. 1999.

Chapter 2

Internal Optical Loss and the Temperature Dependence of the Threshold Current Density of a Quantum Dot Laser

Summary

Internal optical loss in a semiconductor quantum dot (QD) laser couples the confined-carrier level occupancy in QDs to the free-carrier density in the waveguide. Due to this coupling, which is controlled by the threshold condition, the free-carrier density is increased and more temperature-sensitive, and also the confined-carrier level occupancy becomes temperature-dependent. As a result, the characteristic temperature of a laser is considerably reduced. Carrier-density-dependent internal loss also sets an upper limit for operating temperatures of a QD laser and constrains the shallowest potential well depth and the smallest tolerable size of a QD at which the lasing can be attained. The dependences of the characteristic temperature, maximum operating temperature, and shallowest potential well depth on the parameters of the structure are obtained. At the maximum operating temperature or when any parameter of the structure is equal to its critical tolerable value, the characteristic temperature reduces to zero.

2.1. Introduction

Temperature-stable diode lasers are highly desired for optical fiber telecommunication systems. The temperature dependence of the threshold current density of a semiconductor laser can be expressed as [1]

$$j_{\text{th}} \propto \exp\left(\frac{T}{T_0}\right), \tag{2.1}$$

where T_0 is the characteristic temperature – a very important and widely accepted figure of merit of semiconductor lasers defined as

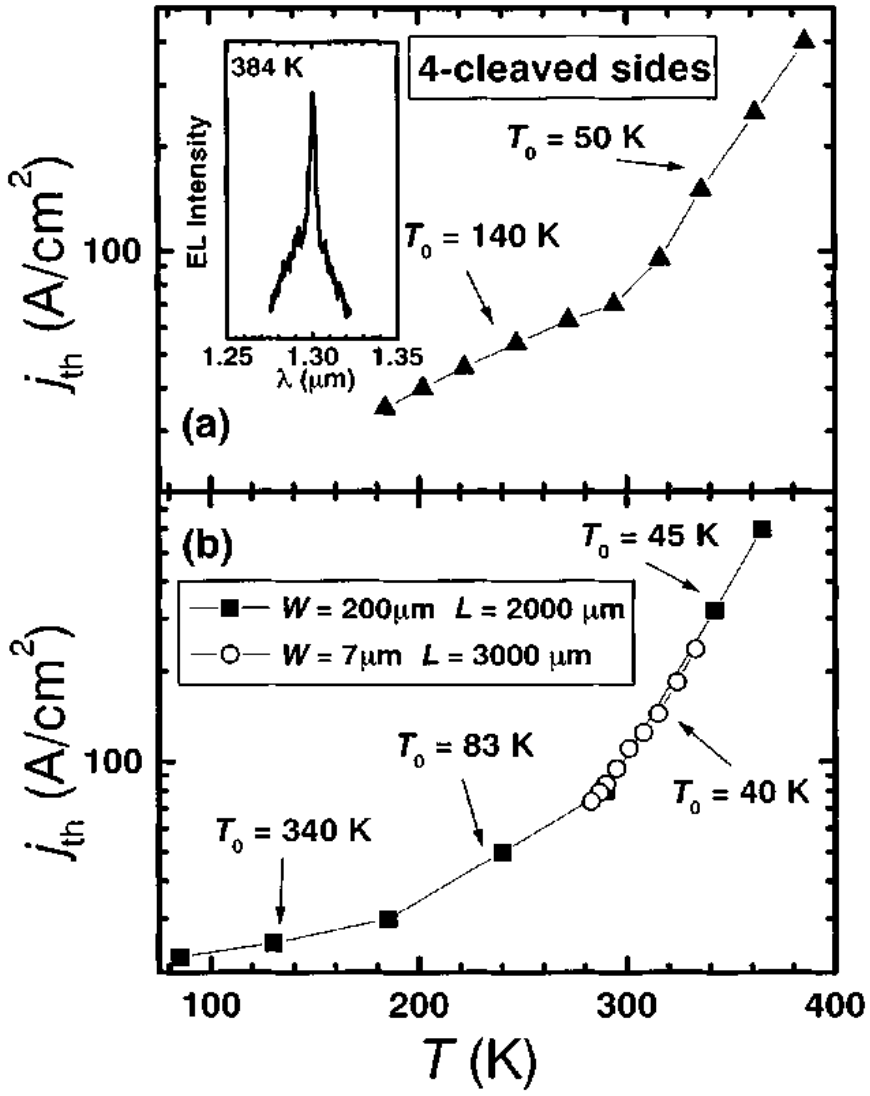

Fig. 2.1. Temperature dependence of the threshold current density of a structure with four-cleaved sides (a) and a stripe device (b). The stripe width (W) and length (L) are indicated. (Fig. 4 of ref. [4], © [2001] IEEE.)

$$T_0 = \left(\frac{\partial \ln j_{th}}{\partial T} \right)^{-1}. \tag{2.2}$$

The less temperature-sensitive is j_{th}, the higher is T_0 (see Fig. 2.1).

High temperature stability of operation is anticipated from semiconductor quantum dot (QD) lasers [2]. This advantage stems from a discrete energy spectrum of carriers in dots (Fig. 1.3).

Improved temperature stability of j_{th} has been first demonstrated by placing QW lasers in strong magnetic fields to achieve three-dimensional confinement of carriers [2, 3].

In an ideal QD laser, the threshold current density j_{th} should remain unchanged with the temperature and the characteristic temperature should be infinitely high [2]. This would be the case if the overall injection current went into QDs, and the recombination current in QDs would be temperature-independent. In actual QD lasers, carriers are first injected from the cladding layers into the optical confinement layer (OCL) (which includes the wetting layer), and then captured into QDs. The presence of carriers in the OCL results in recombination therein. Hence the recombination processes both in QDs and in the OCL control j_{th} and its T-dependence [5, 6]:

$$j_{th} = j_{QD} + j_{OCL}, \tag{2.3}$$

$$\frac{1}{T_0} = \frac{j_{QD}}{j_{QD} + j_{OCL}} \frac{1}{T_0^{QD}} + \frac{j_{OCL}}{j_{QD} + j_{OCL}} \frac{1}{T_0^{OCL}}, \tag{2.4}$$

where j_{QD} and j_{OCL} are the components of j_{th} associated with the recombination in QDs and in the OCL, respectively, and T_0^{QD} and T_0^{OCL} are defined similarly to T_0 but for j_{QD} and j_{OCL}, respectively. The components of j_{th} are given as

$$j_{QD} = \frac{eN_S}{\tau_{QD}} f_n f_p, \qquad j_{OCL} = ebBnp, \tag{2.5}$$

where N_S is the surface density of QDs, τ_{QD} is the spontaneous radiative recombination time in QDs, f_n and f_p are the confined-electron and -hole level occupancies in QDs at the lasing threshold, b is the OCL thickness, B is the radiative constant for the OCL material, and n and p are the free-electron and -hole densities in the OCL at the lasing threshold.

The T-dependence of free-carrier densities, n and p, acts as the major source of such dependence of j_{th} [5, 6]. Thus, when the carrier distribution (below and at the lasing threshold) is described by the equilibrium statistics (relatively high T), n and p depend exponentionally on T,

$$n = n_1 \frac{f_n}{1 - f_n} = N_c^{OCL} \exp\left(-\frac{E_n}{T}\right) \frac{f_n}{1 - f_n}, \tag{2.6}$$

where $n_1 = N_c^{OCL} \exp\left(-E_n/T\right)$, $N_c^{OCL} = 2\left(m_c^{OCL} T / 2\pi\hbar^2\right)^{3/2}$, m_c^{OCL} is the electron effective mass in the OCL, T is the temperature measured in units of energy, and E_n is the carrier excitation

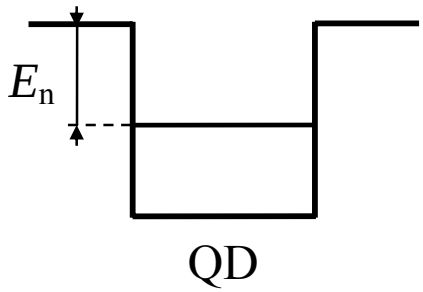

Fig. 2.2. Energy of the carrier excitation from a QD to the OCL.

energy from a QD to the OCL [see Fig. 2.2 and also the inset in Fig. 2.9(a)]. The temperature T here is measured in units of energy. The equation for p is similar to (2.6).

Different factors can contribute to the T-dependence of the confined-carrier level occupancies in QDs, $f_{n,p}$, thus causing the temperature-dependence of the recombination current density in QDs, j_{QD}, and making T_0^{QD} finite. In [6, 7], violation of charge neutrality in QDs ($f_n \neq f_p$) was shown to be such a factor.

2.2. Carrier-density-dependent internal loss in the waveguide

Here we study the effect of carrier-density-dependent internal optical loss in the OCL on the temperature dependence of j_{th} [A1–A3] *). As in other injection lasers [8–16], such a loss can strongly affect the temperature stability of QD lasers [17]. This work is based on [18], where j_{th} has been calculated in the presence of the carrier-density-dependent internal loss. To neatly clarify the effect of internal loss, the charge neutrality [separately in QDs ($f_n = f_p$) and in the OCL ($n = p$)] is assumed here.

In general, several mechanisms can contribute to the internal loss, such as free-carrier absorption in the OCL and scattering at rough surfaces and imperfections in the waveguide (see [18] and the references therein). All these mechanisms can be conveniently grouped into the two categories – one dependent on the carrier density in the OCL and the other independent. Hence, the overall internal loss coefficient α_{int} can be written as a sum of two components – one constant (α_{int}) and the other increasing with the carrier density n,

*) "A" in the reference number indicates the publications of the author of this dissertation.

$$\alpha_{\text{int}} = \alpha_0 + \sigma_{\text{int}} n\,, \tag{2.7}$$

where σ_{int} is the effective cross section for the internal absorption loss processes [18].

With eq. (2.7), the lasing threshold condition (equality of the gain to the loss) can be written as

$$g^{\max}\left(2f_{\text{n}} - 1\right) = \beta + \alpha_0 + \sigma_{\text{int}} n\,, \tag{2.8}$$

where $g^{\max}$ is the maximum (saturation) gain (see eq. (41) in [7]), $\beta = \left(1/L\right)\ln\left(1/R\right)$ is the mirror loss, L is the cavity length, and R is the facet reflectivity.

In the absence of the carrier-density-dependent internal loss ($\sigma_{\text{int}} = 0$), the level occupancy is immediately obtained from (2.8) to be independent of temperature,

$$f_{\text{n}}^{\text{const}} = \frac{1}{2}\left(1 + \frac{\beta + \alpha_0}{g^{\max}}\right). \tag{2.9}$$

Hence, $j_{\text{QD}} = \text{const}(T)$ and $T_0^{\text{QD}} = \infty$ in this case.

As seen from (2.8), the carrier-density-dependent internal loss couples n and f_{n} and, in view of the temperature dependence of n, makes f_{n} and j_{QD} also temperature dependent. Thus, T_0^{QD} becomes finite.

The following expression for f_{n} [which is easily found from (2.6) and (2.8)] has been derived in [18] [see eq. (9) therein]:

$$f_{\text{n}} = \frac{1}{2}\left(1 + f_{\text{n}}^{\text{const}} - \frac{1}{2}\frac{\sigma_{\text{int}} n_1}{g^{\max}}\right) - \sqrt{\frac{1}{4}\left(1 + f_{\text{n}}^{\text{const}} - \frac{1}{2}\frac{\sigma_{\text{int}} n_1}{g^{\max}}\right)^2 - f_{\text{n}}^{\text{const}}}\,, \tag{2.10}$$

where $f_{\text{n}}^{\text{const}}$ is given by (2.9).

As seen from (2.10), the temperature dependence of f_{n} stems from such dependence of n_1 [see eq. (2.6)]. In what follows, a possible T-dependence of σ_{int} is neglected compared to the exponential T-dependence of n_1. Fig. 2.3 shows the temperature-dependence of the confined-carrier level occupancy in QDs (right axis) given by eq. (2.10), the free-carrier density in the OCL and the internal loss (left axis) obtained from eqs. (2.8) and (2.10). In view of a linear character of eq. (2.8), the curve for all these quantities, f_{n}, n, and α_{int}, is the same, and the vertical axes for them are obtained by a simple rescaling from one another. In the presence of the carrier-density-dependent internal loss, the confined-carrier level occupancy increases with

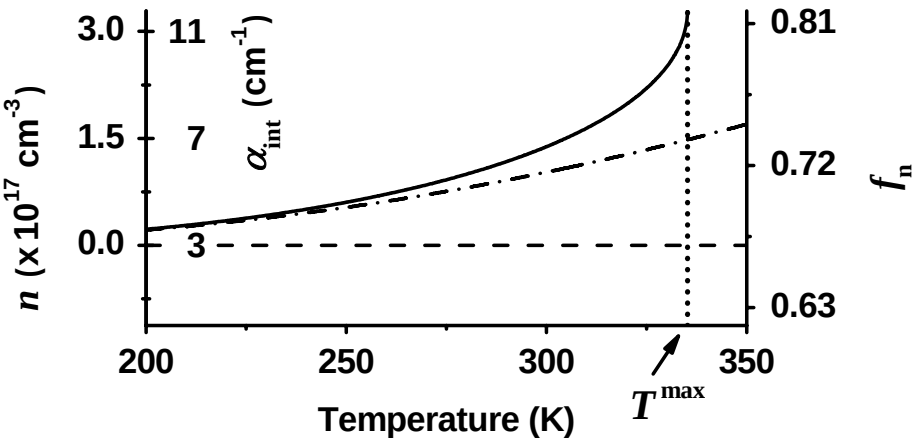

Fig. 2.3. Confined-carrier level occupancy in QDs, f_n (right axis), free-carrier-density in the OCL, n, and internal loss α_{int} (left axis) against temperature in the presence of the carrier-density-dependent internal loss (solid curve). The horizontal dashed line indicates α_{int} and f_n in the absence of the carrier-density-dependent internal loss. The dash-dotted curve shows n in the absence of the carrier-density-dependent internal loss. The vertical dotted line marks the maximum operating temperature T^{max} in the presence of the carrier-density-dependent internal loss [see eq. (2.14)]. The parameters are (the same throughout this chapter unless otherwise specified): the mean size of QDs $a = 150$ Å, the root mean square (RMS) of relative QD size fluctuations $\delta = 0.05$ (Gaussian distribution is assumed), the OCL thickness $b = 0.28$ μm, the surface density of QDs $N_S = 6.11 \times 10^{-10}$ cm^{-2}, the constant component of internal loss $\alpha_0 = 3$ cm^{-1}, the cross section of internal loss $\sigma_{int} = 2.67 \times 10^{-17}$ cm^2, the cavity length $L = 1.628$ mm, and the mirror loss $\beta = 7$ cm^{-1}.

temperature. Both f_n and n are increased compared to their values in the absence of such a loss (the latter are given by the horizontal dashed line and dash-dotted curve, respectively). The vertical dotted line marks the maximum operating temperature T^{max} of a QD laser in the presence of the carrier-density-dependent internal loss (see Section 2.4.1).

GaInAsP/InP heterostructure lasing near 1.55 μm is considered. The parameters are indicated in the caption to Fig. 2.3 and are the same throughout this chapter unless otherwise specified.

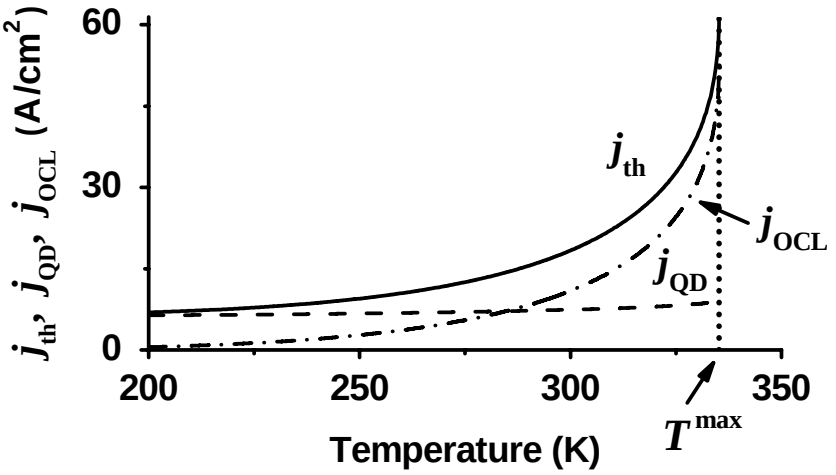

Fig. 2.4. Threshold current density j_{th} (solid curve) and its components j_{QD} (dashed curve) and j_{OCL} (dash-dotted curve) against temperature. The vertical dotted line marks the maximum operating temperature T^{max}.

It is seen from eq. (2.10) that, in order to have a positive real f_n, the expression in the square root should be larger than or equal to zero. Implementing this condition gives the critical value of f_n and hence the critical values of structure parameters. While in the absence of carrier-density-dependent internal loss [5], the critical value of f_n is unity, the critical value of f_n in the presence of such a loss is smaller than unity [see eq. (10) in [18] for the critical value of f_n]. Therefore, the carrier-density-dependent internal loss narrows the range of possible values of the structure parameters, within which lasing action in a QD laser can be attained.

The threshold current density j_{th} and its components j_{QD} and j_{OCL} associated with the recombination in QDs and in the OCL are shown in Fig. 2.4.

Although j_{QD} becomes temperature-dependent in the presence of the carrier-density-dependent internal loss, its temperature dependence is much weaker than that of j_{OCL}. Correspondingly, T_0^{QD} is much higher than T_0^{OCL} (Fig. 2.5). While j_{OCL} is smaller than j_{QD} at relatively low temperature, it increases with temperature much faster than j_{QD} does, and surpasses the latter at relatively high temperature (Fig. 2.4). It is the recombination in the OCL that is a major obstacle to a superior performance of QD lasers at room temperature or higher.

2.3. Characteristic temperature in the presence of carrier-density-dependent internal loss

Assuming the charge neutrality in QDs ($f_n = f_p$) and using (2.5), we have

$$\frac{1}{T_0^{QD}} = \frac{2}{f_n}\frac{\partial f_n}{\partial T}. \tag{2.11}$$

The carrier-density-dependent internal loss formally plays a role similar to that of violation of charge neutrality in QDs [6, 7], affecting the characteristic temperature T_0 via its effect on the level occupancy f_n.

Putting (2.10) into (2.11) yields the following expression for T_0^{QD}:

$$\frac{1}{T_0^{QD}} = \frac{1}{\sqrt{\frac{1}{4}\left(1 + f_n^{const} - \frac{1}{2}\frac{\sigma_{int} n_1}{g^{max}}\right)^2 - f_n^{const}}} \frac{\sigma_{int} n_1}{2g^{max}}\left(\frac{3}{2}\frac{1}{T} + \frac{E_n}{T^2}\right). \tag{2.12}$$

The carrier-density-dependent internal loss also alters the temperature dependence of j_{OCL} since the free-carrier density at the lasing threshold is strongly affected. The expression for T_0^{OCL} in this case can then be expressed as

$$\frac{1}{T_0^{OCL}} = \frac{3}{2}\frac{1}{T} + \frac{2E_n}{T^2} + \frac{1}{1 - f_n}\frac{1}{T_0^{QD}}. \tag{2.13}$$

The sum of the first two terms in the right-hand side of (2.13) presents the reciprocal of T_0^{OCL} in the absence of the carrier-density dependent internal loss [6]. As seen from (2.13), T_0^{OCL} is reduced in the presence of such a loss.

T_0^{QD} and T_0^{OCL} are shown versus temperature in Fig. 2.5. With increasing temperature, the effect of the carrier-density-dependent internal loss becomes more strongly manifested and hence T_0^{QD} (the solid curve) decreases. This is in contrast to the effect of charge neutrality violation in QDs, which is suppressed with increasing temperature — T_0^{QD} controlled by the latter effect increases with temperature (see Fig. 8 in [6]).

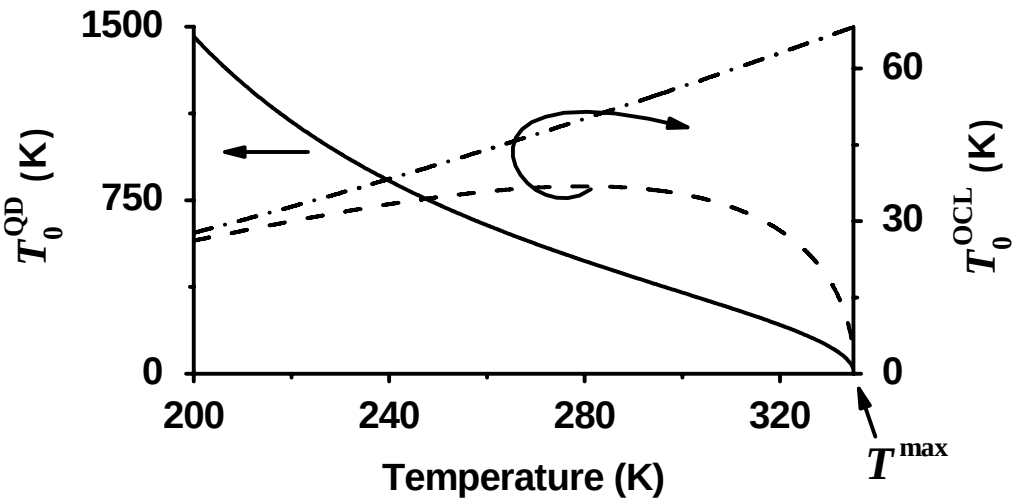

Fig. 2.5. T_0^{QD} (solid curve, left axis) and T_0^{OCL} (dashed curve, right axis) against temperature in the presence of the carrier-density-dependent internal loss. The dash-dotted curve shows T_0^{OCL} in the absence of such a loss.

T_0^{OCL} in the presence of the carrier-density-dependent internal loss (the dashed curve in Fig. 2.5) is also reduced compared to that in the absence of such a loss (the dash-dotted curve), which is again in contrast to the effect of charge neutrality violation in QDs. Due to the latter, T_0^{OCL} was increased (see eq. (25) and Fig. 8 in [6]). A non-monotonic behavior of T_0^{OCL} with temperature should also be noted in the presence of the carrier-density-dependent internal loss. This behavior is controlled by the competition of the sum of the first two terms in (2.13) with the last term. The sum of the first two terms presents the reciprocal of T_0^{OCL} in the absence of the carrier-density-dependent internal loss and decreases with temperature (the dash-dotted curve), the last term is introduced by the carrier-density-dependent internal loss and increases with temperature. At a certain value of the temperature, T^{max}, the third term increases infinitely since T_0^{QD} goes to zero. Hence, T_0^{OCL} goes to zero too at $T = T^{max}$. T^{max} will be discussed in more detail in Section 2.4.1.

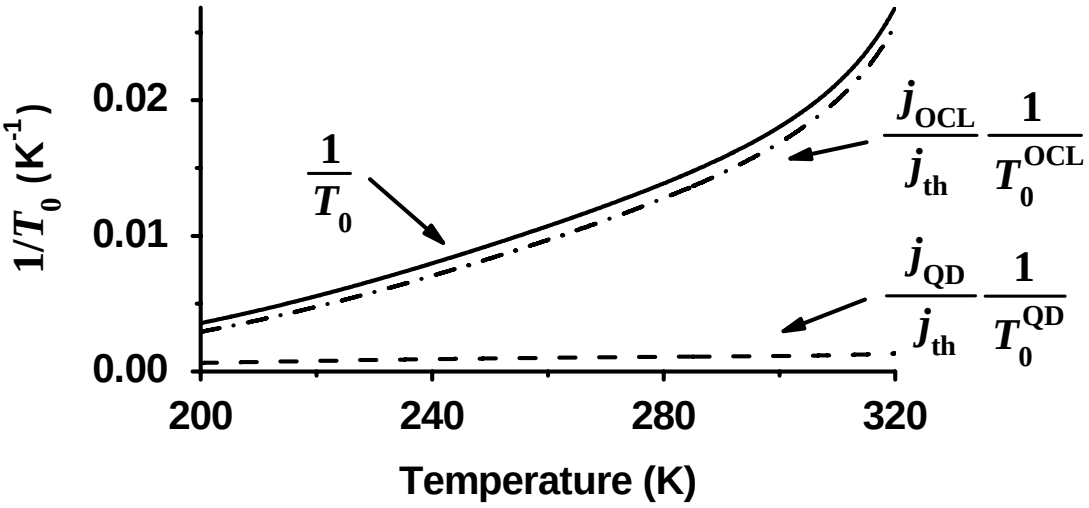

Fig. 2.6. Reciprocal of T_0 and the first and the second terms in the right-hand side of eq. (2.4) against temperature.

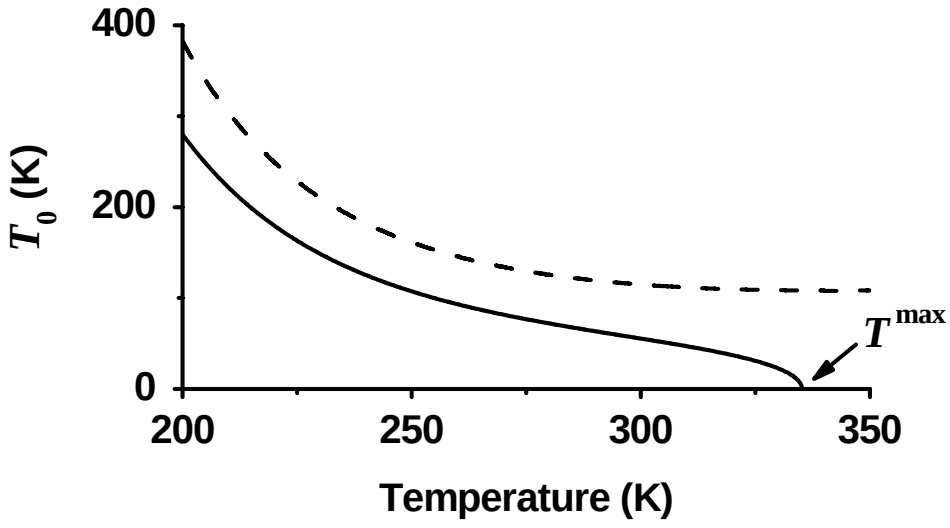

Fig. 2.7. Characteristic temperature against temperature calculated including (solid curve) and neglecting (dashed curve) the carrier-density-dependent internal loss.

Fig. 2.6 shows the reciprocal of T_0 and the first and second terms in the right-hand side of (2.4). As seen from the figure, for the entire temperature range shown, $1/T_0$ is mainly controlled by the second term. Even at low temperature, when j_{QD}/j_{th} is close to unity and hence much larger than j_{OCL}/j_{th}, T_0^{QD} is so high that $(j_{QD}/j_{th})(1/T_0^{QD})$ is smaller than $(j_{OCL}/j_{th})(1/T_0^{OCL})$. At high temperature, j_{QD}/j_{th} is much smaller than j_{OCL}/j_{th}, and, at the same time, T_0^{QD} is still higher than T_0^{OCL}. Although the contribution of the first term in the right-hand side of (2.4) (which is entirely due to the carrier-density-dependent internal loss) into T_0 is minor compared to that of the second term, the latter itself is strongly modified by the carrier-density-dependent internal loss (formally through T_0^{QD}). Hence T_0 is considerably reduced due to such a loss. This is explicitly shown in Fig. 2.7 depicting the characteristic temperature T_0 against the temperature in the presence and in the absence of carrier-density-dependent internal loss. At room temperature, T_0 is about twice as low as that neglecting such a loss.

With eqs. (2.4), (2.6) and (2.11)–(2.13), the characteristic temperature of a QD laser in the presence of carrier-density-dependent internal loss can be calculated and analyzed versus the parameters of the structure (Fig. 2.8).

The maximum gain g^{max} is a function of the RMS of QD size fluctuations δ and the surface density of QDs N_S ($g^{max} \propto N_S/\delta$). As seen from (2.8), varying g^{max} affects f_n and n and hence the temperature characteristics of a laser. The greater δ or the smaller N_S (i.e., the smaller is g^{max}), the lower is T_0 [Figs. 2.8(a) and (b)]. In the presence of the carrier-density-dependent internal loss, T_0 decreases with increasing δ or decreasing N_S faster than that neglecting such a loss [Figs. 2.8(a) and (b)]. While T_0 in the absence of the carrier-density-dependent internal loss remains nonvanishing (though low) with increasing δ (or decreasing N_S), T_0 in the presence of such a loss turns to zero at the critical value $\delta = \delta^{max}$ (or $N_S = N_S^{min}$).

T_0 reduces with decreasing cavity length L [Fig. 2.8(c)]. T_0 in the absence of the carrier-density-dependent internal loss remains nonvanishing with decreasing L while that in the presence of such a loss turns to zero at $L = L^{min}$.

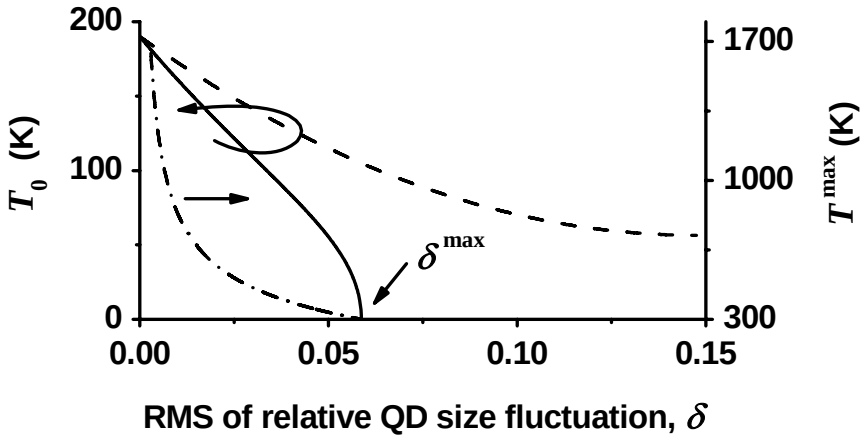
200
100
0
1700
1000
300
T_0 (K)
T^{max} (K)
δ^{max}
0.00
0.05
0.10
0.15
RMS of relative QD size fluctuation, δ

(a)

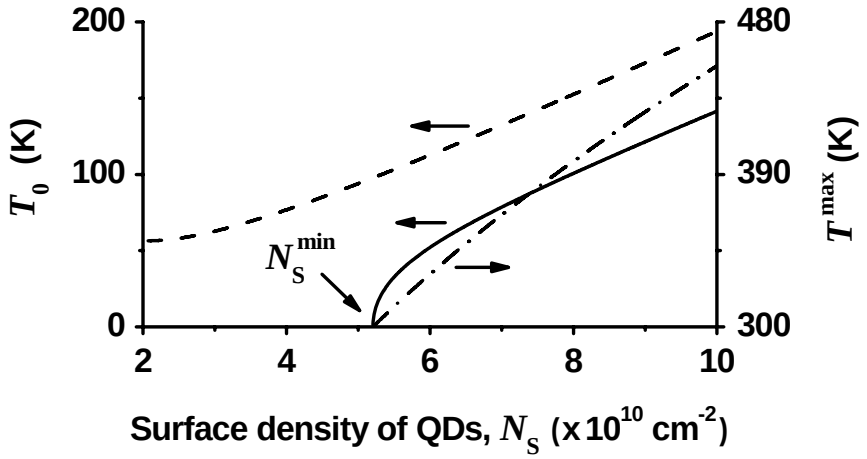
200
100
0
480
390
300
T_0 (K)
T^{max} (K)
N_S^{min}
2
4
6
8
10
Surface density of QDs, N_S (x 10^{10} cm^{-2})

(b)

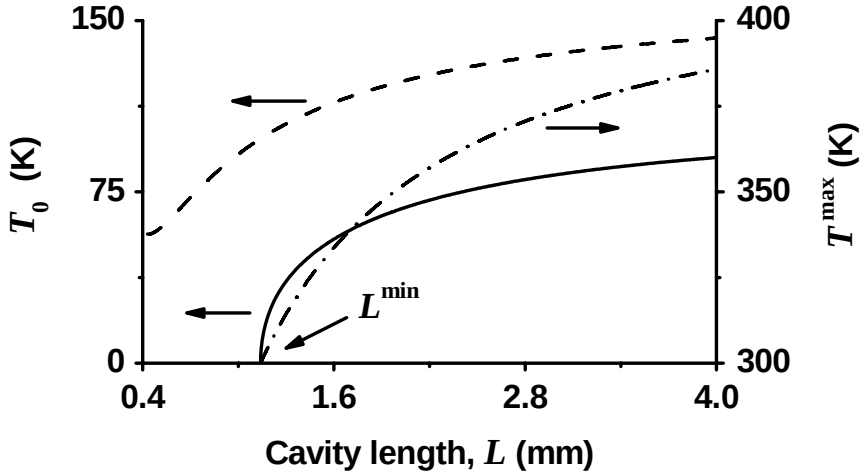
150
75
0
400
350
300
T_0 (K)
T^{max} (K)
L^{min}
0.4
1.6
2.8
4.0
Cavity length, L (mm)

(c)

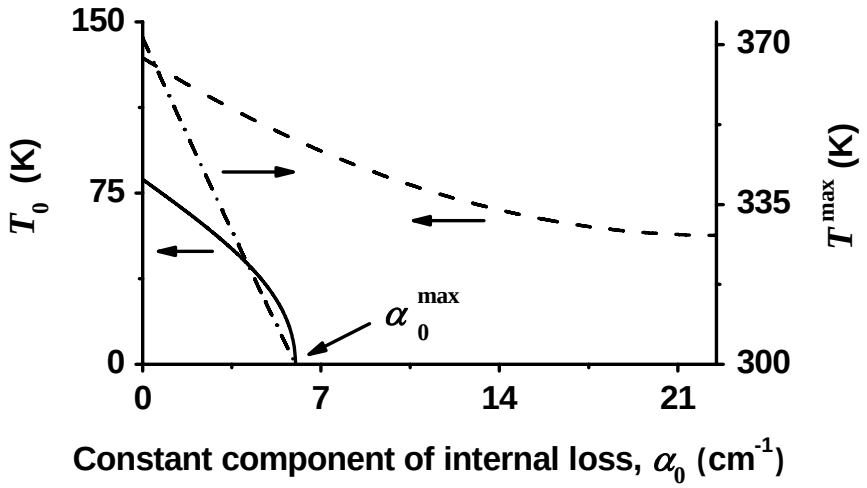

(d)

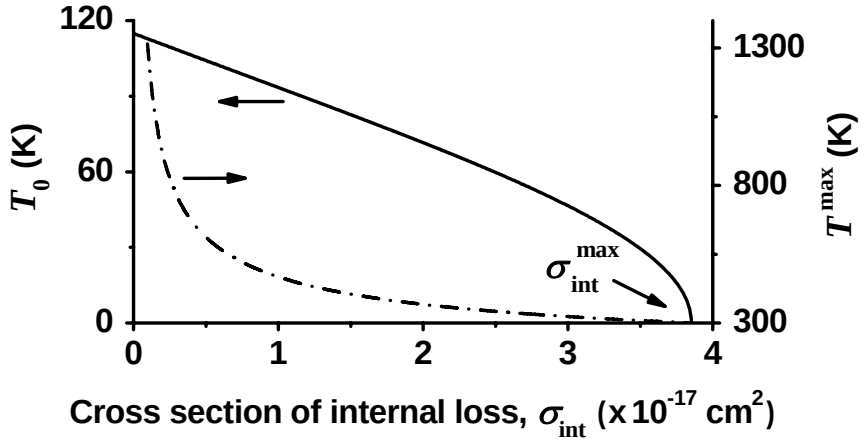

(e)

Fig. 2.8. Characteristic temperature calculated including (solid curve, left axis) and neglecting (dashed curve, left axis) the carrier-density-dependent internal loss, and maximum operating temperature (dash-dotted curve, right axis) against RMS of QD size fluctuations (a), surface density of QDs (b), cavity length (c), constant component of internal loss (d), and cross section of internal loss (e).

Although α_0 and σ_{int} are not easily controllable parameters in a given structure, in order to illustrate their effects on T_0, we also present here the dependence on α_0 and σ_{int} [Figs. 2.8(d) and (e)]. As seen from (2.8), the constant component α_0 of the internal loss does not introduce any

temperature dependence in f_n and acts similarly to the mirror loss β. T_0 decreases with increasing α_0 or σ_{int}; at the critical value $\alpha_0 = \alpha_0^{max}$ or $\sigma_{int} = \sigma_{int}^{max}$, T_0 becomes zero.

As our calculations suggest, the characteristic temperature depends critically on the parameters of the laser structure. At the same time, when the parameters are far from their critical tolerable values, T_0 can be above 100 K, which is in agreement with the experimental data for properly optimized structures (see, e.g., [19–21]).

It can be seen from Fig. 2.8 that, as $\delta \to 0$, $L \to \infty$, $\alpha_0 \to 0$, or $\sigma_{int} \to 0$, the characteristic temperature remains finite. On the contrary, the characteristic temperature goes to infinite with $N_S \to \infty$. These tendencies are discussed in more detail in Appendix II.

Eq. (2.4), where T_0^{QD} and T_0^{OCL} are given by (2.12) and (2.13), respectively, is the general expression for T_0. The asymptotic expressions for T_0 when the parameters are near and far from their critical tolerable values are presented in Appendixes I and II, respectively.

2.4. Critical parameters controlled by the carrier-density-dependent internal loss

2.4.1. Maximum operating temperature

The characteristic temperature falls off profoundly with increasing temperature T (Fig. 2.7). At a certain temperature T^{max}, presenting the maximum operating temperature of the device (T^{max} = 335 K for the specific case considered here), T_0 goes to zero. Hence even in the absence of heating effects, the carrier-density-dependent internal loss itself sets an upper limit for operating temperatures of a QD laser. The point is that, the carrier density in the OCL, n, and hence the internal loss, $\alpha_{int} = \alpha_0 + \sigma_{int} n$, increase continuously with temperature. At the same time, the maximum gain of a laser can not exceed g^{max} [see (2.8)]. For $T > T^{max}$, the lasing condition (2.8) can not be satisfied. The following transcendental equation is derived for T^{max}:

$$\frac{1}{\left(T^{max}\right)^{3/4}} \exp\left(\frac{E_n}{2T^{max}}\right) = \frac{\sqrt{2\left(m_c^{OCL}/2\pi\hbar^2\right)^{3/2}\sigma_{int}}}{\sqrt{2g^{max}} - \sqrt{g^{max} + \beta + \alpha_0}}. \qquad (2.14)$$

$T^{\max}$ is shown versus the structure parameters in Fig. 2.8. The greater δ or the smaller N_S (i.e., the smaller is $g^{\max}$), the lower is $T^{\max}$ [Figs. 2.8(a) and (b)]. As $\delta \to 0$ or $N_S \to \infty$, $g^{\max}$ becomes infinitely high and $T^{\max} \to \infty$ [see eq. (2.14) and Figs. 2.8(a) and (b)].

$T^{\max}$ reduces with decreasing cavity length L [Fig. 2.8(c)]. As $L \to \infty$, i.e., $\beta \to 0$, $T^{\max}$ remains finite [also see eq. (2.14)].

$T^{\max}$ decreases with increasing α_0 or σ_{int}. Like with $g^{\max} \to \infty$, $T^{\max}$ becomes infinitely high when $\sigma_{int} \to 0$ [Fig. 2.8(e) and eq. (2.14)]. This tendency is readily seen also from eq. (2.8) — if $\sigma_{int} \to 0$ (α_{int} becomes temperature-independent: $\alpha_{int} \to \alpha_0$) or $g^{\max} \to \infty$, the solution for f_n exists at any temperature T.

In the presence of the carrier-density-dependent internal loss, the critical tolerable parameters depend on temperature. In Fig. 2.8, room-temperature values of the critical parameters are used. That is why when any of the parameters (δ, N_S, L, α_0, or σ_{int}) approaches its critical value ($\delta^{\max}$, $L^{\min}$, $N_S^{\min}$, $\alpha_0^{\max}$, or $\sigma_{int}^{\max}$, respectively), $T^{\max}$ reduces to 300 K. Beyond the critical tolerable value of any parameter, $T^{\max}$ goes below 300 K, i.e., no room-temperature lasing is possible.

2.4.2. Shallowest potential well depth and smallest tolerable size of a QD

The carrier density n in the OCL [eq. (2.6)] is also strongly controlled by the excitation energy E_n from a QD. The smaller E_n, the easier for carriers to escape to the OCL and hence the higher are n and α_{int}. Just as $T^{\max}$ exists, there is a lowest excitation energy, $E_n^{\min}$, below which no lasing is attainable in a structure. From (2.14), an explicit expression is apparent for $E_n^{\min}$,

$$E_n^{\min} = T \ln\left[\frac{\sigma_{int} N_c^{OCL}}{\left(\sqrt{2g^{\max}} - \sqrt{g^{\max} + \beta + \alpha_0}\right)^2}\right]. \tag{2.15}$$

For $E_n < E_n^{\min}$, the thermal escapes from QDs to the OCL will be so intensive that the population inversion required for the lasing can not be attained.

Since E_n decreases with reducing QD size [E_n is the separation between the quantized energy level and the top of the well — see the inset in Fig. 2.9(a)], there also exists the smallest

tolerable QD size $a^{\min}$. It has been known (see, e.g., [22]) that, in contrast to one-dimensional symmetrical potential well (which supports the quantized energy level no matter how thin it is), there is a smallest size of a three-dimensional (even symmetrical) well (QD), beyond which no bound state can exist. As seen from the present analysis, a more strict condition should be satisfied to attain lasing in the presence of the carrier-density-dependent internal loss. Just having a confined energy level in a QD is not sufficient — the level should be so deeply localized that the carrier density in the OCL and the internal loss are low enough for holding the lasing condition (2.8).

Figure 2.9 shows the minimum tolerable excitation energy $E_n^{\min}$ as a function of the structure parameters. As also readily seen from eq. (2.15), $E_n^{\min}$ decreases with decreasing RMS of relative QD size fluctuations δ [Fig. 2.9(a)], increasing surface density of QDs N_S [Fig. 2.9(b)], increasing cavity length L [Fig. 2.9(c)], decreasing constant component of internal loss α_0 [Fig. 2.9(d)], or reducing cross section of internal loss σ_{int} [Fig. 2.9(e)]. At certain values of $g^{\max}$ (i.e., certain values of δ or N_S, since $g^{\max} \propto N_S/\delta$ — see eq. (41) in [7]) or σ_{int} given by

$$\left(g^{\max}\right)^* = \left(\sqrt{2\sigma_{int} N_c^{OCL}} + \sqrt{\sigma_{int} N_c^{OCL} + \beta + \alpha_0}\right)^2, \tag{2.16}$$

$$\sigma_{int}^* = \frac{\left(\sqrt{2g^{\max}} - \sqrt{g^{\max} + \beta + \alpha_0}\right)^2}{N_c^{OCL}}, \tag{2.17}$$

the minimum tolerable excitation energy turns to zero, $E_n^{\min} = 0$. On further increasing $g^{\max}$ (i.e., decreasing δ or increasing N_S) or further decreasing σ_{int}, eq. (2.15) would formally give negative $E_n^{\min}$. Hence, for $g^{\max} \ge \left(g^{\max}\right)^*$ (i.e., $\delta \le \delta^*$ or $N_S \ge N_S^*$) or $\sigma_{int} \le \sigma_{int}^*$, the restriction placed by the carrier-density-dependent internal loss on the shallowest potential well depth or the smallest QD size is removed — the minimum size is solely determined by the condition of existence of a bound state. For a specific structure considered here, $\left(g^{\max}\right)^* = 74.64\ \text{cm}^{-1}$ (i.e., $\delta^* = 0.02$ or $N_S^* = 1.54\times10^{11}\ \text{cm}^{-2}$), and $\sigma_{int}^* = 0.57\times10^{-17}\ \text{cm}^2$.

Since $E_n^{\min}$ depends on the structure parameters, so does $a^{\min}$. The smaller β (the longer L), α_0 or δ, or the larger N_S, the smaller is $a^{\min}$.

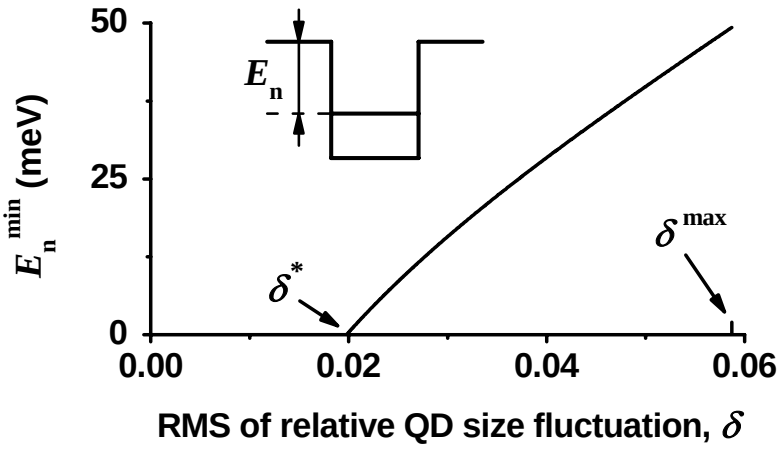
50
25
0
0.00
0.02
0.04
0.06
E_n^{min} (meV)
E_n
δ^*
δ^{max}
RMS of relative QD size fluctuation, δ

(a)

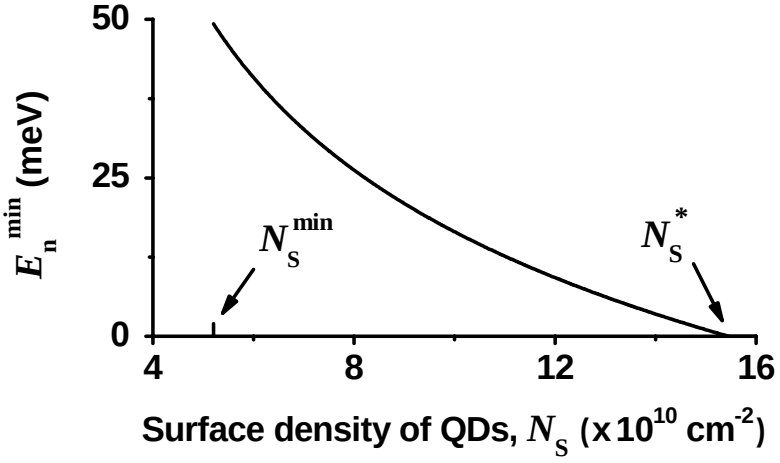
50
25
0
4
8
12
16
E_n^{min} (meV)
N_S^{min}
N_S^*
Surface density of QDs, N_S (x10^{10} cm^{-2})

(b)

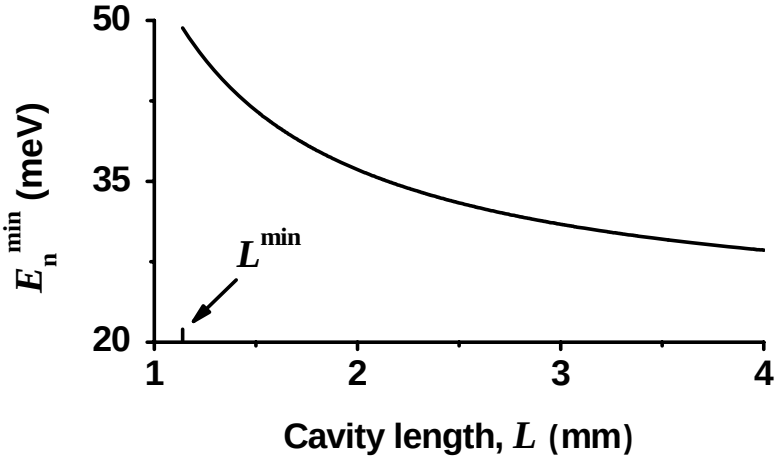
50
35
20
1
2
3
4
E_n^{min} (meV)
L^{min}
Cavity length, L (mm)

(c)

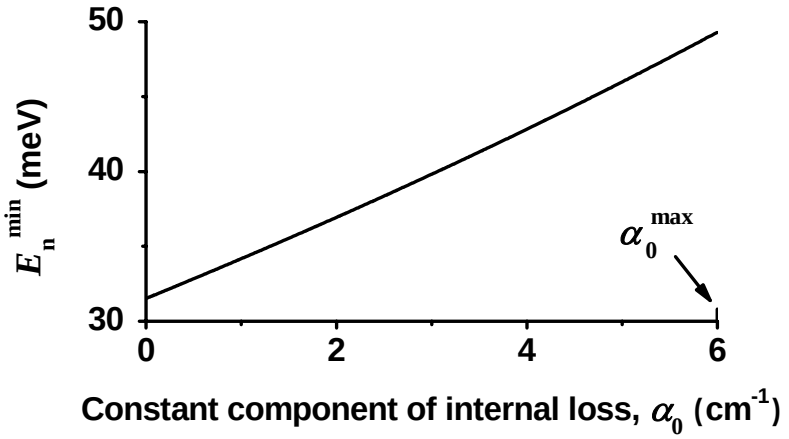

(d)

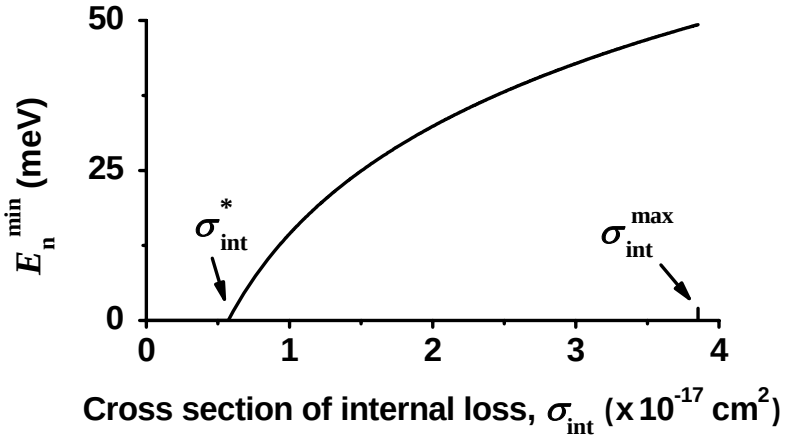

(e)

Fig. 2.9. Minimum tolerable excitation energy from a QD against RMS of QD size fluctuations (a), surface density of QDs (b), cavity length (c), constant component of internal loss (d), and cross section of internal loss (e). The inset in (a) shows schematically the potential well of a QD and the excitation energy E_n.

As shown previously [5, 18, 23] there exist the critical tolerable values of the parameters of a QD structure beyond which no lasing is attainable. These critical quantities are the maximum RMS of QD-size fluctuations δ^{max}, the minimum surface density of QDs N_S^{min}, the minimum cavity length L^{min}, and the maximum cross-section of internal loss σ_{int}^{max}. As shown here, there

are three more critical parameters ($T^{\max}$, $E_{\mathrm{n}}^{\min}$, and $a^{\min}$) in the presence of the carrier-density-dependent internal loss.

2.5. Conclusion

A detailed theoretical analysis has been carried out on the temperature dependence of the threshold current density of a semiconductor QD laser in the presence of the carrier-density-dependent internal optical loss in the waveguide (OCL). In the presence of such a loss, the confined-carrier level occupancy in QDs is coupled to the free-carrier density in the OCL by the threshold condition. Due to this coupling, the free-carrier density is increased and more temperature-sensitive, and also the confined-carrier level occupancy becomes temperature-dependent. As a result, the characteristic temperature of a laser is considerably reduced; at room temperature, for a specific structure considered in this chaper, T_0 is about twice as low as that neglecting the internal loss. Carrier-density-dependent internal loss also sets an upper limit for the operating temperatures of a QD laser and constrains the shallowest potential well depth and the smallest tolerable size of a QD at which the lasing can be attained. The dependences of the characteristic temperature, maximum operating temperature, and shallowest potential well depth on the parameters of the structure are obtained. At the maximum operating temperature or when any parameter of the structure is equal to its critical tolerable value, the characteristic temperature reduces to zero.

Appendix I

Characteristic temperature near the critical point

Near the critical point [when any of the parameters of the structure is close to its critical tolerable value, or the temperature is close to $T^{\max}$ (which will be presented and discussed later)], the denominator in eq. (2.12) tends to zero and hence $1/T_0^{\mathrm{QD}}$ increases infinitely, i.e., $T_0^{\mathrm{QD}} \to 0$. Hence the first two terms in the right-hand side of (2.13) can be neglected compared to the last term, yielding

$$\frac{1}{T_0^{\mathrm{OCL}}} \approx \frac{1}{1-f_{\mathrm{n}}} \frac{1}{T_0^{\mathrm{QD}}}. \tag{A1}$$

Putting (A1) into (2.4) gives

$$T_0 \approx \frac{1}{1+\dfrac{j_{\mathrm{OCL}}}{j_{\mathrm{QD}}+j_{\mathrm{OCL}}} \dfrac{f_{\mathrm{n}}}{1-f_{\mathrm{n}}}} T_0^{\mathrm{QD}} \to 0. \tag{A2}$$

T_0^{QD} and hence T_0 go to zero as the square root of the parameter deviation from its critical tolerable value. Thus, for example, when $\delta \to \delta^{\max}$, we have

$$T_0 \approx \frac{1+\dfrac{N_{\mathrm{S}}/\tau_{\mathrm{QD}}}{bBn_1^2} \dfrac{\sigma_{\mathrm{int}} n_1}{2g^{\max}}}{1+\dfrac{N_{\mathrm{S}}/\tau_{\mathrm{QD}}}{bBn_1^2} \left(\dfrac{\sigma_{\mathrm{int}} n_1}{2g^{\max}} \right)^{\frac{3}{2}}} \frac{1}{\dfrac{3}{2}\dfrac{1}{T}+\dfrac{E_{\mathrm{n}}}{T^2}} \left[\frac{1}{2} \left(1+\frac{\beta+\alpha_0}{\sigma_{\mathrm{int}} n_1} \right) \right]^{\frac{1}{4}} \left(1-\frac{\delta}{\delta^{\max}} \right)^{\frac{1}{2}}. \tag{A3}$$

The expressions for T_0 when other parameters are close to the critical values are similar to the above equation and not listed here. The square root dependence of T_0 on one parameter near the critical value can be seen from Fig. 2.8.

The general tendency is that the further the parameter from its critical tolerable value, the less pronounced is the effect of the internal loss, i.e., the closer T_0 to its value in the absence of the internal loss.

Appendix II

Characteristic temperature far from the critical point

As $\alpha_0 \to 0$ or $\beta \to 0$ ($L \to \infty$), T_0^{QD} remains finite and can not be neglected either in (2.13) or (2.4).

As $\sigma_{int} \to 0$ or $\delta \to 0$, T_0^{QD} increases as the reciprocal of σ_{int} or δ, correspondingly, and can be neglected both in (2.13) and (2.4). For the limiting case of ideally uniform QDs ($\delta = 0$), the expression for T_0 is

$$T_0 \approx \left(1 + \frac{1}{4}\frac{N_S/\tau_{QD}}{bBn_1^2}\right)\left(\frac{3}{2}\frac{1}{T} + \frac{2E_n}{T^2}\right)^{-1}. \qquad \text{(A4)}$$

None of the quantities β, α_0, or σ_{int} characterizing the mirror and internal loss enter into (A4), which is easily understood — the maximum gain $g^{max} = \infty$ and $f_n = 1/2$ if $\delta = 0$, no matter what are the above quantities [see eq. (2.8)].

At $N_S \to \infty$, T_0^{QD} increases proportionally to N_S. The last term in the right-hand side of (2.13) containing $1/T_0^{QD}$ can be neglected. The first term in the right-hand side of (2.4) containing $1/T_0^{QD}$, which is of the order of $1/N_S$, should nevertheless be kept; the point is that the second term there contains the small quantity $j_{OCL}/j_{th} \approx j_{OCL}/j_{QD}$ of the same order $1/N_S$. The following equation is obtained for T_0:

$$\frac{1}{T_0} \approx \frac{4\sigma_{int}n_1}{2g^{max}}\left(\frac{3}{2}\frac{1}{T} + \frac{E_n}{T^2}\right) + \frac{4bBn_1^2}{N_S/\tau_{QD}}\left(\frac{3}{2}\frac{1}{T} + \frac{2E_n}{T^2}\right). \qquad \text{(A5)}$$

Note that since $g^{max} \propto N_S$, T_0 is proportional to N_S.

REFERENCES [*)]

[A1] L. Jiang and L.V. Asryan, "Internal-loss-limited maximum operating temperature and characteristic temperature of quantum dot laser," *Laser Phys. Lett.*, vol. 4, no. 4, pp. 265–269, Apr. 2007.

[A2] L. Jiang and L.V. Asryan, "Maximum operating temperature and characteristic temperature of a quantum dot laser in the presence of internal loss," *Proceedings of SPIE's International Symposium Photonics West*. San Jose, California, Jan. 20–25 2007. vol. 6481, pp. 648107-1–648107-6.

[A3] L. Jiang and L. V. Asryan, "Maximum operating temperature of quantum dot laser," *Abstracts of International Symposium and Spring School "Nano and Giga Challenges in Electronics and Photonics"*. Phoenix, Arizona, Mar. 12–16, 2007. p. 37.

[1] J. I. Pankove, "Temperature dependence of emission efficiency and lasing threshold in laser diodes," *IEEE J. Quantum Electron.*, vol. 4, no. 4, pp. 119–122, Apr. 1968.

[2] Y. Arakawa and H. Sakaki, "Multidimensional quantum well laser and temperature dependence of its threshold current," *Appl. Phys. Lett.*, vol. 40, no. 11, pp. 939–941, June 1982.

[3] K. Vahala, Y. Arakawa, and A. Yariv, "Reduction of the field spectrum linewidth of a multiple quantum-well laser in a high magnetic-field - spectral properties of quantum dot lasers," *Appl. Phys. Lett.*, vol. 50, no. 7, pp. 365–367, Feb. 1987.

[4] M. V. Maximov, L. V. Asryan, Yu. M. Shernyakov, A. F. Tsatsul'nikov, I. N. Kaiander, V. V. Nikolaev, A. R. Kovsh, S. S. Mikhrin, V. M. Ustinov, A. E. Zhukov, Zh. I. Alferov, N. N. Ledenstov, and D. Bimberg, "Gain and threshold characteristics of long wavelength lasers based on InAs/GaAs quantum dots formed by activated alloy phase separation," *IEEE J. Quantum Electron.*, vol. 37, no. 5, pp. 676–683, May 2001.

[*)] "A" in the reference number indicates the publications of the author of this dissertation.

[5] L. V. Asryan and R. A. Suris, "Inhomogeneous line broadening and the threshold current density of a semiconductor quantum dot laser," *Semicond. Sci. Technol.*, vol. 11, no. 4, pp. 554–567, Apr. 1996.

[6] L. V. Asryan and R. A. Suris, "Temperature dependence of the threshold current density of a quantum dot laser," *IEEE J. Quantum Electron.*, vol. 34, no. 5, pp. 841–850, May 1998.

[7] L. V. Asryan and R. A. Suris, "Charge neutrality violation in quantum dot lasers," *IEEE J. Select. Topics Quantum Electron.*, vol. 3, no. 2, pp. 148–157, Apr. 1997.

[8] M. Asada, A. R. Adams, K. E. Stubkjaer, Y. Suematsu, Y. Itaya, and S. Arai, "The temperature dependence of the threshold current of GaInAsP-InP DH lasers," *IEEE J. Quantum Electron.*, vol. QE-17, no. 5, pp. 611–619, May 1981.

[9] C. H. Henry, R. A. Logan, F. R. Merritt, and J. P. Luongo, "The effect of intervalence band absorption on the thermal-behavior of InGaAsP lasers," *IEEE J. Quantum Electron.*, vol. QE-19, no. 6, pp. 947–952, June 1983.

[10] M. Asada, A. Kameyama, and Y. Suematsu, "Gain and intervalence band absorption in quantum-well lasers," *IEEE J. Quantum Electron.*, vol. QE-20, no. 7, pp. 745–753, July 1984.

[11] D. Z. Garbuzov, A. V. Ovchinnikov, N. A. Pikhtin, Z. N. Sokolova, I. S. Tarasov, and V. B. Khalfin, "Experimental and theoretical investigations of singularities of the threshold and power characteristics of InGaAsP/InP separate-confinement double-heterostructure lasers (λ = 1.3 μm)," *Sov. Phys. Semicond.*, vol. 25, no. 5, pp. 560–564, May 1991.

[12] P. S. Zory Jr., Ed., *Quantum Well Lasers*. Boston, MA: Academic, 1993, p. 504.

[13] L. A. Coldren and S. W. Corzine, *Diode Lasers and Photonic Integrated Circuits*. New York: Wiley, 1995, p. 594.

[14] D. A. Ackerman, G. E. Shtengel, M. S. Hybertsen, P. A. Morton, R. F. Kazarinov, T. Tanbun-Ek, and R. A. Logan, "Analysis of gain in determining T_0 in 1.3 μm semiconductor lasers," *IEEE J. Select. Topics Quantum Electron.*, vol. 1, no. 2, pp. 250–263, June 1995.

[15] T. Higashi, T. Yamamoto, S. Ogita, and M. Kobayashi, "Experimental analysis of characteristic temperature in quantum-well semiconductor lasers," *IEEE J. Select. Topics Quantum Electron.*, vol. 3, no. 2, pp. 513–521, Apr. 1997.

[16] N. A. Gun'ko, V. B. Khalfin, Z. N. Sokolova, and G. G. Zegrya, "Optical loss in InAs-based long-wavelength lasers," *J. Appl. Phys.*, vol. 84, no. 1, pp. 547–554, July 1998.

[17] N.-H. Kim, J.-H. Park, L. J. Mawst, T. F. Kuech, and M. Kanskar, "Temperature sensitivity of InGaAs quantum-dot lasers grown by MOCVD," *IEEE Photon. Technol. Lett.*, vol. 18, no. 8, pp. 989-991, Apr. 2006.

[18] L. V. Asryan and S. Luryi, "Effect of internal optical loss on threshold characteristics of semiconductor lasers with a quantum-confined active region," *IEEE J. Quantum Electron.*, vol. 40, no. 7, pp. 833–843, July 2004.

[19] O. B. Shchekin and D. G. Deppe, "1.3 μm InAs quantum dot laser with T_0 = 161 K from 0 to 80 °C," *Appl. Phys. Lett.*, vol. 80, no. 18, pp. 3277–3279, May 2002.

[20] A. R. Kovsh, N. A. Maleev, A. E. Zhukov, S. S. Mikhrin, A. P. Vasil'ev, Yu. M. Shernyakov, M. V. Maximov, D. A. Livshits, V. M. Ustinov, Zh. I. Alferov, N. N. Ledentsov, and D. Bimberg, "InAs/InGaAs/InAs quantum dot lasers of 1.3 μm range with high (88%) differential efficiency," *Electron. Lett.*, vol. 38, no. 19, pp. 1104–1106, Sep. 2002.

[21] V. Tokranov, M. Yakimov, A. Katsnelson, M. Lamberti, and S. Oktyabrsky, "Enhanced thermal stability of laser diodes with shape-engineered quantum dot medium," *Appl. Phys. Lett.*, vol. 83, no. 5, pp. 833–835, Aug. 2003.

[22] K. J. Vahala, "Quantum box fabrication tolerance and size limits in semiconductors and their effect on optical gain," *IEEE J. Quantum Electron.*, vol. 24, no. 3, pp. 523–530, Mar. 1988.

[23] L. V. Asryan and R. A. Suris, "Longitudinal spatial hole burning in a quantum-dot laser," *IEEE J. Quantum Electron.*, vol. 36, no. 10, pp. 1151–1160, Oct. 2000.

Chapter 3

Excited States in Quantum Dots and the Light-Current Curve of a Laser

Summary

We develop a comprehensive theory of the output power of a quantum dot (QD) laser in the presence of excited states in QDs. The carrier capture from the three-dimensional reservoir (optical confinement layer – OCL) into the QD ground-state and escape from the ground-state to the OCL are assumed to occur via the QD excited-state. Such a two-step capture places a fundamental limitation on ground-state lasing—the output power saturates at high injection currents. The saturation power is controlled by the transition time between the excited- and ground-state in a QD. The longest, cut-off transition time exists, beyond which no ground-state lasing is possible. The following characteristics are analyzed versus the injection current density and the transition time: occupancies of the ground- and excited-state, free carrier density in the OCL, threshold current density, number of stimulated photons emitted, output power, internal and external differential quantum efficiencies.

3.1. Introduction

Operating characteristics of quantum dot (QD) lasers are controlled by a number of factors. Among them are excited states, which are present in QDs in addition to the ground-state. In an ideal situation, there should be one electron and one hole energy level in a QD. If the size of QDs or the bandgap difference between the materials of the optical confinement layer (OCL) and QDs is sufficiently large, excited states can appear in QDs (see, e.g., [1, 2] and the references in [2]). There can be more than one excited states in each of the conduction and valence bands (see, e.g., [3, 4]).

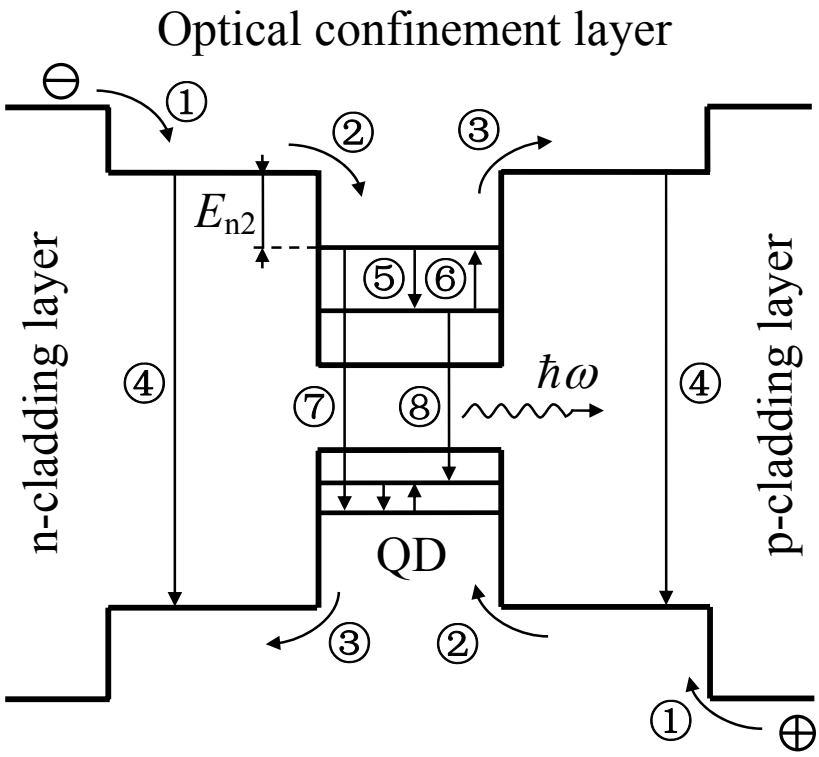

Fig. 3.1. Energy band diagram of a QD laser (the layers are not drawn to scale). The main processes (shown by arrows) are as follows: 1) carrier injection from the cladding layers into the OCL, 2) carrier capture from the OCL into the QD excited state, 3) carrier escape from the QD excited state to the OCL, 4) spontaneous radiative recombination in the OCL, 5) carrier capture from the excited- to ground-state, 6) carrier escape from the ground- to excited-state, 7) spontaneous and stimulated radiative recombinations of an excited-state electron with an excited-state hole in a QD, and 8) spontaneous and stimulated radiative recombinations of a ground-state electron with a ground-state hole in a QD.

Excited states can affect the capture of carriers from the OCL (Fig. 3.1) into the lasing ground state. Besides, carriers can recombine through the excited states rather than contribute to ground-state lasing.

In [5, 6], Asryan *et al* examined the effect of excited states on the gain and the threshold current density of a QD laser. In this chapter, a comprehensive theory of the output optical power

of a QD laser is developed in the presence of excited states [A1–A3] [*)].

It should be emphasized that there have been theoretical works on the power characteristics of a QD laser in the presence of excited states (see for example [7–11]), which were based on several assumptions. First, the bulk barrier (waveguide) layers and the processes therein were not considered, which means the carriers were assumed to be directly injected either into the wetting layer or QD excited states. Second, in the works, which included the wetting layer, the recombination therein was assumed to be monomolecular (see below). And third, the capture from the wetting layer into QDs was described in terms of a time constant, which did not depend on the surface density of QDs. The output powers of the ground- and excited-state lasing were calculated as linearly increasing functions of the pump current. In [12], the carrier capture from the reservoir surrounding QDs (wetting layer or OCL) into the QD excited states was assumed to be faster than the relaxation from the excited- to ground-state and hence was not considered. Other processes (recombination in the reservoir, thermal escape of carriers from QDs to the reservoir) were also not considered and thus the reservoir was not included into the model. In [7] and [8], the wetting layer was treated as a discrete level. In [9], the effect of homogeneous broadening on the ground- and excited-state lasing was discussed. In [10] and [11], two different models of carrier capture into QDs were considered again revealing linear increase in the output power with the pump current.

Indirect (noninstantaneous) carrier injection into QDs is an essential component of our model and it describes the actual situation for QD lasers. Except for the tunneling-injection QD laser [13, 14], the carriers are indirectly supplied to QDs in all the types of QD lasers. We consider the carrier capture from the OCL into QDs self-consistently using the corresponding rate and cross-section, rather than a constant capture time into a single QD, which, strictly speaking, can not be introduced adequately [15]. As discussed earlier in [15], the time of capture can be formally introduced only for the entire ensemble of QDs, which thus depends on the surface density of QDs and is simply related to the capture cross-section (see eq. (42) in [15]).

Another important feature of our model is a superlinear (in the carrier density n) recombination rate outside QDs: bimolecular spontaneous radiative recombination in the OCL is included here, which rate is quadratic in n; Auger recombination (which rate is cubic in n) can

---

[*)] "A" in the reference number indicates the publications of the author of this dissertation.

also be easily included into our model. It is this superlinearity of the recombination rate, which, combined with the noninstantaneous capture of carriers from the OCL into QDs, strongly couples the free-carrier density outside QDs with the number of stimulated photons (and hence the output power) and causes the saturation of the output power of the ground-state lasing with increasing injection current (see below).

The assumption of monomolecular (linear in n) recombination rate outside QDs, i.e., the use of a constant time of the spontaneous recombination, which does not depend on n, is unrealistic for both the OCL and wetting layer. Bimolecular (quadratic in n) rate should be used for the recombination outside QDs. With increasing injection current, i.e., with increasing n, the Auger recombination may become a dominant mechanism with a rate cubic in n. Monomolecular recombination outside QDs can not cause the saturation of the output power of ground-state lasing – an important derivation from our model. It was the assumption of monomolecular recombination in the wetting layer that lead to the linear increase of the output power with current in the previous works.

3.2. Main assumptions and model used

Continuous-wave operation is considered here and hence the steady-state rate equations are used to calculate the output optical power. To mainly focus on the effect of excited-states, several assumptions are made. 1) The carrier capture into and escape from the QD ground-state occur via the excited-state (Fig. 3.1). For the case of direct capture from the OCL into single-state QDs, the optical power was calculated in [15]. 2) Heating effects are not considered. 3) The free-carrier distribution in the transverse direction in the OCL is uniform. 4) The electron and hole densities are equal in the OCL, and the occupancies of the electron and hole ground-states (excited-states) are equal in a QD (charge neutrality assumption). 5) In view of a large volume of the cavity of edge-emitting lasers considered here, the fraction of spontaneous emission in the lasing mode is ignored. 6) To separate the effect of excited-state-mediated capture on ground-state lasing, the internal optical loss is ignored in this chapter.

3.3. Rate equations and main notations

The steady-state rate equations for carriers confined in the ground- and excited-states of a

QD, free carriers in the OCL, and photons are $\partial(f_{n1}, f_{n2}, n, N)/\partial t = 0$. In an explicit form, these equations are

$$\frac{f_{n2}(1-f_{n1})}{\tau_{21}} - \frac{f_{n1}(1-f_{n2})}{\tau_{21}} - \frac{f_{n1}^2}{\tau_{QD1}} - \frac{c}{\sqrt{\in_{g1}}}\frac{g_1^{max}}{N_S S}(2f_{n1}-1)N_1 = 0, \tag{3.1}$$

$$\sigma_{n2} v_n n(1-f_{n2}) - \sigma_{n2} v_n n_2 f_{n2} + \frac{f_{n1}(1-f_{n2})}{\tau_{21}} - \frac{f_{n2}(1-f_{n1})}{\tau_{21}} - \frac{f_{n2}^2}{\tau_{QD2}} = 0, \tag{3.2}$$

$$\sigma_{n2} v_n n_2 \frac{N_S}{b} f_{n2} - \sigma_{n2} v_n n \frac{N_S}{b}(1-f_{n2}) - Bn^2 + \frac{j}{eb} = 0, \tag{3.3}$$

$$\frac{c}{\sqrt{\in_{g1}}} g_1^{max}(2f_{n1}-1)N_1 - \frac{c}{\sqrt{\in_{g1}}}\beta_1 N_1 = 0. \tag{3.4}$$

The physical quantities and terms entering (3.1)–(3.4) are presented in Tables 3.1 and 3.2, respectively.

In (3.1) and (3.2), the downward and upward transition rates in a QD can be combined to yield $(f_{n2} - f_{n1})/\tau_{21}$. Thus eq. (3.1) can be written as

$$\frac{f_{n2} - f_{n1}}{\tau_{21}} = \frac{f_{n1}^2}{\tau_{QD1}} + \frac{c}{\sqrt{\in_{g1}}}\frac{g_1^{max}}{N_S S}(2f_{n1}-1)N_1, \tag{3.5}$$

which is simply the condition that the net downward transition rate from the excited- to ground-state (the left-hand side) goes into spontaneous and stimulated recombinations via the ground-state (the first and second terms in the right-hand side).

3.4. Solutions of rate equations: level occupancies in a QD, free-carrier density in the OCL, photon number, and output power

Above the lasing threshold (when $N_1 \neq 0$), it follows immediately from (3.4) that the ground-state occupancy pins at its threshold value (Fig. 3.2),

$$f_{n1} = \frac{1}{2}\left(1 + \frac{\beta_1}{g_1^{max}}\right), \tag{3.6}$$

Table 3.1. Physical quantities in eqs. (3.1)–(3.4)

f_{n1}	Occupancy of the ground state
f_{n2}	Occupancy of the excited state
τ_{QD1}	Ground-state spontaneous radiative lifetime in a QD
τ_{QD2}	Excited-state spontaneous radiative lifetime in a QD
τ_{21}	Transition time between the excited- and ground-state
c	Light velocity in vacuum
$\sqrt{\epsilon_{g1}}$	Group index of the dispersive OCL material at the energy of the ground-state transition
N_S	Surface density of QDs
$S=WL$	QD layer area (the cross-section of the junction)
W	QD layer width (the lateral size of the device)
L	QD layer length (the cavity length)
g_1^{max}	Maximum (saturation) value of the modal gain for the ground-state transitions
N_1	Number of photons in the ground-state lasing mode
σ_{n2}	Cross-section of carrier capture from the OCL into the QD excited-state
v_n	Free carrier thermal velocity in the OCL
N	Free carrier density in the OCL
b	OCL thickness
B	Radiative constant for the OCL
j	Injection current density
$\beta_1 = (1/L)\ln(1/R_1)$	Mirror loss coefficient for the ground-state lasing
R_1	Facet reflectivity at the energy of the ground-state transition
$n_2 = N_c^{OCL}\exp(-E_{n2}/T)$	Describes thermal escape from the QD excited state to the OCL
$N_c^{OCL} = 2\left(m_c^{OCL}T/2\pi\hbar^2\right)^{3/2}$	Effective density of states in the OCL
E_{n2}	Carrier excitation energy from the QD excited-state to the OCL
m_c^{OCL}	Effective mass in the OCL
T	Temperature measured in units of energy
$\hbar$	Plank's constant

Table 3.2. Rates of different processes in eqs. (3.1)–(3.4)

$\frac{f_{n2}(1-f_{n1})}{\tau_{21}}$	Downward transition in a QD: capture from the excited- to ground-state
$\frac{f_{n1}(1-f_{n2})}{\tau_{21}}$	Upward transition in a QD: escape from the ground- to excited-state
$\frac{f_{n1}^2}{\tau_{QD1}}$	Spontaneous radiative recombination via the ground state of a QD
$\frac{c}{\sqrt{\epsilon_{g1}}}\frac{g_1^{max}}{N_S S}(2f_{n1}-1)N_1$	Stimulated radiative recombination via the ground state of a QD
$\sigma_{n2} v_n n(1-f_{n2})$	Capture from the OCL to the excited state of a QD
$\sigma_{n2} v_n n_2 f_{n2}$	Escape from the excited state of a QD to the OCL
$\frac{f_{n2}^2}{\tau_{QD2}}$	Spontaneous radiative recombination via the excited state of a QD
Bn^2	Spontaneous radiative recombination in the OCL
$\frac{j}{eb}$	Carrier injection into the OCL
$\frac{c}{\sqrt{\epsilon_{g1}}} g_1^{max}(2f_{n1}-1)N_1$	Stimulated generation of photons in the active region
$\frac{c}{\sqrt{\epsilon_{g1}}}\beta_1 N_1$	Mirror loss of photons

From (3.1), the excited-state occupancy can be expressed as a linear function of the photon number N_1,

$$f_{n2} = f_{n1} + \tau_{21}\left[\frac{f_{n1}^2}{\tau_{QD1}} + \frac{c}{\sqrt{\varepsilon_{g1}}}\frac{g_1^{max}}{N_S S}(2f_{n1}-1)N_1\right] = f_{n1} + \tau_{21}\left[\frac{f_{n1}^2}{\tau_{QD1}} + \frac{c}{\sqrt{\varepsilon_{g1}}}\frac{\beta_1}{N_S S}N_1\right], \quad (3.7)$$

From (3.2), the free carrier density in the OCL is

$$n = n_2\frac{f_{n2}}{1-f_{n2}} + \frac{1}{\sigma_{n2} v_n}\frac{1}{1-f_{n2}}\left(\frac{f_{n2}-f_{n1}}{\tau_{21}} + \frac{f_{n2}^2}{\tau_{QD2}}\right), \quad (3.8)$$

or, taking into account (3.5) and (3.6), as

$$n = n_2 \frac{f_{n2}}{1-f_{n2}} + \frac{1}{\sigma_{n2} v_n} \frac{1}{1-f_{n2}} \left(\frac{f_{n1}^2}{\tau_{QD1}} + \frac{f_{n2}^2}{\tau_{QD2}} + \frac{c}{\sqrt{\epsilon_{g1}}} \frac{\beta_1}{N_S S} N_1 \right). \tag{3.9}$$

From (3.2) and (3.3), the injection current density is

$$j = ebBn^2 + \frac{eN_S}{\tau_{21}} \left(f_{n2} - f_{n1} \right) + \frac{eN_S}{\tau_{QD2}} f_{n2}^2 , \tag{3.10}$$

or, taking into account (3.5) and (3.6),

$$j = ebBn^2 + \frac{eN_S}{\tau_{QD1}} f_{n1}^2 + \frac{eN_S}{\tau_{QD2}} f_{n2}^2 + \frac{e}{S} \frac{c}{\sqrt{\epsilon_{g1}}} \beta_1 N_1 . \tag{3.11}$$

Eq. (3.11) is the condition that the injection current goes into spontaneous radiative recombination (in the OCL and via the QD ground- and excited-states), and stimulated radiative recombination (via the QD ground state). The corresponding current densities are the first, second, third and last terms in the right-hand side of eq. (3.11), respectively.

In eqs. (3.9) and (3.11), f_{n2} is a function of N_1 given by (3.7). Inserting f_{n2} and n given by (3.7) and (3.9) into (3.11) yields the expression for the injection current density as an explicit function of the photon number N_1. Our task is to calculate the inverse function, i.e., N_1 versus j, and then f_{n2}, n, and the output power versus j. This can be done and a closed form expression can be obtained from the solution of a quartic equation. This expression is however rather cumbersome and, for this reason, we use a different procedure to plot the functional dependences here. As mentioned above, all the quantities (including j) are explicit functions of N_1. Hence, we first consider N_1 as a variable, change it throughout the entire range of its possible values (from 0 to N_1^{max} – see below), and calculate f_{n2}, n, and j versus N_1. The dependence of N_1 on j is then simply obtained by exchanging the X and Y axes. Then the output power [eq. (3.12)] is easily calculated versus the injection current density (light-current characteristic – LCC). The dependences of f_{n2} and n on j are easily obtained from those on N_1 by converting the X-axis for N_1 into the X-axis for $j(N_1)$.

Figs. 3.2, 3.3, and 3.4 show f_{n2}, n and N_1 versus the excess of the injection current density j over the threshold current density j_{th1} for the ground-state lasing [see (3.18) for j_{th1}].

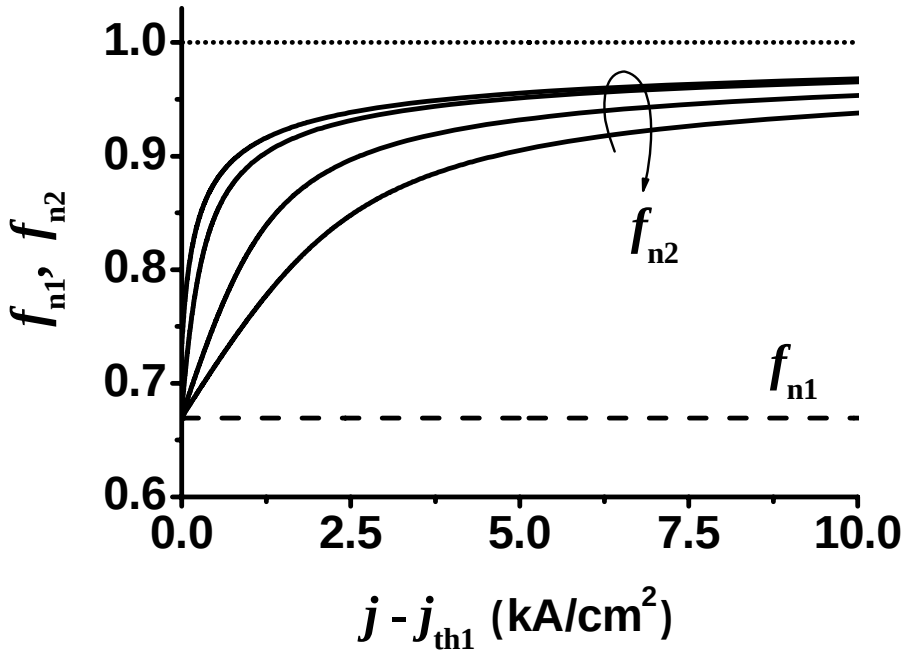

Fig. 3.2. Ground- (horizontal dashed line) and excited-state (solid curves) occupancies against excess injection current density. Horizontal dotted line indicates the maximum possible value (unity) for the level occupancies. GaInAsP/InP heterostructure lasing near 1.55 μm is considered here for illustration. The parameters, which apply to Figs. 2–7, are as follows: the root mean square of QD size fluctuations $\delta = 0.05$ (Gaussian distribution is assumed); $N_S = 6.11 \times 10^{10}$ cm^{-2}, $\tau_{QD1} = 0.71$ ns, $\tau_{QD2} = 2.31$ ns, $g_1^{max} = 29.52$ cm^{-1}, $g_2^{max} = 7.92$ cm^{-1}, $\sigma_{n2} = 10^{-13}$ cm^2, $L = 0.114$ cm, and $T = 300$ K. The mirror reflectivity at the ground- and excited-state transition energies is put the same, $R_1 = R_2 = 0.32$ (as-cleaved facets at both ends), and hence the mirror loss $\beta_1 = \beta_2 = 10$ cm^{-1}. The values of τ_{21} for different curves (from the top down) are 100, 10, 2, and 1 ps. The corresponding values of j_{th1} are 90.51, 55.47, 53.31, and 53.05 A/cm^2. (Fig. 1(a) of ref. [A1], © [2006] IEEE.)

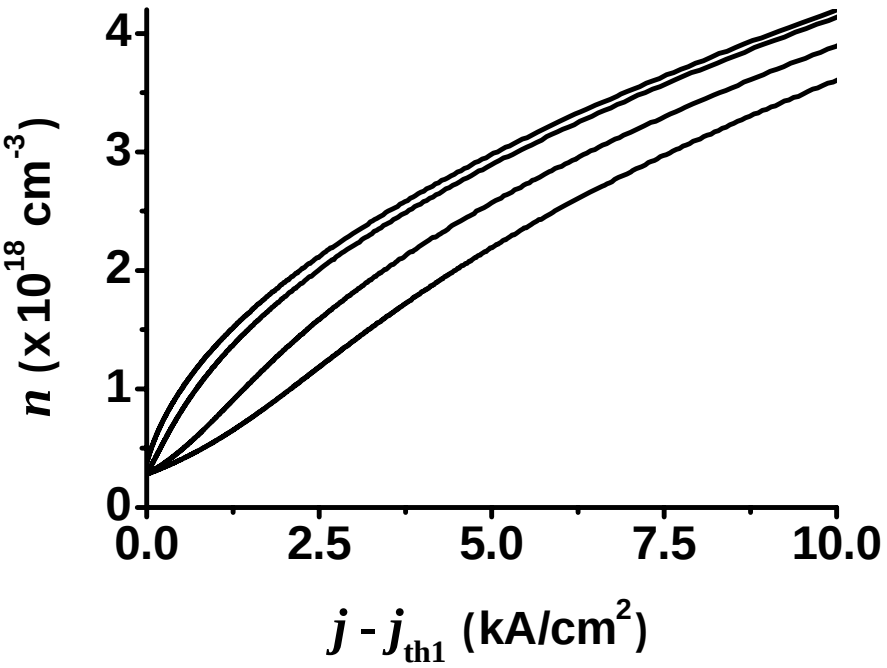

Fig. 3.3. Free carrier density against excess injection current density. The values of τ_{21} for different curves (from the top down) are 100, 10, 2, and 1 ps. (Fig. 1(b) of ref. [A1], © [2006] IEEE.)

Since we discuss the effect of excited states on the optical power of ground-state lasing, the transition time between the excited- and ground-state, τ_{21}, plays a crucial role. Table 3.3 shows τ_{21} (both measured and calculated) from different sources [7, 16–31]. In view of a wide scatter of reported values of τ_{21} (from below a picosecond to several hundred picoseconds), we analyze the laser characteristics for a wide range of τ_{21} values. Thus, in Figs. 3.2–3.4, four different values of τ_{21} (ranging from 10^{-12} to 10^{-10} s) are used.

The output power P_1 of the ground-state lasing is related to the corresponding number of photons N_1 as follows (as before, the internal optical loss is neglected):

$$P_1 = \hbar\omega_1 \frac{c}{\sqrt{\epsilon_{g1}}} \beta_1 N_1 = \hbar\omega_1 \frac{N_1}{\tau_{ph1}}, \tag{3.12}$$

where $\hbar\omega_1$ is the energy of photons emitted via the ground-state transitions (Fig. 3.1), and we introduced the photon lifetime in the cavity for the ground-state transition

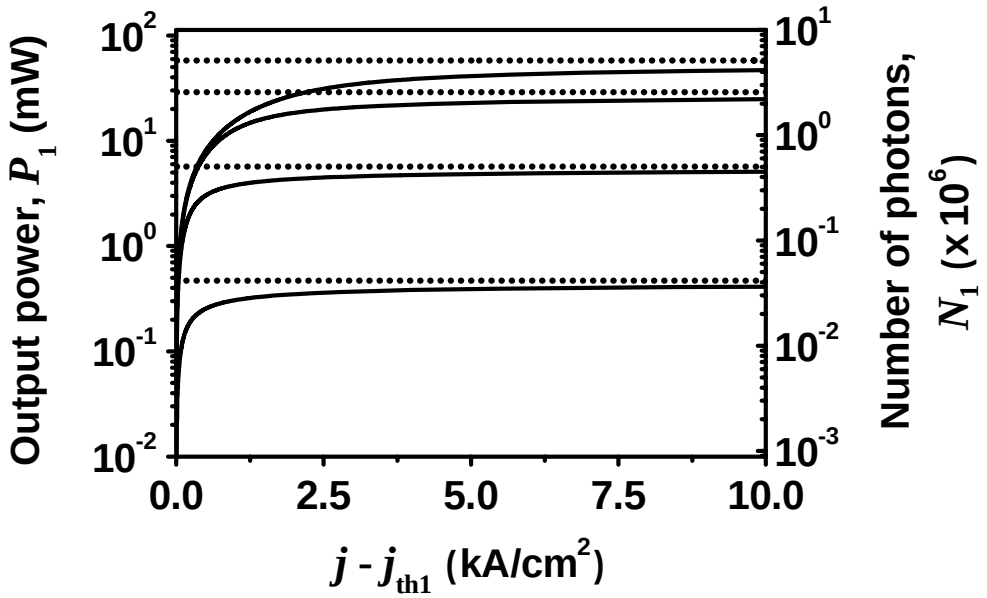

Fig. 3.4. Output power P_1 (left axis) and number of photons N_1 (right axis) of ground-state lasing against excess injection current density. Both P_1 and N_1 go to zero at the lasing threshold ($j = j_{th1}$); the lowest shown values of P_1 and N_1 are nonvanishing since the log-scale is used for the vertical axes. The horizontal dotted lines show P_1^{max} and N_1^{max} [eq. (3.24)]. The values of τ_{21} for different curves (from bottom to top) are 100, 10, 2, and 1 ps. Since all these τ_{21} values are much smaller than τ_{21}^{max} = 521 ps [eq. (3.22)], P_1^{max} is inversely proportional to τ_{21} [eq. (3.24)]. (Fig. 2 of ref. [A1], © [2006] IEEE.)

$$\tau_{ph1} = \frac{\sqrt{\epsilon_{g1}}}{c}\frac{1}{\beta_1}. \tag{3.13}$$

The output power of the ground-state lasing is plotted against injection current density in Fig. 3.4. With increasing j, the output power saturates (Fig. 3.4). In [15], the light-current curve (curve for optical power versus injection current) was shown to be sublinear in the case of direct carrier capture from the OCL into single-state QDs. The sublinearity was attributed to noninstantaneous capture from the OCL into the QD level and recombination in the OCL, which rate is superlinear in carrier density (quadratic or cubic for spontaneous radiative or nonradiative Auger recombinations). In the case under study here, the capture into the lasing state in a QD is a

Table 3.3. Reported values of τ_{21}

Time	Temperature	Spacing between the excited- and ground-states	Material system	Source
7 ps	RT		$InAs/In_{0.15}Ga_{0.85}As/GaAs$	[7, 16]
570 ps	Low (12K)	11 meV	$In_{0.1}Ga_{0.9}As$ well/GaAs barrier/InP islands	[17]
1 ps				
19 ps		< 2 meV	$GaAs/Al_{0.3}Ga_{0.7}As$	[18]
2.7–17 ps	12K	11 meV	$In_{0.1}Ga_{0.9}As$ well/GaAs barrier/InP islands	[19]
150 ps	RT	50 meV	GaAs-AlGaAs	[20]
~30–50 ps	RT		$In_{0.4}Ga_{0.6}As/GaAs$	[21]
0.6–6 ps	2K	40 meV	$InP/Ga_{0.5}In_{0.5}P$	[22]
30 ps, 100 ps			Typical InGaAs/GaAs	[23]
>30 ps	Liquid Helium		InAs/GaAs	[24]
Order of ps	Varied	Varied	InGaAs/InP	[25]
> 13 ps	0K	Varied		[26]
10 ps	40K		4-layer $In_{0.4}Ga_{0.6}As$	[27]
5.6 ps	10K	~60 meV	In(Ga)As/GaAs	[28]
7 ps	40 K		$In_{0.4}Ga_{0.6}As/GaAs$	[29]
360 ps	10K		InAs	[30]
320 ps	RT			
5.2 ps	40K	60 meV	$In_{0.4}Ga_{0.6}As/GaAs$	[31]

two-step process. Transition from the excited- to ground-state controls the carrier supply to the lasing ground-state. This strongly limits the output power and causes its saturation at high injection currents: the light-current curve asymptotically approaches the saturation value (horizontal dotted line in Fig. 3.4). It is reasonable that the saturation power is governed by the transition time between the excited- and ground-state [see eq. (3.20) below].

3.4.1. Characteristics at the lasing threshold

Putting $N_1 = 0$ into (3.7), (3.3), and (3.10), the values of f_{n2}, n and j at the ground-state lasing threshold (or simply lasing threshold in this particular case) are obtained

$$f_{n2,th1} = f_{n1} + \frac{\tau_{21}}{\tau_{QD1}} f_{n1}^2, \tag{3.14}$$

$$n_{th1} = n_2 \frac{f_{n2,th1}}{1 - f_{n2,th1}} + \frac{1}{\sigma_{n2} v_n} \frac{1}{1 - f_{n2,th1}} \left(\frac{f_{n2,th1} - f_{n1}}{\tau_{21}} + \frac{f_{n2,th1}^2}{\tau_{QD2}} \right), \tag{3.15}$$

$$j_{th1} = ebBn_{th1}^2 + \frac{eN_S}{\tau_{21}} (f_{n2,th1} - f_n) + \frac{eN_S}{\tau_{QD2}} f_{n2,th1}^2 . \tag{3.16}$$

Taking into account (3.14), we can express n_{th1} and j_{th1} as

$$n_{th1} = n_2 \frac{f_{n2,th1}}{1 - f_{n2,th1}} + \frac{1}{\sigma_{n2} v_n} \frac{1}{1 - f_{n2,th1}} \left(\frac{f_{n1}^2}{\tau_{QD1}} + \frac{f_{n2,th1}^2}{\tau_{QD2}} \right), \tag{3.17}$$

$$j_{th1} = ebBn_{th1}^2 + \frac{eN_S}{\tau_{QD1}} f_{n1}^2 + \frac{eN_S}{\tau_{QD2}} f_{n2,th1}^2 . \tag{3.18}$$

The first, second and third terms in the right-hand side of (3.18) are the threshold values of the spontaneous radiative recombination current density in the OCL, and via the ground- and excited-states in QDs, respectively.

It is seen from eq. (3.14) that when $\tau_{21} << \tau_{QD1}/f_{n1}$, ($\tau_{QD1}/f_{n1} = 1.05 \times 10^{-9}$ s for the specific example considered here), the second term in the right-hand side is much smaller than the first term, hence the threshold value of f_{n2}, $f_{n2,th1}$, is close to f_{n1} (Fig. 3.2). This is the case for the entire range of τ_{21} values considered here (10^{-12} to 10^{-10} s). Even for $\tau_{21} = 10^{-10}$ s, the deviation of $f_{n2,th1}$ from f_{n1} is only 8.5%. For $\tau_{21} = 10^{-12}$, 2×10^{-12}, and 10^{-11} s, the values of n_{th1} and j_{th1} are also close to those at $f_{n2,th1} = f_{n1}$. For $\tau_{21} = 10^{-10}$ s, the deviation of n_{th1} from its value at $f_{n2,th1} = f_{n1}$ is about 32% and hence is still small (Fig. 3.3), although it is larger than the deviation of $f_{n2,th1}$ from f_{n1}; this is because of the factor $1/(1 - f_{n2,th1})$ in (3.17). For $\tau_{21} = 10^{-10}$ s, the deviation of j_{th1} from its value at $f_{n2,th1} = f_{n1}$ is not negligible (it is about 70%, see the caption to Fig. 3.2); this is because of the first term in the right-hand side of (3.18), which is the radiative

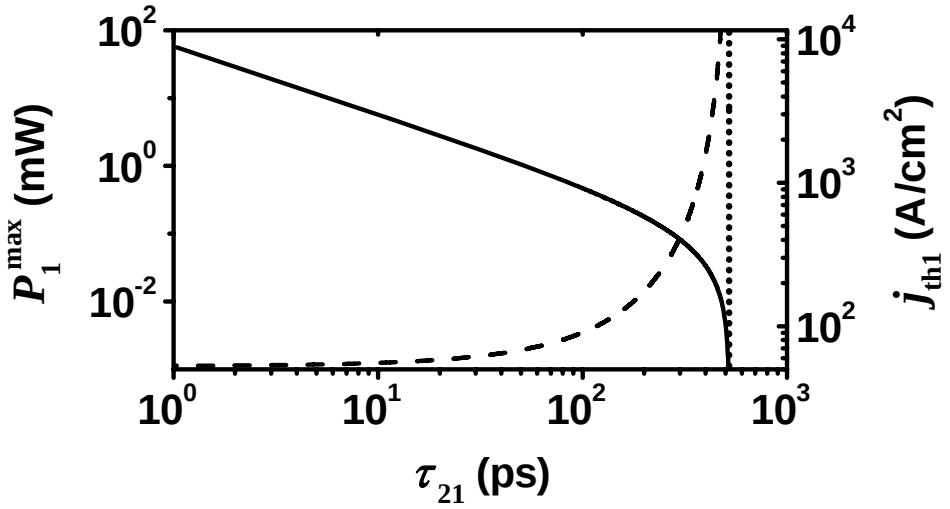

Fig. 3.5. Maximum output power (solid curve, left axis) and threshold current density of ground-state lasing (dashed curve, right axis) as a function of the transition time between the excited- and ground-state. Vertical dotted line marks $\tau_{21}^{max} = 521$ ps, at which the lasing becomes unattainable. (Fig. 3 of ref. [A1], © [2006] IEEE.)

recombination current density in the OCL at the lasing threshold and is proportional to n_{th1}^2, i.e., contains the factor $1/(1-f_{n2,th1})^2$.

3.4.2. Maximum output power and necessary condition for ground-state lasing

The level occupancy can not exceed unity: it is clear from (3.7) that as f_{n2} tends to unity (Fig. 3.2), the photon number N_1 remains finite and tends to its maximum value. Putting $f_{n2} = 1$ into (3.7) yields:

$$N_1^{max} = \frac{\frac{1-f_{n1}}{\tau_{21}} - \frac{f_{n1}^2}{\tau_{QD1}}}{\frac{1}{\tau_{ph1}}} N_S S, \tag{3.19}$$

where $N_S S$ is the total number of QDs.

Then the maximum value of the output power of the ground-state lasing can be obtained

$$P_1^{\max} = \hbar\omega_1 \frac{N_1^{\max}}{\tau_{\text{ph1}}} = \hbar\omega_1 \left(\frac{1-f_{\text{n1}}}{\tau_{21}} - \frac{f_{\text{n1}}^2}{\tau_{\text{QD1}}} \right) N_S S \,. \tag{3.20}$$

Fig. 3.5 shows the threshold current density and the maximum power of the ground-state lasing versus τ_{21}. As seen from the figure and eq. (3.20), $P_1^{\max}$ is a decreasing function of the transition time τ_{21}. At a certain value of τ_{21}, $P_1^{\max}$ vanishes. Hence the condition for lasing can be formulated as

$$\tau_{21} < \tau_{21}^{\max}, \tag{3.21}$$

where $\tau_{21}^{\max}$ is obtained from (3.20) putting $P_1^{\max} = 0$ there

$$\tau_{21}^{\max} = \tau_{\text{QD1}} \frac{1-f_{\text{n1}}}{f_{\text{n1}}^2} \,. \tag{3.22}$$

As can be seen from (3.22) and (3.14), at $\tau_{21} = \tau_{21}^{\max}$, the excited-state occupancy is unity already at the ground-state lasing threshold ($f_{\text{n2,th1}} = 1$), and hence both n_{th1} and j_{th1} are infinitely high [see eqs. (3.17) and (3.18), and Fig. 3.5].

$\tau_{21}^{\max}$ presents the maximum, cut-off value of the transition time, above which no ground-state lasing is possible. It depends on f_{n1}, i.e., on the mirror loss β_1 and the maximum gain $g_1^{\max}$. As seen from (3.6), the ground-state occupancy f_{n1} at and above the lasing threshold can range from 1/2 (when $\beta_1 = 0$ or $g_1^{\max} = \infty$) to 1 (when $\beta_1 = g_1^{\max}$). As seen from (3.22), $\tau_{21}^{\max}$ decreases from $2\tau_{\text{QD1}}$ to 0 as f_{n1} increases from 1/2 to 1. Hence

$$\tau_{21}^{\text{abs\_max}} = 2\tau_{\text{QD1}}, \tag{3.23}$$

presents an absolute upper limit of τ_{21}. For $\tau_{21} > \tau_{21}^{\text{abs\_max}}$, no lasing is possible even in a structure with no mirror loss (infinitely long cavity) or with infinitely high maximum gain $g_1^{\max}$ (since the maximum gain is inversely proportional to inhomogeneous line broadening [32], $g_1^{\max} = \infty$ corresponds to the case of ideally uniform QDs, for which the gain spectrum is a delta-function).

At the shortest possible cavity length, when $\beta_1 = g_1^{\max}$ ($f_{\text{n1}} = 1$), the cut-off value of τ_{21} reduces to zero, i.e., no lasing is possible even if transitions from the excited- to ground-state are instant.

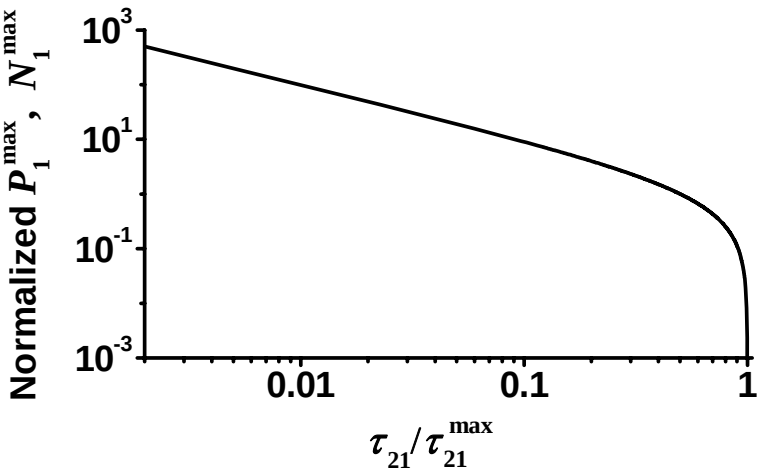

Fig. 3.6. Normalized maximum photon number and maximum output power [eqs. (3.24)] of the ground-state lasing as a universal function of normalized transition time between the excited- and ground-states.

The existence of the longest τ_{21}, at which the device can operate, is another manifestation of the critical dependence of threshold and power characteristics of a QD laser on the structure parameters (such as the surface density of QDs, QD size dispersion, cavity length, and cross section of absorption loss processes), which was revealed earlier (see [15], [32] and [33]).

The asymptotic expression for the LCC at high injection currents is presented in Appendix I. At high j, n increases as $\sqrt{j}$ [eq. (A8)]. The excited-state occupancy f_{n2} and the output power P_1/P_1^{max} asymptotically approach their saturation values according to $1-\text{const}/\sqrt{j}$ [eq. (A7)].

With (3.22), the maximum stimulated radiative recombination rate per QD, $\frac{1}{N_S S}\frac{N_1^{max}}{\tau_{ph1}} = \frac{1}{N_S S}\frac{P_1^{max}}{\hbar\omega_1}$, normalized to the spontaneous radiative recombination rate per QD ground-state, f_{n1}^2/τ_{QD1}, can be written as the following universal function of the normalized transition time $\tau_{21}/\tau_{21}^{max}$:

$$\frac{\frac{1}{N_S S}\frac{N_1^{max}}{\tau_{ph1}}}{\frac{f_{n1}^2}{\tau_{QD1}}} = \frac{\frac{1}{N_S S}\frac{P_1^{max}}{\hbar\omega_1}}{\frac{f_{n1}^2}{\tau_{QD1}}} = \frac{1}{\frac{\tau_{21}}{\tau_{21}^{max}}} - 1, \qquad (3.24)$$

The normalized $N_1^{\max}$ and $P_1^{\max}$ are a simple decaying function of the normalized transition time $\tau_{21}/\tau_{21}^{\max}$ (Fig. 3.6). When $\tau_{21}/\tau_{21}^{\max} \to 0$, the normalized $N_1^{\max}$ and $P_1^{\max}$ are inversely proportional to $\tau_{21}/\tau_{21}^{\max}$ (the linear portion of the curve in Fig. 3.6 in log-scale; see also the horizontal dotted lines in Fig. 3.4).

When deriving the ground-state lasing threshold condition (equality of the gain to the mirror loss) and then the expression for f_{n1} at and above the lasing threshold [eq. (3.6)], nonvanishing N_1 was assumed. Inequality (3.21) presents the necessary condition for nonvanishing N_1 and hence for ground-state lasing. It is written in terms of allowed values of τ_{21} at a given f_{n1}, i.e., given $g_1^{\max}$ and β_1. This condition can be rewritten in terms of allowed values of $g_1^{\max}$ at given τ_{21} and β_1. Thus we obtain

$$g_1^{\max} > \frac{\beta_1}{\dfrac{1}{\dfrac{1}{4}+\sqrt{\dfrac{1}{16}+\dfrac{1}{4}\dfrac{\tau_{21}}{\tau_{QD1}}}}-1}. \tag{3.25}$$

For the entire range of possible values of τ_{21}, the right-hand side of (3.25) is larger than or equal to β_1. Indeed, the denominator of the expression in the right-hand side is less then or equivalent to unity: it changes from 1 to 0 as τ_{21} changes from 0 to $\tau_{21}^{\text{abs\_max}} = 2\tau_{QD1}$.

Hence when the carrier capture into the QD ground state is excited-state-mediated, a simple excess of the maximum gain $g_1^{\max}$ over the mirror loss β_1 is not sufficient for the ground-state lasing to occur. A stronger condition [inequality (3.25)] should be satisfied. Only in the case of instant carrier transition from the excited- to ground-state ($\tau_{21} = 0$), (3.25) reduces to the condition $g_1^{\max} > \beta_1$. The longer τ_{21}, the higher should be $g_1^{\max}$. In the case of the slowest allowed carrier transition from the excited- to ground-state ($\tau_{21} = \tau_{21}^{\text{abs\_max}} = 2\tau_{QD1}$), the maximum gain for the ground-state transitions $g_1^{\max}$ should be infinitely high, i.e., the QD ensemble should be perfectly uniform, or the cavity should be infinitely long ($\beta_1 = 0$).

3.4.3. Internal and external differential quantum efficiencies

Above the lasing threshold ($j \geq j_{\mathrm{th1}}$), the internal differential quantum efficiency of a semiconductor laser is defined as the fraction of the excess of the injection current over the threshold current that results in stimulated emission

$$\eta_{\mathrm{int}} = \frac{j_{\mathrm{stim1}}}{j - j_{\mathrm{th1}}}, \tag{3.26}$$

where

$$j_{\mathrm{stim1}} = e\frac{1}{S}\frac{c}{\sqrt{\epsilon_{\mathrm{g1}}}}\beta_1 N_1, \tag{3.27}$$

is the current density of stimulated recombination via the QD ground state.

With (3.11) and (3.18) for j and j_{th1}, (3.26) becomes

$$\eta_{\mathrm{int}} = \frac{1}{1 + \dfrac{\dfrac{N_S}{\tau_{\mathrm{QD2}}}\left(f_{\mathrm{n2}}^2 - f_{\mathrm{n2,th1}}^2\right) + bB\left(n^2 - n_{\mathrm{th1}}^2\right)}{\dfrac{1}{S}\dfrac{c}{\sqrt{\epsilon_{\mathrm{g1}}}}\beta_1 N_1}} = \frac{1}{1 + \dfrac{\tau_{21}}{\tau_{\mathrm{QD2}}}\left(f_{\mathrm{n2}} + f_{\mathrm{n2,th1}}\right) + \dfrac{bB\left(n^2 - n_{\mathrm{th1}}^2\right)}{\dfrac{1}{S}\dfrac{c}{\sqrt{\epsilon_{\mathrm{g1}}}}\beta_1 N_1}}. \tag{3.28}$$

In the latter expression in (3.28), eqs. (3.7) and (3.14) for f_{n2} and $f_{\mathrm{n2,th1}}$ were used. In (3.28), f_{n2}, n and N_1 are functions of the injection current density j.

So far, only the ground-state lasing is considered, therefore the external differential quantum efficiency is

$$\eta_{\mathrm{ext}} = \frac{1}{\dfrac{\hbar\omega_1}{e}}\frac{\partial P_1}{\partial I} = \frac{1}{\dfrac{\hbar\omega_1}{e}}\frac{1}{S}\frac{\partial P_1}{\partial j} = e\frac{1}{S}\frac{c}{\sqrt{\epsilon_{\mathrm{g1}}}}\beta_1\frac{\partial N_1}{\partial j} = \frac{\partial j_{\mathrm{stim1}}}{\partial j}, \tag{3.29}$$

where $I = Sj$ is the injection current. With (3.7), (3.3) and (3.10), the following expression is obtained for η_{ext}:

$$\eta_{\mathrm{ext}} = \frac{1}{1 + 2\dfrac{\tau_{21}}{\tau_{\mathrm{QD2}}}f_{\mathrm{n2}} + 2\dfrac{\tau_{21}}{N_{\mathrm{S}}}bBn\dfrac{1}{1 - f_{\mathrm{n2}}}\left[n + n_2 + \dfrac{1}{\sigma_{\mathrm{n2}}v_{\mathrm{n}}}\left(\dfrac{1}{\tau_{21}} + \dfrac{2f_{\mathrm{n2}}}{\tau_{\mathrm{QD2}}}\right)\right]}, \tag{3.30}$$

where f_{n2} and n are functions of j.

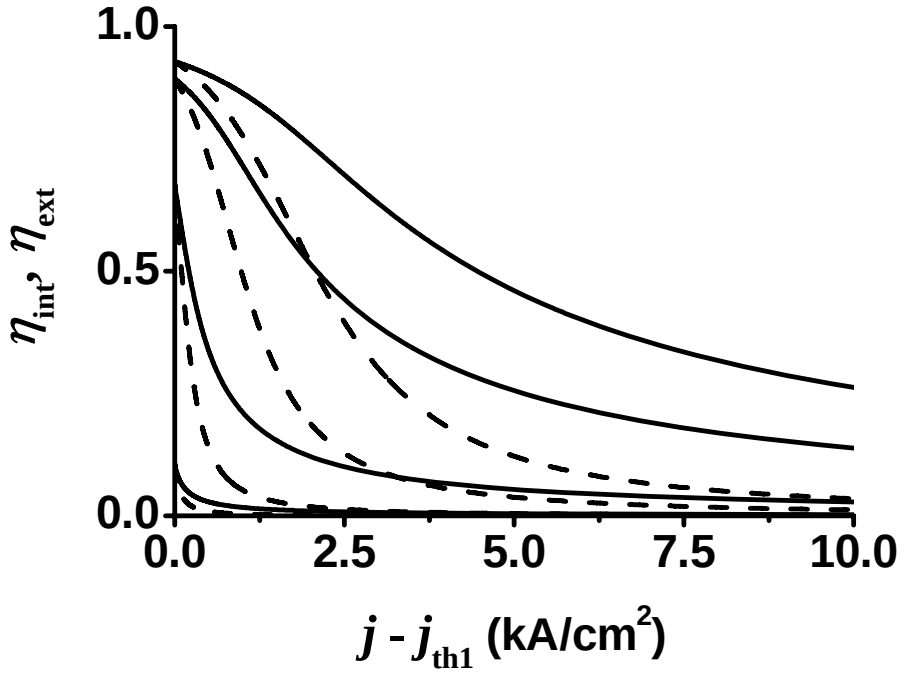

Fig. 3.7. Internal and external efficiencies (solid and dashed curves, respectively) against excess injection current density. The values of τ_{21} for different curves (from bottom to top) are 100, 10, 2, and 1 ps.

The internal and external efficiencies are less than unity even at the lasing threshold (Fig. 3.7). At $j = j_{th1}$, $\eta_{int,th1}$ and $\eta_{ext,th1}$ are equal to each other and given by (3.30), wherein $f_{n2,th1}$ and n_{th1} enter instead of f_{n2} and n. This threshold value of the efficiencies can be obtained also from (3.28) using (3.7) and (3.3).

At $j > j_{th1}$, η_{ext} is smaller than η_{int} (Fig.3.7). Predominantly due to the free-carrier density increase above j_{th1}, both efficiencies decrease rapidly with increasing j (Fig. 3.7). The asymptotic expressions for η_{int} and η_{ext} at high j are presented in Appendix I. At high j, η_{int} and η_{ext} decay as $1/j$ and $1/j^{3/2}$, respectively [eqs. (A9) and (A10)].

The shorter the transition time τ_{21}, the higher η_{int} and η_{ext} (Fig. 3.7). The limiting case of instant carrier exchange between the excited-and ground-states ($\tau_{21} = 0$) is considered in Appendix II.

3.5. Conclusion

While the ground-state occupancy is pinned above the ground-state lasing threshold, the excited-state occupancy and the free carrier density continuously increase with the injection current as a consequence of noninstantaneous capture from the OCL to the excited state and from the excited- to ground-state. Indirect or cascade capture of carriers from the OCL into the QD ground-state, combined with the superlinear (in carrier density) recombination rate in the OCL, causes the saturation of the output power of the ground-state lasing with increasing injection current – the power asymptotically approaches its maximum value. The threshold current density and the saturation power of the ground-state lasing depend critically on the transition time – as the transition time increases and approaches a certain value, the threshold current density increases infinitely, and the saturation power decreases and vanishes. This cut-off transition time marks the slowest carrier exchange between the excited- and ground-state, beyond which no ground-state lasing is possible. In an ideally uniform QD ensemble, this cut-off time is twice the spontaneous radiative recombination time through the QD ground state. The normalized maximum power of the ground-state lasing is obtained as a simple universal function of the transition time normalized to the cut-off value.

We considered the three-dimensional reservoir (OCL), wherefrom carriers are captured into QDs. The capture from the two-dimensional wetting layer in addition to (or instead of) the capture from the OCL can be easily included into our model. To do this, the corresponding quantities for the two-dimensional region should be properly used in addition to (instead of) the bulk quantities. In view of qualitatively similar character of the recombination rates in the OCL and the wetting layer (both are superlinear in the corresponding carrier density), and of the captures from the three-dimensional and two-dimensional regions into QDs, such an extension of the model will not introduce significantly new results.

Appendix I

LCC at high injection currents

Using eq. (3.13) for τ_{ph1} and eq. (3.22) for $\tau_{21}^{\max}$, we have from (3.24):

$$\frac{c}{\sqrt{\epsilon_{\mathrm{g1}}}}\frac{\beta_1}{N_{\mathrm{S}}S}=\frac{\dfrac{1}{\tau_{21}}-\dfrac{1}{\tau_{21}^{\max}}}{N_1^{\max}}\left(1-f_{\mathrm{n1}}\right). \tag{A1}$$

With (A1) and (3.22), (3.7) can be written as

$$f_{\mathrm{n2}}=f_{\mathrm{n1}}+\left(1-f_{\mathrm{n1}}\right)\left[\frac{\tau_{21}}{\tau_{21}^{\max}}+\left(1-\frac{\tau_{21}}{\tau_{21}^{\max}}\right)\frac{N_1}{N_1^{\max}}\right]. \tag{A2}$$

That is

$$1-f_{\mathrm{n2}}=\left(1-f_{\mathrm{n1}}\right)\left(1-\frac{\tau_{21}}{\tau_{21}^{\max}}\right)\left(1-\frac{N_1}{N_1^{\max}}\right). \tag{A3}$$

Inserting $1-f_{\mathrm{n2}}$ from (A3) into (3.3) yields

$$n=\left[n_2 f_{\mathrm{n2}}+\frac{1}{\sigma_{\mathrm{n2}}v_{\mathrm{n}}}\left(\frac{f_{\mathrm{n2}}-f_{\mathrm{n1}}}{\tau_{21}}+\frac{f_{\mathrm{n2}}^2}{\tau_{\mathrm{QD2}}}\right)\right]\frac{1}{\left(1-f_{\mathrm{n1}}\right)\left(1-\dfrac{\tau_{21}}{\tau_{21}^{\max}}\right)\left(1-\dfrac{N_1}{N_1^{\max}}\right)}. \tag{A4}$$

As N_1 tends to $N_1^{\max}$, the free carrier density n in the OCL tends to infinity. The asymptotic expression for n at $N_1\to N_1^{\max}$ ($f_{\mathrm{n2}}\to 1$) is apparent from (A4)

$$n_{\mathrm{asympt}}=\frac{n_2+\dfrac{1}{\sigma_{\mathrm{n2}}v_n}\left(\dfrac{1}{\tau_{\mathrm{QD2}}}+\dfrac{1-f_{\mathrm{n1}}}{\tau_{21}}\right)}{\left(1-f_{\mathrm{n1}}\right)\left(1-\dfrac{\tau_{21}}{\tau_{21}^{\max}}\right)}\frac{1}{1-\dfrac{N_1}{N_1^{\max}}}\propto\frac{1}{1-\dfrac{N_1}{N_1^{\max}}}. \tag{A5}$$

As n tends to infinity, the last two terms in the right-hand side of (3.10) (which remain finite) can be ignored compared to the first term. Accordingly, we have for j when $N_1\to N_1^{\max}$

$$j=ebBn_{\mathrm{asympt}}^2\propto\frac{1}{\left(1-\dfrac{N_1}{N_1^{\max}}\right)^2}. \tag{A6}$$

Hence the asymptotic expression for the LCC at high j is

$$\frac{P_1}{P_1^{\max}} = \frac{N_1}{N_1^{\max}} = 1 - \frac{n_2 + \frac{1}{\sigma_{n2} v_n}\left(\frac{1}{\tau_{QD2}} + \frac{1-f_{n1}}{\tau_{21}}\right)}{(1-f_{n1})\left(1-\frac{\tau_{21}}{\tau_{21}^{\max}}\right)}\sqrt{\frac{ebB}{j}} = 1 - \frac{\text{const}}{\sqrt{j}}. \tag{A7}$$

The asymptotic expression for the free carrier density in the OCL versus j is apparent from (A6)

$$n_{\text{asympt}} = \sqrt{\frac{j}{ebB}}. \tag{A8}$$

At high current density (when $N_1 \to N_1^{\max}$), the asymptotic expression for η_{int} is easily obtained from (3.26)

$$\eta_{\text{int,asympt}} = \frac{j_{\text{stim1}}^{\max}}{j} = \frac{e\frac{1}{S}\frac{c}{\sqrt{\epsilon_{g1}}}\beta_1 N_1^{\max}}{j}, \tag{A9}$$

where we introduced the saturation value of the stimulated recombination current density via the QD ground state, $j_{\text{stim1}}^{\max}$.

The asymptotic expression for η_{ext} at high j can be found from the general equation (3.30). It is however easier to derive this equation using (3.29) and the asymptotic expression (A7) for $P_1(j)$. Thus we obtain

$$\eta_{\text{ext,asympt}} = \frac{1}{2} j_{\text{stim1}}^{\max} \frac{n_2 + \frac{1}{\sigma_{n2} v_n}\left(\frac{1}{\tau_{QD2}} + \frac{1-f_{n1}}{\tau_{21}}\right)}{(1-f_{n1})\left(1-\frac{\tau_{21}}{\tau_{21}^{\max}}\right)}\frac{\sqrt{ebB}}{j^{3/2}}. \tag{A10}$$

Appendix II

Instant carrier exchange between excited- and ground-states in a QD

In the limiting case of instant transition between the excited- and ground-states ($\tau_{21} = 0$), eqs (3.7), (3.9) and (3.11) become

$$f_{n2} = f_{n1}, \tag{A11}$$

$$n = n_2 \frac{f_{n1}}{1-f_{n1}} + \frac{1}{\sigma_{n2} v_n} \frac{1}{1-f_{n1}} \left[f_{n1}^2 \left(\frac{1}{\tau_{QD1}} + \frac{1}{\tau_{QD2}} \right) + \frac{c}{\sqrt{\epsilon_{g1}}} \frac{\beta_1}{N_S S} N_1 \right], \tag{A12}$$

$$j = ebBn\big|_{\tau_{21}\to 0}^2 + eN_S f_{n1}^2 \left(\frac{1}{\tau_{QD1}} + \frac{1}{\tau_{QD2}} \right) + e \frac{1}{S} \frac{c}{\sqrt{\epsilon_{g1}}} \beta_1 N_1 . \tag{A13}$$

It can be seen from (A11)–(A13) that at $\tau_{21} = 0$, the model developed here is reduced to that for a single-transition QD considered in [15], except that n_1 and σ_{n1} are now replaced by n_2 and σ_{n2} in view of the fact that the carrier exchange between QDs and the OCL occurs through the excited-state; also, $\frac{1}{\tau_{QD1}} + \frac{1}{\tau_{QD2}}$ effectively replaces $\frac{1}{\tau_{QD}}$. Particularly, the expression for $\eta_{int,th1}$ [given by (3.30) at the threshold values of f_{n2} and n] will go into eq. (47) of [15]

$$\eta_{int,th1} = \frac{1}{1 + 2\dfrac{j_{th1}^{OCL}}{j_{capt,th1}}}, \tag{A14}$$

where

$$j_{th1}^{OCL} = ebBn_{th1}^2, \tag{A15}$$

with n_{th1} being given by (A12) at $N_1 = 0$, and σ_{n2} entering the current density of the carrier capture into the QD excited-states at the lasing threshold

$$j_{capt,th1} = ebn_{th1} \left[\sigma_{n2} v_n \frac{N_S}{b} (1 - f_{n2}) \right]. \tag{A16}$$

REFERENCES [*)]

[A1] L. Jiang and L. V. Asryan, "Excited-state-mediated capture of carriers into the ground state and the saturation of optical power in quantum-dot lasers," *IEEE Photon. Technol. Lett.*, vol. 18, no. 24, pp. 2611–2613, Dec. 2006.

[A2] L. Jiang and L.V. Asryan, "Effect of excited states on light-current characteristic of a quantum dot laser," *Proceedings of SPIE's International Symposium Photonics West*. San Jose, California, Jan. 20–25, 2007. vol. 6481, pp. 648108-1–648108-7.

[A3] L. Jiang and L.V. Asryan, "Indirect capture and ground-state lasing in quantum dot structures," *Proceedings of 15th International Symposium "Nanostructures: Physics and Technology"*. Novosibirsk, Russia, June 25–29, 2007. pp. 38–39.

[1] P. N. Brounkov, A. Polimeni, S. T. Stoddart, M. Henini, L. Eaves, P. C. Main, A. R. Kovsh, Y. G. Musikhin, and S. G. Konnikov, "Electronic structure of self-assembled InAs quantum dots in GaAs matrix," *Appl. Phys. Lett.*, vol. 73, no. 8, pp. 1092–1094, Aug. 1998.

[2] P. Bhattacharya and Z. Mi, "Quantum-dot optoelectronic devices," *Proc. IEEE*, vol. 95, no. 9, pp. 1723–1740, Sept. 2007.

[3] M. V. Maximov, L. V. Asryan, Y. M. Shernyakov, A. F. Tsatsul'nikov, I. N. Kaiander, V. V. Nikolaev, A. R. Kovsh, S. S. Mikhrin, V. M. Ustinov, A. E. Zhukov, Zh. I. Alferov, N. N. Ledenstov, and D. Bimberg, "Gain and threshold characteristics of long wavelength lasers based on InAs/GaAs quantum dots formed by activated alloy phase separation," *IEEE J. Quantum Electron.*, vol. 37, no. 5, pp. 675–683, May 2001.

[4] I. C. Sandall, P. M. Smowton, C. L. Walker, H. Y. Liu, M. Hopkinson, and D. J. Mowbray, "Recombination mechanisms in 1.3-μm InAs quantum-dot lasers," *IEEE Photon. Technol. Lett.*, vol. 18, no. 5–8, pp. 965–967, Apr. 2006.

[5] L. V. Asryan, M. Grundmann, N. N. Ledentsov, O. Stier, R. A. Suris, and D. Bimberg, "Effect of excited-state transition on the threshold characteristics of a quantum dot laser,"

[*)] "A" in the reference number indicates the publications of the author of this dissertation.

IEEE J. Quantum Electron., vol. 37, no. 3, pp. 418–425, Mar. 2001.

[6] L. V. Asryan, M. Grundmann, N. N. Ledentsov, O. Stier, R. A. Suris, and D. Bimberg, "Maximum modal gain of a self-assembled InAs/GaAs quantum-dot laser," *J. Appl. Phys.*, vol. 90, no. 3, pp. 1666–1668, Aug. 2001.

[7] A. Markus, J. X. Chen, O. Gauthier-Lafaye, J. G. Provost, C. Paranthoen, and A. Fiore, "Impact of intraband relaxation on the performance of a quantum-dot laser," *IEEE J. Select. Topics Quantum Electron.*, vol. 9, no. 5, pp. 1308–1314, Sept./Oct. 2003.

[8] A. Markus and A. Fiore, "Modeling carrier dynamics in quantum-dot lasers," *Phys. Stat. Sol. A*, vol. 201, No. 2, 338–344, Jan. 2004.

[9] M. Sugawara, N. Hatori, H. Ebe, M. Ishida, Y. Arakawa, T. Akiyama, K. Otsubo, and Y. Nakata, "Modeling room-temperature lasing spectra of 1.3-μm self-assmebled InAs/GaAs quantum-dot lasers: homogeneous broadening of optical gain under current injection," *J. Appl. Phys.*, vol. 97, no. 4, Article 043523, Feb. 2005.

[10] K. Veselinov, F. Grillot, P. Miska, E. Homeyer, P. Caroff, C. Platz, J. Even, X. Marie, O. Dehaese, S. Loualiche, and A. Ramdane, "Carrier dynamics and saturation effect in (113)B InAs/InP quantum dot lasers," *Opt. Quantum Electron.*, vol. 38, no. 4–6, pp. 369–379, Mar. 2006.

[11] K. Veselinov, F. Grillot, J. Even, and S. Loualiche, "Numerical modeling of the two-state lasing in 1.55 μm (113)B InAs/InP quantum dot lasers," *International Workshop on Semiconductor Quantum Dot Based Devices and Applications*, Paris (France), pp. 16–17, Mar. 2006.

[12] A. E. Zhukov, A. R. Kovsh, D. A. Livshits, V. M. Ustinov, and Zh. I. Alferov, "Output power and its limitation in ridge-waveguide 1.3 μm wavelength quantum-dot lasers," *Semicond. Sci. Technol.*, vol. 18, no. 8, pp. 774–781, Aug. 2003.

[13] L. V. Asryan and S. Luryi, "Tunneling-injection quantum-dot laser: ultrahigh temperature stability," *IEEE J. Quantum Electron.*, vol. 37, no. 7, pp. 905–910, July 2001.

[14] L. V. Asryan and S. Luryi, *Semiconductor laser with reduced temperature sensitivity*. U.S. Patent 6870178, Mar. 2005.

[15] L. V. Asryan, S. Luryi and R. A. Suris, "Internal efficiency of semiconductor lasers with a quantum-confined active region," *IEEE J. Quantum Electron.*, vol. 39, no. 3, pp. 404–418, Mar. 2003.

[16] A. Markus, J. X. Chen, C. Paranthoen, A. Fiore, C. Platz, and O. Gauthier-Lafaye, "Simultaneous two-state lasing in quantum-dot lasers," *Appl. Phys. Lett.*, vol. 82, no. 12, pp. 1818–1820, Mar. 2003.

[17] S. Grosse, J. H. H. Sandmann, G. von Plessen, J. Feldmann, H. Lipsanen, M. Sopanen, J. Tulkki, and J. Ahopelto, "Carrier relaxation dynamics in quantum dots - Scattering mechanisms and state-filling effects," *Phys. Rev. B*, vol. 55, no. 7, pp. 4473–4476, Feb. 1997.

[18] D. Gammon, E. S. Snow, B. V. Shanabrook, D. S. Katzer, and D. Park., "Homogeneous linewidths in the optical spectrum of a single Gallium Arsenide quantum dot," *Science*, vol. 273, no. 5271, pp. 87–90, July 1996.

[19] J. H. H. Sandmann, S. Grosse, G. von Plessen, J. Feldmann, G. Hayes, R. Phillips, H. Lipsanen, M. Sopanen, and J. Ahopelto, "Carrier relaxation in (GaIn)As quantum dots," *Phys. Status Solidi A*, vol. 164, no. 1, pp. 421–425, Nov. 1997.

[20] J. Singh, "Possibility of room temperature intra-band lasing in quantum dot structures," *IEEE Photon. Technol. Lett.*, vol. 8, no. 4, pp. 488–490, Apr. 1996.

[21] D. Klozkin, K. Kamath, and P. Bhattacharya, "Quantum capture times at room temperature in high-speed $In_{0.4}Ga_{0.6}As$-GaAs self-organized quantum-dot lasers," *IEEE Photon. Technol. Lett.*, vol. 9, no. 10, pp. 1301–1303, Oct. 1997.

[22] I. V. Ignatiev, I. E. Kozin, S. V. Nair, H. W. Ren, S. Sugou, and Y. Masumoto, "Carrier relaxation dynamics in InP quantum dots studied by artificial control of nonradiative losses," *Phys Rev. B*, vol. 61, no. 23, pp. 15633–15636, June 2000.

[23] M. Grundmann, "How a quantum-dot laser turns on," *Appl. Phys. Lett.*, vol. 77, no. 10, pp. 1428–1430, Sept. 2000.

[24] P. Boucaud, K. S. Gill, J. B. Williams, M. S. Sherwin, W. V. Schoenfeld, and P. M. Petroff, "Saturation of THz-frequency intraband absorption in InAs/GaAs quantum dot molecules," *Appl. Phys. Lett.*, vol. 77, no. 4, pp. 510–512, July 2000.

[25] U. Bockelmann and T. Egeler, "Electron relaxation in quantum dots by means of Auger processes," *Phys. Rev. B*, vol. 46, no. 23, pp. 15574–15577, Dec. 1992.

[26] U. Bockelmann, "Exciton relaxation and radiative recombination in semiconductor quantum dots," *Phys. Rev. B*, vol. 48, no. 23, pp. 17637–17640, Dec. 1993.

[27] J. Urayama, T. B. Norris, H. Jiang, J. Singh, and P. Bhattacharya, "Differential

transmission measurement of phonon bottleneck in self-assembled quantum dot intersubband relaxation," *Physica B*, vol. 316–317, pp. 74–80, May 2002.

[28] P. Bhattacharya, S. Krishna, J. Phillips, P. J. McCann, and K. Namjou, "Carrier dynamics in self-organized quantum dots and their application to long-wavelength sources and detectors," *J. Cryst. Growth*, Vol. 227–228, pp. 27–35, July 2001.

[29] J. Urayama, T. B. Norris, J. Singh, and P. Bhattacharya, "Observation of phonon bottleneck in quantum dot electronic relaxation," *Phys. Rev. Lett.*, vol. 86, no. 21, pp. 4930–4933, May 2001.

[30] T. Kitamura, R. Ohtsubo, M. Murayama, T. Kuroda, K. Yamaguchi, and A. Tackeuchi, "Direct observation of phonon relaxation bottleneck in InAs quantum dots of high-uniformity," *Phys. Status Solidi C*, vol. 0, no. 4, pp. 1165–1168, Jun. 2003.

[31] T. B. Norris, K. Kim, J. Urayama, Z. K. Wu, J. Singh, and P. K. Bhattacharya, "Density and temperature dependence of carrier dynamics in self-organized InGaAs quantum dots," *J. Phys. D*, vol. 38, no. 13, pp. 2077–2087, July 2005.

[32] L. V. Asryan and R. A. Suris, "Inhomogeneous line broadening and the threshold current density of a semiconductor quantum dot laser," *Semicond. Sci. Technol.*, vol. 11, no. 4, pp. 554–567, Apr. 1996.

[33] L. V. Asryan and S. Luryi, "Effect of internal optical loss on threshold characteristics of semiconductor lasers with a quantum-confined active region," *IEEE J. Quantum Electron.*, vol. 40, no. 7, pp. 833–843, July 2004.

Chapter 4

Multimode Emission and Optical Power in a Quantum Dot Laser

Summary

Effect of spatial hole burning (SHB) and multi-longitudinal-mode generation on high power operation of a quantum dot (QD) laser is studied. We use a set of rate equations for confined carriers in QDs, free carriers in the optical confinement layer, and photons. The number of modes is shown to remain limited with increasing injection current. The maximum number of modes that can oscillate in a QD laser is analytically estimated. While this number increases with increasing surface density of QDs or cavity length, it remains limited (first increases and then decreases) with increasing scatter in the QD-size. The critical tolerable values of the structure parameters are derived beyond which higher-order longitudinal modes can not oscillate. It is notable that, in addition to the maximum tolerable scatter, there also exists the minimum scatter in the QD-size for each higher-order mode to start lasing. The threshold currents and output powers of modes are computed numerically. The power of the main mode is reduced due to lasing of higher-order modes and spatially nonuniform carrier distribution. As a new mode turns on, kinks appear in the light-current curves (LCCs) of existing modes. SHB reduces the total optical power of a laser and contributes to nonlinearity of the overall LCC. The effect is more significant when any of the structure parameters is close to its critical tolerable value. The LCC becomes more linear with improving QD-size uniformity or increasing surface density of QDs or cavity length.

4.1. Introduction

Delta-function density-of-states [1, 2] and ultra narrow optical gain spectrum in an ideally uniform ensemble of quantum dots (QDs) could potentially ensure a single-mode generation in a

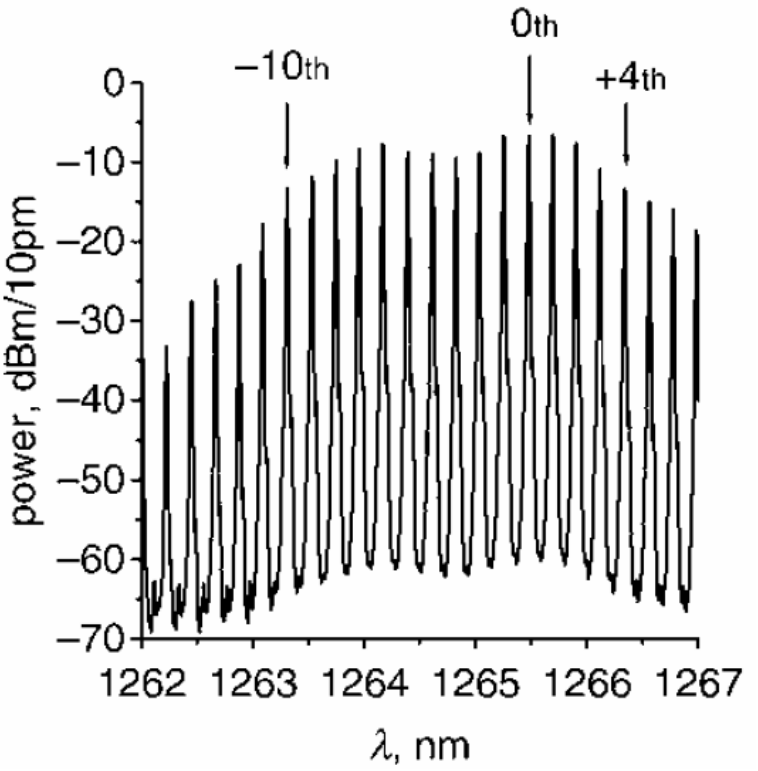

Fig. 4.1. Lasing spectrum of a QD laser around the maximum-intensity wavelength. (Fig. 1(a) of ref. [5], © [2007] IEEE.)

QD laser. In self-organized QD ensembles, due to fluctuations in QD parameters (primarily size) during the structure growth [3], the gain spectrum is inhomogeneously broadened [4] thus making for multimode lasing. Fig. 4.1 shows an experimental lasing spectrum with multiple peaks corresponding to the longitudinal modes of a Fabry-Perot cavity. Fig. 4.2 illustrates the emergence of new modes with increasing injection current density.

Multimode generation is an interesting phenomenon, which can strongly affect the operating characteristics of semiconductor lasers [7–17]. One possible mechanism for multimode emission is spatial hole burning (SHB) in the population inversion in the laser active region.

Due to the standing wave character, the optical mode intensity and hence the stimulated recombination rate are spatially nonuniform along the laser cavity. Nonuniformity of stimulated recombination can cause nonuniform carrier distributions. In semiconductor quantum well or bulk-active-region lasers, nonuniform carrier distributions are effectively smoothed out by

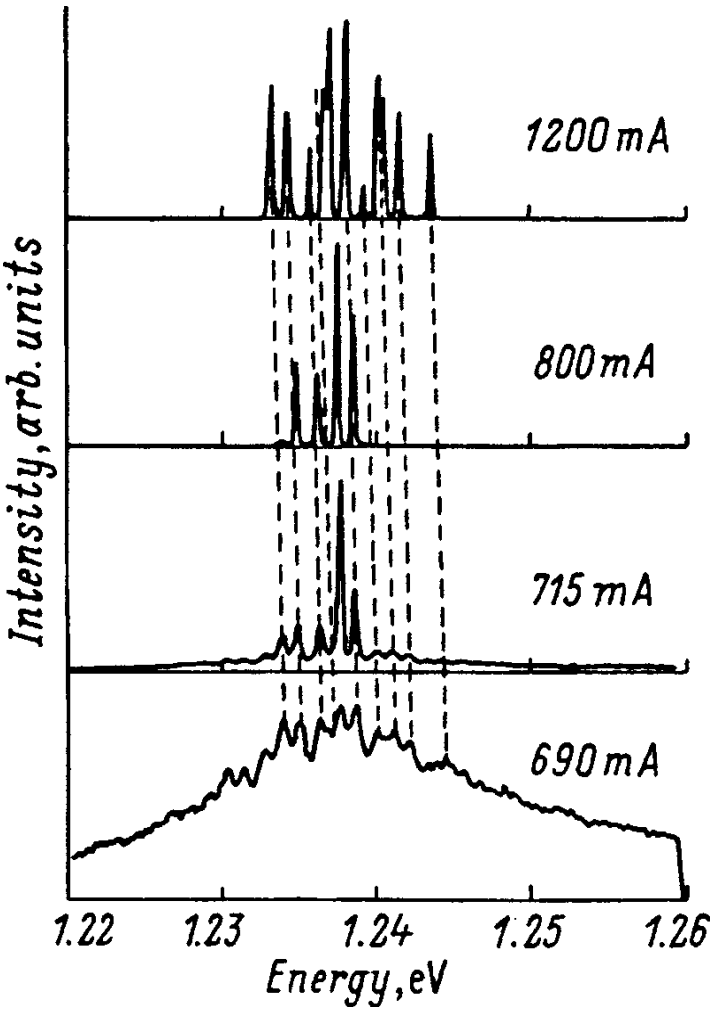

Fig. 4.2. Electroluminescence spectra of a QD laser at various pump currents. (Fig. 3 of ref. [6], reprinted with kind permission of Springer Science and Business Media.)

diffusion processes. In quantum dot (QD) lasers, carriers that contribute to the stimulated emission are spatially localized in QDs. For this reason, smoothing out nonuniform carrier distributions requires thermal excitation from overfilled QDs, diffusion to depleted QDs, and capture into the latter (Fig. 4.3). This delayed, three-step carrier exchange between neighboring QDs can result in a strongly nonuniform population inversion and hence SHB. With increasing pump current, the light intensity will rise and the conditions for lasing of higher-order longitudinal modes (in addition to the main mode) can be satisfied in overfilled QDs [18, 19].

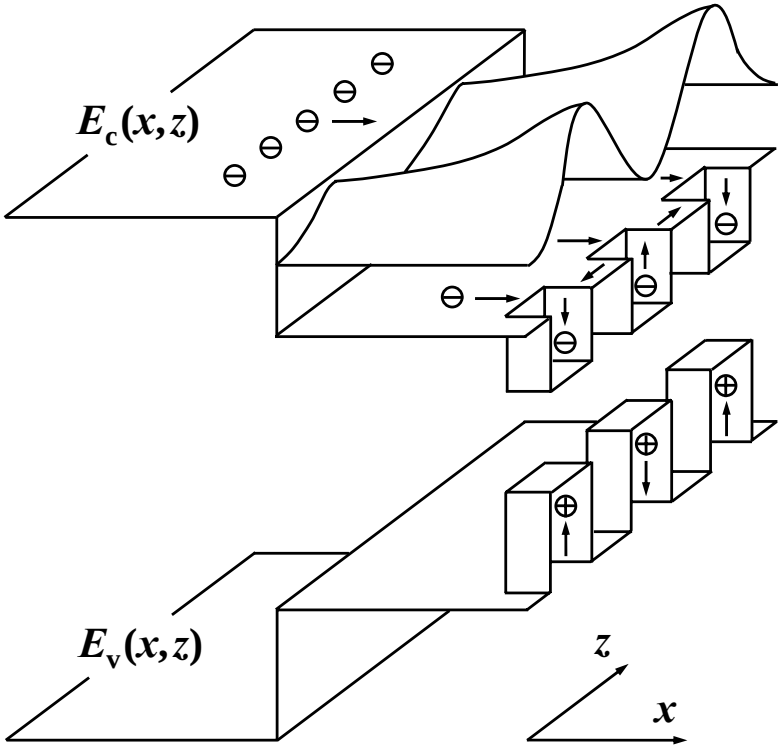

Fig. 4.3. Energy band diagram of a QD laser in the directions of current injection and light output. Half of the diagram with a section through the QD layer is shown. $E_{c,v}(x, z)$ are the conduction and valence band edges. Electron injection from the n-cladding to the OCL and from the OCL to QDs is indicated by the horizontal arrows. Capture into QDs and thermal escape from QDs are indicated by the vertical arrows. Electron diffusion in the OCL between neighboring QDs is indicated by the diagonal arrows. The wavy surface schematically sketches the light intensity distribution in the OCL. (Fig. 1 of ref. [A1], reprinted with permission of IOP Publishing Ltd.)

Several QDs are typically accommodated within a period of the optical mode intensity (half-wavelength in the medium). SHB occurs therefore on the half-wavelength scale. This SHB is specific to QD lasers. There will be an additional nonuniformity of the population inversion caused by a nonuniform distribution of the total light intensity of the lasing modes. The latter nonuniformity develops on the cavity-length scale (see Section 4.5); in contrast to the

nonuniformity on the half-wavelength scale, it is not totally smoothed out by diffusion processes in bulk and quantum well Fabry-Perot cavity lasers and can be viewed as SHB occurring on the cavity-length scale.

4.2. Rate equations in the presence of SHB

As in previous works (see for example, [20, 21]), we use the rate equations model to calculate the threshold current densities and output powers of longitudinal modes. The steady-state rate equations [$\partial\left(f_{\mathrm{n}}, f_{\mathrm{p}}, n, p, N_l\right)/\partial t = 0$] for carriers confined in QDs, free carriers in the optical confinement layer (OCL), and photons are [18, 19, A1] *)

$$\begin{aligned}&\sigma_{\mathrm{n}} v_{\mathrm{n}} n(0,z)\left[1-f_{\mathrm{n}}(z)\right]-\sigma_{\mathrm{n}} v_{\mathrm{n}} n_{\mathrm{1}} f_{\mathrm{n}}(z)-\frac{f_{\mathrm{n}}(z) f_{\mathrm{p}}(z)}{\tau_{\mathrm{QD}}}\\&\quad-\left[f_{\mathrm{n}}(z)+f_{\mathrm{p}}(z)-1\right]\frac{c}{\sqrt{\epsilon_{\mathrm{g}}}}\frac{g^{\max}}{N_{\mathrm{S}} S}\sum_{l} G_l N_l\left(1+\cos 2k_l z\right)=0\,,\end{aligned} \tag{4.1}$$

$$\begin{aligned}&\sigma_{\mathrm{p}} v_{\mathrm{p}} p(0,z)\left[1-f_{\mathrm{p}}(z)\right]-\sigma_{\mathrm{p}} v_{\mathrm{p}} p_{\mathrm{1}} f_{\mathrm{p}}(z)-\frac{f_{\mathrm{n}}(z) f_{\mathrm{p}}(z)}{\tau_{\mathrm{QD}}}\\&\quad-\left[f_{\mathrm{n}}(z)+f_{\mathrm{p}}(z)-1\right]\frac{c}{\sqrt{\epsilon_{\mathrm{g}}}}\frac{g^{\max}}{N_{\mathrm{S}} S}\sum_{l} G_l N_l\left(1+\cos 2k_l z\right)=0\,,\end{aligned} \tag{4.2}$$

$$\begin{aligned}&\sigma_{\mathrm{n}} v_{\mathrm{n}} n_{\mathrm{1}} f_{\mathrm{n}}(z) N_{\mathrm{S}}\delta(x)-\sigma_{\mathrm{n}} v_{\mathrm{n}} n(x,z)\left(1-f_{\mathrm{n}}(z)\right) N_{\mathrm{S}}\delta(x)\\&\quad-Bn(x,z)p(x,z)+D_{\mathrm{n}}\left(\frac{\partial^2 n(x,z)}{\partial x^2}+\frac{\partial^2 n(x,z)}{\partial z^2}\right)=0\,,\end{aligned} \tag{4.3}$$

$$\begin{aligned}&\sigma_{\mathrm{p}} v_{\mathrm{p}} p_{\mathrm{1}} f_{\mathrm{p}}(z) N_{\mathrm{S}}\delta(x)-\sigma_{\mathrm{p}} v_{\mathrm{p}} p(x,z)\left(1-f_{\mathrm{p}}(z)\right) N_{\mathrm{S}}\delta(x)\\&\quad-Bn(x,z)p(x,z)+D_{\mathrm{p}}\left(\frac{\partial^2 p(x,z)}{\partial x^2}+\frac{\partial^2 p(x,z)}{\partial z^2}\right)=0\,,\end{aligned} \tag{4.4}$$

$$N_l\frac{c}{\sqrt{\epsilon_{\mathrm{g}}}}\int_0^L g^{\max} G_l\left[f_{\mathrm{n}}(z)+f_{\mathrm{p}}(z)-1\right]\left(1+\cos 2k_l z\right)\frac{dz}{L}-N_l\frac{c}{\sqrt{\epsilon_{\mathrm{g}}}}\beta=0\,, \tag{4.5}$$

*) "A" in the reference number indicates the publications of the author of this dissertation.

where $\sigma_{n,p}$ are the cross sections of electron and hole capture into a QD, $v_{n,p}$ and $D_{n,p}$ are the thermal velocities and diffusion constants of electrons and holes, respectively, τ_{QD} is the spontaneous radiative lifetime in a QD, c is the light velocity in vacuum, $\sqrt{\epsilon_g}$ is the group index of the dispersive OCL material, which is assumed to be the same for all modes, B is the radiative constant for the OCL, N_S is the surface density of QDs, $S = WL$ is the cross-section of the junction, W is the lateral size of the device, L is the cavity length, $\beta = (1/L)\ln(1/R)$ is the mirror loss, and R is the facet reflectivity. We assume that R (and hence β) is the same for all modes.

The expression for the maximum value of the modal gain is [4]

$$g^{\max} = \frac{\xi}{4}\left(\frac{\lambda_1}{\sqrt{\epsilon_g}}\right)^2 \frac{1}{\tau_{QD}} \frac{\hbar}{(\Delta\varepsilon)_{inhom}} \frac{\Gamma}{a} N_S, \tag{4.6}$$

where $\xi = 1/\sqrt{2\pi}$ for the Gaussian QD-size distribution, λ_1 is the wavelength of the main mode in vacuum, Γ is the optical confinement factor in the QD layer [along the transverse (x) direction in the waveguide], and a is the mean size of QDs.

In (4.6),

$$(\Delta\varepsilon)_{inhom} = (q_n\varepsilon_n + q_p\varepsilon_p)\delta \tag{4.7}$$

is the inhomogeneous line broadening [4], where δ is the root mean square (RMS) of relative QD-size fluctuations, $\varepsilon_{n,p}$ are the quantized energy levels of an electron and hole in a mean-sized QD (measured from the corresponding band edges), and $q_{n,p} = -\partial\varepsilon_{n,p}/\partial \ln a$.

The quantities n_1 and p_1 are equal to $N_{c,v}^{OCL} \exp\left[-(\Delta E_{c,v} - \varepsilon_{n,p})/T\right]$, where $N_{c,v}^{OCL} = 2\left(m_{c,v}^{OCL} T/2\pi\hbar^2\right)^{3/2}$ are the conduction- and valence-band effective densities of states in the OCL, $m_{c,v}^{OCL}$ are the electron and hole effective masses in the OCL, $\Delta E_{c,v}$ are the conduction- and valence-band offsets at the QD–OCL heteroboundary, and temperature T is measured in units of energy.

In the rate equations, $f_{n,p}(z)$ are the electron and hole level occupancies in QDs and $n(x, z)$ and $p(x, z)$ are the free-electron and -hole densities in the OCL. The longitudinal-coordinate- (z-) dependence of $f_{n,p}$ is caused by such dependence of the light intensity. Since n and p are coupled to $f_{n,p}$ through the processes of capture/escape into/from QDs, nonuniformity of the level

occupancies in QDs leads to nonuniform carrier distributions in the OCL along the z-direction. The free-carrier densities also depend on the transverse coordinate x (direction of current injection – see Fig. 4.3). The nonuniformity of n and p along the z-direction becomes less manifested away from the QD layer toward the boundaries between the OCL and the cladding layers ($x = \pm b/2$).

Since the QD size is much smaller than the OCL thickness, the QD layer is considered as a delta-layer placed in the plane $x = 0$ [hence the delta-function enters into eqs. (4.3) and (4.4)].

The number of photons in the l-th longitudinal mode is denoted N_l. The z-dependence of the light intensity of the l-th mode is accounted for by the factor $1 + \cos 2k_l z$ (which reflects the standing-wave nature of the mode – see Fig. 4.3), where $k_l = \left(2\pi/\lambda_l\right)\sqrt{\in_{\mathrm{g}}}$ is the wavenumber and λ_l is the wavelength of the mode in vacuum.

G_l is the lineshape factor of the gain for the l-th mode [18, 19]. For the Gaussian distribution of QD size fluctuations (see also Fig. 4.4),

$$G_l = \exp\left\{-\frac{1}{2}\left[\frac{(l-1)\Delta E}{(\Delta\varepsilon)_{\mathrm{inhom}}}\right]^2\right\}, \tag{4.8}$$

where $\Delta E = \hbar\left(c/\sqrt{\in_{\mathrm{g}}}\right)(\pi/L)$ is the separation between the photon energies of neighboring longitudinal modes in a Fabry-Perot cavity. The main mode ($l = 1$) is assumed to coincide with the gain spectrum peak ($G_1 = 1$). In Fig. 4.4, each vertical column indicates the value of G_l for a certain longitudinal mode. The dashed curve shows the continuous envelope function. From this figure we can see the rapid decreasing of the gain with increasing mode order.

The injection current density flowing in the transverse (x) direction can be presented as

$$\begin{aligned} j = eB\left\langle \int_{-b/2}^{b/2} n(x,z)p(x,z)\,dx \right\rangle + \frac{eN_{\mathrm{S}}}{\tau_{\mathrm{QD}}}\left\langle f_{\mathrm{n}}(z)f_{\mathrm{p}}(z)\right\rangle \\ + eN_{\mathrm{S}}\left\langle \left[f_{\mathrm{n}}(z)+f_{\mathrm{p}}(z)-1\right]\frac{c}{\sqrt{\in_{\mathrm{g}}}}\frac{g^{\max}}{N_{\mathrm{S}}S}\sum_l G_l N_l\left(1+\cos 2k_l z\right)\right\rangle, \end{aligned} \tag{4.9}$$

where b is the OCL thickness, and $\langle\ \rangle$ means averaging in the z-direction. The first and second terms in the right-hand side are the current densities of spontaneous recombination in the OCL and in QDs; the third term is the current density of stimulated recombination in QDs.

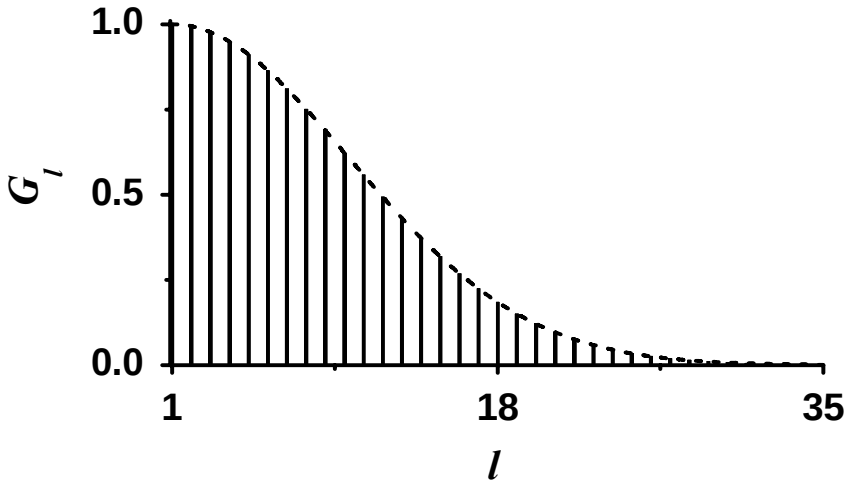

Fig. 4.4. Lineshape factor of the gain against longitudinal mode order in a Fabry-Perot cavity QD laser.

The optical power output from the mirrors is

$$P = \sum_l \hbar\omega_l \frac{N_l}{\tau_{\text{mirror}}} = \sum_l \hbar\omega_l \frac{c}{\sqrt{\epsilon_g}} \beta N_l , \tag{4.10}$$

where $\hbar\omega_l$ is the energy of photons in the l-th mode and we used the expression

$$\frac{1}{\tau_{\text{mirror}}} = \frac{c}{\sqrt{\epsilon_g}} \beta \tag{4.11}$$

for the rate at which photons escape the cavity through the mirrors [14].

For illustration of results, a GaInAsP-InP heterostructure is considered in this chapter. Room temperature continuous-wave operation near 1.55 μm is assumed. The values of parameters are (the same throughout this chapter unless otherwise specified): a = 150 Å, b = 0.28 μm, δ = 0.025, $N_S = 6.11 \times 10^{-10}$ cm^{-2}, L = 500 μm, and β = 22.79 cm^{-1}.

4.3. Maximum number of longitudinal modes

As mentioned in the introduction to this chapter, with increasing injection current, the lasing conditions for higher-order modes can be satisfied and hence more modes will appear in the

cavity. However, as shown in this section [A2, A3], the number of modes remains limited with increasing injection current.

From eq. (4.5), we obtain the following lasing condition for the l-th mode:

$$g^{\max} G_l \int_0^L \left[f_{\rm n}(z) + f_{\rm p}(z) - 1\right]\left(1 + \cos 2k_l z\right)\frac{dz}{L} = \beta\,, \tag{4.12}$$

which is the equality of the gain of the mode [weighted by the function $(1+\cos 2k_l z)$ presenting the spatial nonuniformity of the light intensity of the mode along the cavity length L in the z-direction and averaged over that direction] to the mirror loss.

It is seen from eq. (4.8) (and also Fig. 4.4) that, with increasing l, G_l decreases and hence satisfying (4.12) becomes more difficult. Also, since $f_{\rm n,\,p}(z) \le 1$, the integral in eq. (4.12) is limited by unity. Therefore, the lasing condition (4.12) can only be satisfied for a certain number of modes, which means the number of oscillating modes will remain limited with increasing injection current density j. The use of the maximum value of the integral (unity) will give us an upper estimate for the maximum number of modes,

$$l^{\max} = 1 + \left[\frac{(\Delta\varepsilon)_{\rm inhom}}{\Delta E}\sqrt{2\ln\frac{g^{\max}}{\beta}}\right]. \tag{4.13}$$

In eqs. (4.13) and (4.14)–(4.17) below, $[x]$ means the integer part of x (the largest integer less than or equal to x). With (4.6) and using the expressions for $(\Delta\varepsilon)_{\rm inhom}$ [eq. (4.7)], ΔE, and β, we can express $l^{\max}$ in terms of the QD structure parameters (δ, $N_{\rm S}$, and L),

$$l^{\max}(\delta) = 1 + \left[\frac{\left(q_{\rm n}\varepsilon_{\rm n} + q_{\rm p}\varepsilon_{\rm p}\right)\delta}{\Delta E}\sqrt{2\ln\frac{\delta_1^{\max}}{\delta}}\right], \tag{4.14}$$

$$l^{\max}(N_{\rm S}) = 1 + \left[\frac{(\Delta\varepsilon)_{\rm inhom}}{\Delta E}\sqrt{2\ln\frac{N_{\rm S}}{N_{\rm S,1}^{\min}}}\right], \tag{4.15}$$

$$l^{\max}(L) = 1 + \left[\left\{L\Big/\left(\hbar\frac{c}{\sqrt{\in_{\rm g}}}\frac{\pi}{(\Delta\varepsilon)_{\rm inhom}}\right)\right\}\sqrt{2\ln\frac{L}{L_1^{\min}}}\right], \tag{4.16}$$

where $\delta_1^{\max}$, $N_{S,1}^{\min}$, and $L_1^{\min}$ are the critical values of δ, N_S, and L beyond which the main mode can not lase (see [4, 19, 22] for the expressions for $\delta_1^{\max}$, $N_{S,1}^{\min}$, and $L_1^{\min}$). As will be seen later, for each higher-order longitudinal mode, there also exist unique critical values of parameters.

The dependence of $l^{\max}$ on each of the structure parameters is shown by the boundary between the two regions in Fig. 4.5.

As seen from Fig. 4.5(a), the maximum number of modes remains limited (first increases and then decreases) with varying δ, $l^{\max} \to 1$ both as $\delta \to 0$ and $\delta \to \delta_1^{\max}$ — the point is that if $\delta \to 0$, we have an ideally uniform QD-ensemble with a delta-function gain spectrum, and there should be only main mode lasing; if $\delta \to \delta_1^{\max}$, lasing of the main mode itself (the mode with the highest gain) becomes hard to attain.

At a certain values of δ given by $\delta_1^{\max}/\sqrt{e}$, where e is the base of the natural logarithm, $l^{\max}$ peaks [Fig. 4.5(a)]. The expression for the peak value of $l^{\max}$ is

$$1+\left[\frac{\left(q_n\varepsilon_n+q_p\varepsilon_p\right)\left(\delta_1^{\max}/\sqrt{e}\right)}{\Delta E}\right] \tag{4.17}$$

[in Fig. 4.5(a), this peak value is 15]. This nonmonotonic behavior is also readily seen from eq. (4.14). Taking into account that ΔE is the separation between the photon energies of the neighboring modes, expression (4.17) simply gives the number of modes that can be accommodated within the inhomogeneous linewidth $(\Delta\varepsilon)_{\text{inhom}} = \left(q_n\varepsilon_n + q_p\varepsilon_p\right)\delta$ corresponding to the RMS of QD size fluctuations $\delta = \delta_1^{\max}/\sqrt{e}$.

It should be noted that there is homogeneous broadening of the gain spectrum in addition to inhomogeneous broadening. Even if the QD ensemble is ideally uniform ($\delta \to 0$), the gain spectrum will not be a delta-function, and there can be more than one mode lasing depending on other parameters of the structure. Within the framework of our model, this can be formally accounted for by considering the inhomogeneous broadening $(\Delta\varepsilon)_{\text{inhom}} = (q_n\varepsilon_n + q_p\varepsilon_p)\delta$ values down to the homogeneous linewidth $(\Delta\varepsilon)_{\text{hom}}$, i.e., by considering the values of δ down to $(\Delta\varepsilon)_{\text{hom}}/(q_n\varepsilon_n + q_p\varepsilon_p)$.

With increasing surface density of QDs or cavity length, the maximum number of modes that can oscillate in a laser increases [see eqs. (4.15) and (4.16), and also Figs. 4.5(b) and (c)].

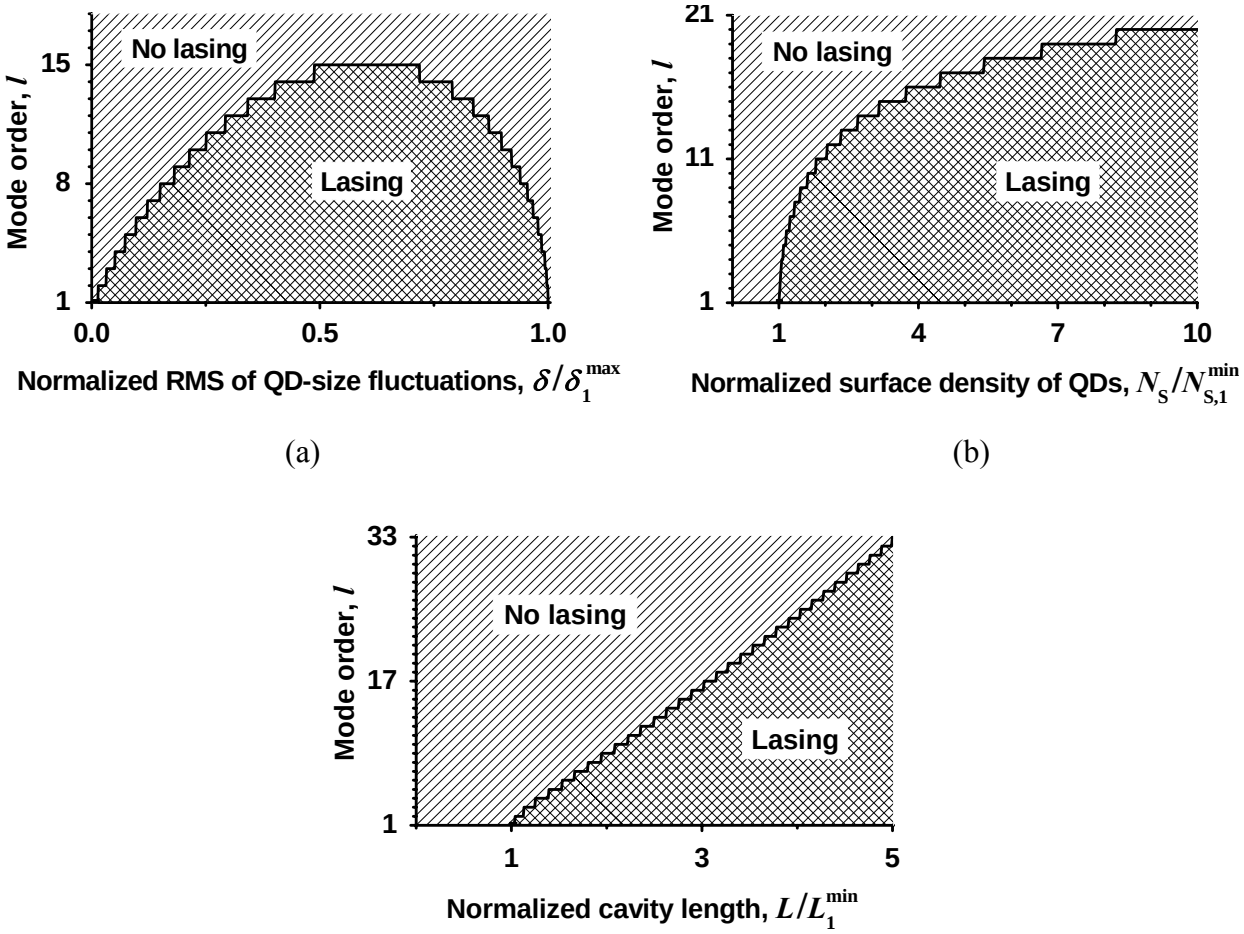

Fig. 4.5. "Lasing" and "no lasing" regions of values of the structure parameter and longitudinal mode order. The parameter is normalized to its critical tolerable value for the main ($l = 1$) mode. The boundary of "lasing" and "no lasing" regions represents the maximum number of modes which can oscillate at a given structure parameter [(4.14), (4.15), and (4.16) for (a), (b), and (c), respectively]. (Fig. 1 of ref. [A2], © [2008] IEEE.)

The cross-hatched area in Fig. 4.5 presents the two-dimensional region of the values of the structure parameter and mode order l for which the lasing is attainable. As already discussed above, the boundary of the "lasing" and "no lasing" regions gives the maximum number l^{max} of modes that can oscillate at a given structure parameter. Alternatively, if the functional relationship between the abscissa and ordinate is interchanged, the same boundary represents the critical tolerable value of the parameter for lasing of a given l-th mode. These critical tolerable

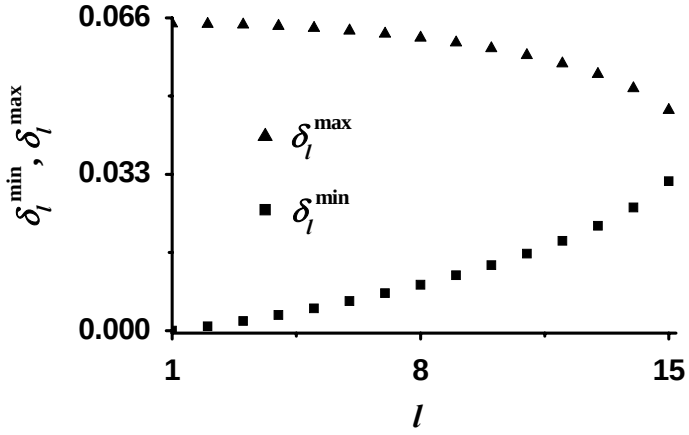

(a)

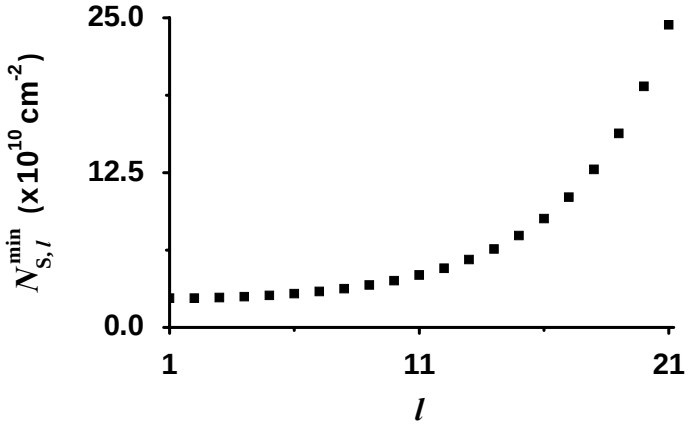

(b)

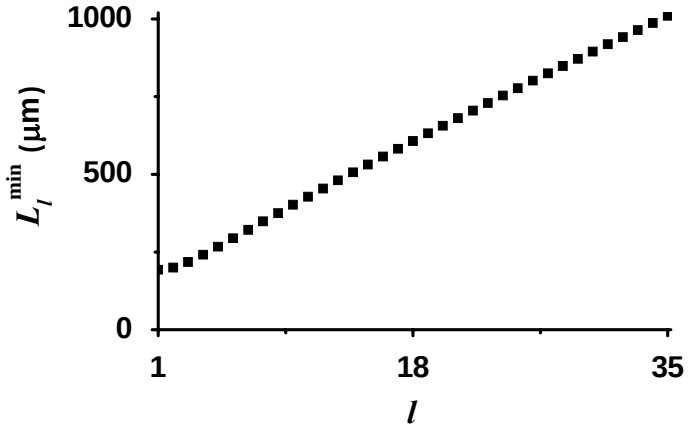

(c)

Fig. 4.6. Critical values of δ (a), N_S (b), and L (c) for the l-th mode. Lasing of the l-th mode is only possible if $\delta_l^{\min} \le \delta \le \delta_l^{\max}$, $N_S \ge N_{S,l}^{\min}$, and $L \ge L_l^{\min}$.

parameters are the maximum RMS of QD-size fluctuations $\delta_l^{\max}$ [the declining portion of the boundary in Fig. 4.5(a)], minimum surface density of QDs $N_{\mathrm{S},l}^{\min}$, and minimum cavity length $L_l^{\min}$. It is notable that for each higher-order ($l \geq 2$) mode there also exists a nonvanishing, minimum RMS of QD-size fluctuations $\delta_l^{\min}$ [the rising portion of the boundary in Fig. 4.5(a)] — the QD ensemble should be nonuniform enough, i.e., the gain spectrum sufficiently broad for a given higher-order mode to appear.

Using eqs. (4.14)–(4.16), the critical tolerable parameters can be found as functions of mode order l – see Fig. 4.6. The equations for $\delta_l^{\min}$, $\delta_l^{\max}$, and $L_l^{\min}$ are transcendental and thus can only be solved numerically; the expression for $N_{\mathrm{S},l}^{\min}$ is

$$N_{\mathrm{S},l}^{\min} = N_{\mathrm{S},1}^{\min} \exp\left\{\frac{1}{2}\left[\frac{(l-1)\Delta E}{(\Delta\varepsilon)_{\mathrm{inhom}}}\right]^2\right\}. \tag{4.18}$$

Hence the l-th mode can only oscillate when δ is between $\delta_l^{\min}$ and $\delta_l^{\max}$ [Fig. 4.6(a)], N_{S} is larger than $N_{\mathrm{S},l}^{\min}$ [Fig. 4.6(b)], and L is longer than $L_l^{\min}$ [Fig. 4.6(c)].

4.4. Numerical approach

In the previous section, the maximum number of modes that can oscillate in a QD laser was estimated analytically using the lasing condition (4.12) [derived from the rate equation (4.5) for photons]. To obtain the threshold current density of each mode and the output power at a given injection current density, we need to solve the entire set of rate equations (4.1)–(4.5) [A1].

In [18, 19], the consideration of SHB was restricted to the case of injection currents slightly exceeding the threshold current for the main mode (small output powers); the set of rate equations was linearized and the solutions were found analytically.

Here, the effect of SHB on high power operation of the laser is studied. We therefore consider high injection currents when the set of eqs. (4.1)–(4.5) can only be solved numerically. We use the finite difference method. The method has been extensively used for simulation of semiconductor devices [23], and particularly optoelectronic devices [24]. Eqs. (4.3) and (4.4) are nonlinear partial differential equations. By applying the finite difference method, eqs. (4.1)–(4.5)

are discretized and a set of nonlinear algebraic equations is obtained. Newton's iteration method [25] is used to solve this set of algebraic equations.

Calculation of the threshold current density j_{th1} for the first mode is a one-dimensional problem in the transverse (x) direction. This is because there is no stimulated emission (and hence no SHB) at the injection current density values $j < j_{th1}$; the level occupancies and carrier densities are uniform along the longitudinal (z) direction.

Starting with the second mode, the problem of calculation of the threshold current density becomes two-dimensional (in x and z directions) since it involves the stimulated-light intensities of existing modes. These intensities are nonuniform in the z-direction, and so are the level occupancies and carrier densities.

Only the main mode oscillates in the cavity at $j_{th1} < j < j_{th2}$, where j_{th2} is the threshold current density for the second mode. The light intensity is periodic in the z-direction with period equal to the half-wavelength of the main mode in the OCL, $\lambda_1 / \left(2\sqrt{\epsilon_g}\right)$. For this reason, the level occupancies in QDs and carrier densities in the OCL are also periodic. We therefore took advantage of the fact that only one period in the z-direction can be considered in the computation of j_{th2} and of output power at $j_{th1} < j < j_{th2}$.

Computation of the threshold current densities of the third and higher modes, and of powers of the second and higher modes is more time-consuming since the periodic condition can not be used. This is because above the second mode threshold ($j > j_{th2}$), the total light intensity is not periodic in the z-direction — it presents the superposition of the intensities of individual modes, each having a slightly different period $\lambda_l / \left(2\sqrt{\epsilon_g}\right)$. Consequently, the level occupancies and free-carrier densities, being coupled to the overall light intensity, are also not periodic.

If the mirror reflectivity is the same at both edges of the cavity, the total light intensity and hence the level occupancies in QDs and carrier densities in the OCL will be symmetric with respect to the center of the cavity. The z-dependences can be computed for half of the cavity length $L/2$ in this case.

The numerical computation results and discussions are presented in Sections 4.5–4.8.

4.5. Spatial distribution of the optical intensity and population inversion in QDs

Fig. 4.7 shows the population inversion in QDs versus the longitudinal coordinate within the length range equal to $\lambda_1/\left(2\sqrt{\epsilon_g}\right)$. As seen from the figure, nonuniformity of the population inversion becomes stronger away from the cavity center toward its edge. The reason is, at the injection current density used in the figure (j = 10 kA/cm^2), there is more than one mode lasing in the cavity. Due to the standing wave nature, superposition of the light intensities of the modes results in an envelope function for the total light intensity. The spatial variation of the envelope occurs on the cavity-length scale, i.e., it is much slower compared to rapid undulations of the intensities of individual modes, which occur on the length scale of $\lambda_l/\left(2\sqrt{\epsilon_g}\right)$. A simple analytical consideration below shows that the total light intensity is maximum at the cavity edge. Consequently, SHB is most strongly manifested and the population inversion is most nonuniform at the mirrors.

The z-dependence of the total optical intensity is given by the sum in (4.1) and (4.2). Denote the sum by $s(z)$,

$$s(z) = \sum_l G_l N_l \left(1 + \cos 2k_l z\right). \tag{4.19}$$

Taking into account that $k_l = \left(2\pi/\lambda_l\right)\sqrt{\epsilon_g} = \left(\pi/L\right) m_l$, where m_l is an integer number [number of half-wavelengths $\lambda_l/\left(2\sqrt{\epsilon_g}\right)$ of the l-th mode in the OCL material, which are accommodated within the Fabry-Perot cavity length L], we can write $s(z)$ as

$$s(z) = \sum_l G_l N_l \left(1 + \cos\frac{2\pi}{L} m_l z\right). \tag{4.20}$$

At either edge of the cavity (z = 0 or L), all the cosine terms in (4.20) are equal to unity, and thus $s(z)$ is maximum,

$$s(0) = s(L) = \sum_l 2G_l N_l \,. \tag{4.21}$$

In the center of the cavity ($z = L/2$), the cosine terms in (4.20) are equal to $(-1)^{m_l}$,

$$s\left(\frac{L}{2}\right)=\sum_l G_l N_l\left(1+\cos\pi m_l\right)=\sum_l\left[1+\left(-1\right)^{m_l}\right]G_l N_l\,. \tag{4.22}$$

Every other term $[1+(-1)^{m_l}]$ (namely, every term with an odd m_l) is zero in (4.22), and hence $s(z)$ is minimum.

As seen from (4.21) and (4.22), the larger is the number of modes, the more nonuniform is the envelope of the optical intensity (the larger is the ratio of maximum to minimum intensity). If only the main mode is lasing, the envelope is uniform — the intensity averaged over the length $\lambda_1/\left(2\sqrt{\epsilon_g}\right)$ is uniform along the z-direction.

Thus, the variation of the population inversion within the half-wavelength range $\lambda_1/\left(2\sqrt{\epsilon_g}\right)$ (each of the two curves in Fig. 4.7) is the manifestation of SHB, which is inherent in QD lasers. The variation of the population inversion within the cavity-length range (i.e., the fact that the curves in Fig. 4.7 differ from each other) is the manifestation of SHB, which generally occurs in Fabry-Perot cavity diode lasers.

We used $\cos k_l z$ for the z-dependence of the electric field of the l-th mode. The use of the general form, $\cos(k_l z + \varphi)$, where the phase φ is a function of the mirror reflectivity R, will not significantly affect the results. The point is that SHB, which is specific to QD lasers, occurs on the half-wavelength scale and is caused by a standing-wave nature of the mode intensity, which is adequately accounted for by $\cos k_l z$. As for SHB on the cavity-length scale, the use of φ will shift the intensities of modes and the envelope function of the total light intensity. As seen from

$$\cos\left(k_l z+\varphi\right)=\cos k_l\left(z+\varphi/k_l\right), \tag{4.23}$$

the shift is equal to φ/k_l. Since the absolute value of the phase can not exceed 2π ($|\varphi|\le 2\pi$), then $\left|\varphi/k_l\right|=\left|\varphi/2\pi\right|\lambda_l/\sqrt{\epsilon_g}\le\lambda_l/\sqrt{\epsilon_g}$, i.e., the shift is less than the wavelength in the medium. Hence the position of the maximum (minimum) of the envelope function of the total light intensity will shift from the edge (center) of the cavity by less than $\lambda_l/\sqrt{\epsilon_g}$, which is negligible compared to the cavity length L.

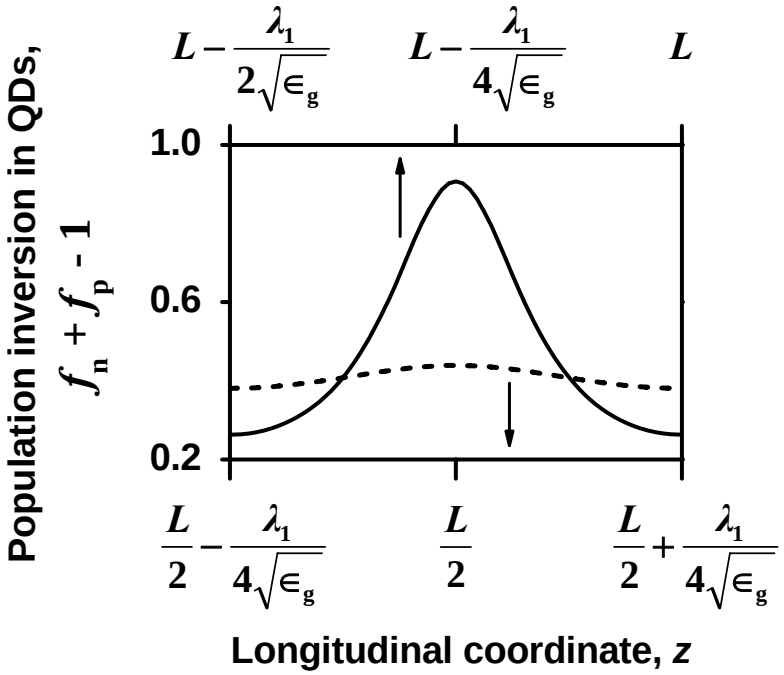

Fig. 4.7. Spatial distribution of the population inversion in QDs at the edge (solid curve, top axis) and center (dashed curve, bottom axis) of the cavity. In both the top and bottom axes, the length range is the period of the light intensity of the main mode in the OCL material, $\lambda_1/\left(2\sqrt{\epsilon_g}\right)$. The injection current density is $j = 10$ kA/cm^2; five modes oscillate in the cavity at this value of j. (Fig. 2 of ref. [A1], reprinted with permission of IOP Publishing Ltd.)

4.6. Threshold current densities for the main and higher-order modes

In Section 4.3, to estimate the maximum number of longitudinal modes that can oscillate in a QD laser, we used the maximum values of the level occupancies ($f_{n,p} = 1$) and hence the maximum value of the integral (unity) in (4.12). For this reason, eq. (4.13) presents an upper estimate for the number of longitudinal modes in a QD laser. The actual number of modes will be less than that given by (4.13). Hence the boundary between the "lasing" and "no lasing" regions (Fig. 4.5) will be lowered — the actual region of allowed values of the structure parameters ("lasing" region) will be more restricted compared to that in Fig. 4.5. For $l \geq 2$, the actual $\delta_l^{\min}$ ($\delta_l^{\max}$) will be greater (smaller) than that obtained from (4.14), $N_{S,l}^{\min}$ will be higher

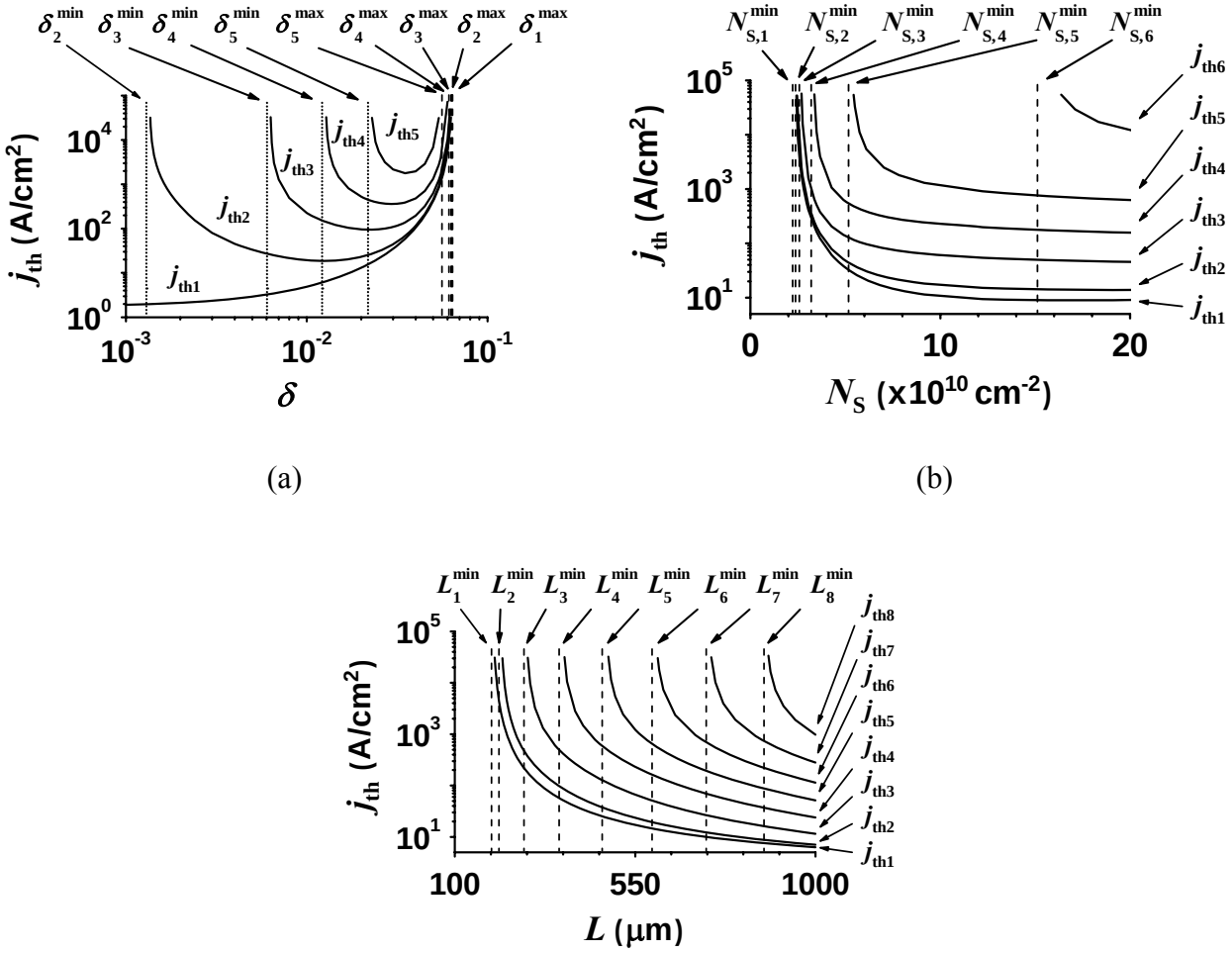

Fig. 4.8. Threshold current densities for the main ($l = 1$) and higher-order longitudinal modes against (a) RMS of QD-size fluctuations, (b) surface density of QDs, and (c) cavity length. The vertical dashed lines in (a) show δ_l^{max} ($l \geq 1$), the vertical dotted lines show δ_l^{min} ($l \geq 2$). The vertical dashed lines in (b) and (c) show $N_{S,l}^{min}$ and L_l^{min}, respectively. (Fig. 3 of ref. [A1], reprinted with permission of IOP Publishing Ltd.)

than that given by (4.18), and L_l^{min} will be longer than that obtained from (4.16). To calculate the actual number of modes and critical values of δ, N_S, and L requires knowledge of the level occupancies $f_{n,p}$. Not only do $f_{n,p}$ depend on the coordinate z and injection current density j, but they also depend on the parameters describing the physical processes in the structure. Thus, in

the case of spatial hole burning, a key process is the carrier exchange between neighboring QDs [18, 19]. For this reason, the number of lasing modes (and the critical values of δ, N_S, and L for $l \geq 2$) will depend on the electron and hole escape times from QDs and diffusion coefficients in the OCL [18, 19].

Fig. 4.8 shows the threshold current densities for the lasing modes versus the structure parameters: RMS of QD-size fluctuations δ, surface density of QDs N_S, and cavity length L. The tendencies of the curves clearly demonstrate the existence of critical values of the structure parameters for each longitudinal mode, which is qualitatively in consistence with the analytical results of Section 4.3. The positions of the critical values are approximately indicated by the vertical lines.

With increasing δ [Fig. 4.8(a)], the threshold current densities for the higher-order modes first decrease and then increase.

With increasing N_S [Fig. 4.8(b)], the threshold current densities decrease rapidly away from the critical values of N_S; the decrease then becomes much slower. The threshold current densities for all modes will finally increase with N_S.

With increasing L [Fig. 4.8(c)], the threshold current density for each mode decreases, hence more modes will lase at a given injection current density.

4.7. Output optical power

Figs. 4.9–4.11 show the output powers of the lasing modes versus the injection current density (light-current curves – LCCs) at different values of the structure parameters.

The QD ensemble is so uniform in Fig. 4.9(a) that only the main mode lases. As discussed above, the number of the lasing modes first increases [Fig. 4.9(b)] and then decreases [Fig. 4.9(c)] with increasing QD-size nonuniformity; there will be no lasing at $\delta > \delta_1^{\max}$.

As a higher-order mode starts lasing with increasing j, redistribution of stimulated recombination occurs among the modes — the stimulated recombination in the newly appeared mode consumes a fraction of injected carriers. The redistribution leads to kinks in the LCCs of existing modes at j equal to the threshold current density of a new mode; this finding is in line with that of [15]. The kinks are seen in the inset in Fig. 4.9(b) and also in Fig. 4.9(c) and Fig. 4.11(a). The more modes lase in the cavity, the weaker is the effect of an extra mode.

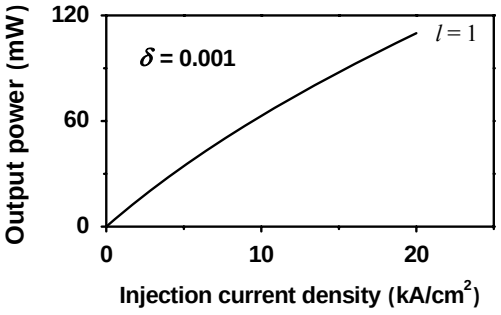

(a)

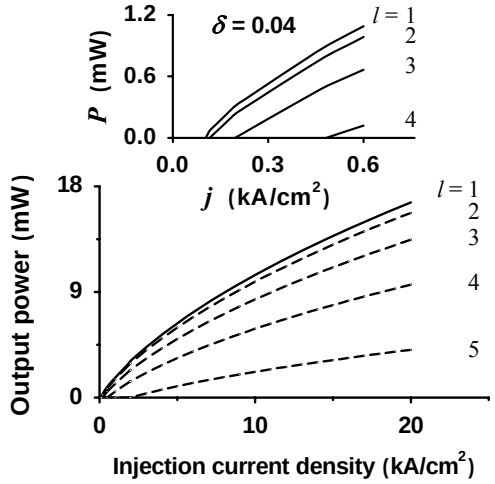

(b)

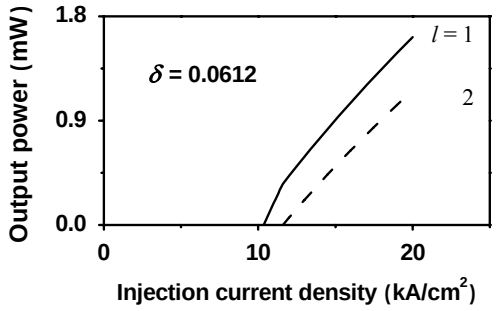

(c)

Fig. 4.9. Optical power of the main (solid curve) and higher-order longitudinal modes (dashed curves) against injection current density at different values of the RMS of QD-size fluctuations δ. The kink in the LCC of the main mode at the second mode threshold ($j = j_{th2}$) is seen in (c). Three, two, and one kink in the LCCs of the first (main), second, and third modes, respectively, are seen in the inset in (b). (Fig. 4 of ref. [A1], reprinted with permission of IOP Publishing Ltd.)

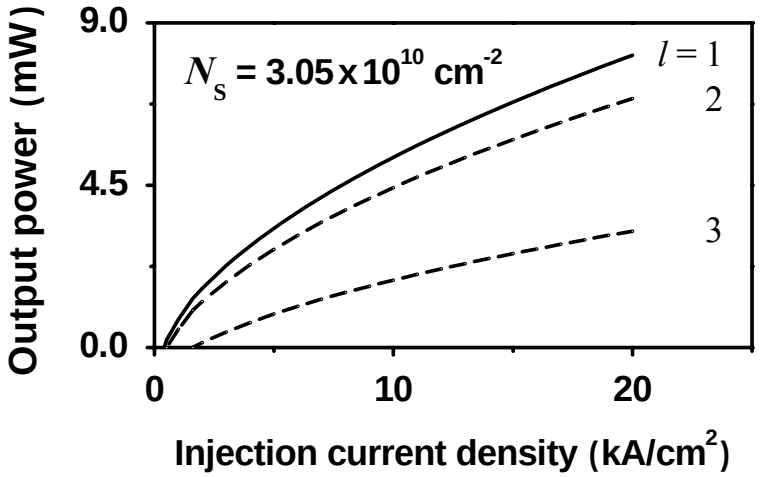

(a)

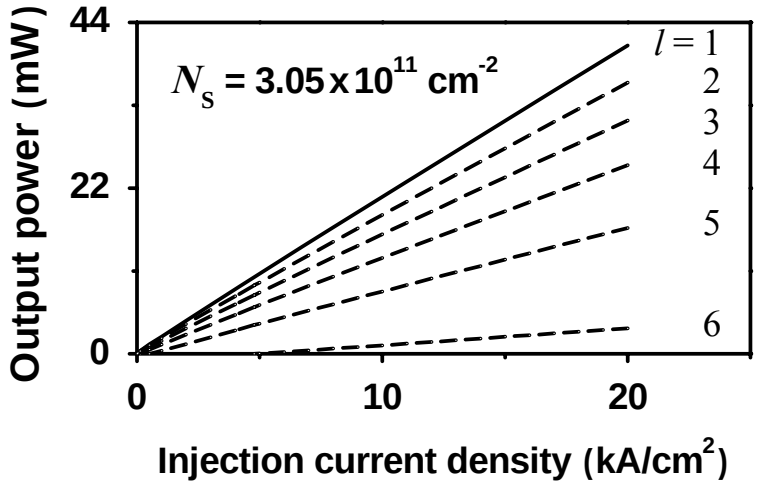

(b)

Fig. 4.10. Optical power of the main (solid curve) and higher-order longitudinal modes (dashed curves) against injection current density at different values of the surface density of QDs N_S. (Fig. 5 of ref. [A1], reprinted with permission of IOP Publishing Ltd.)

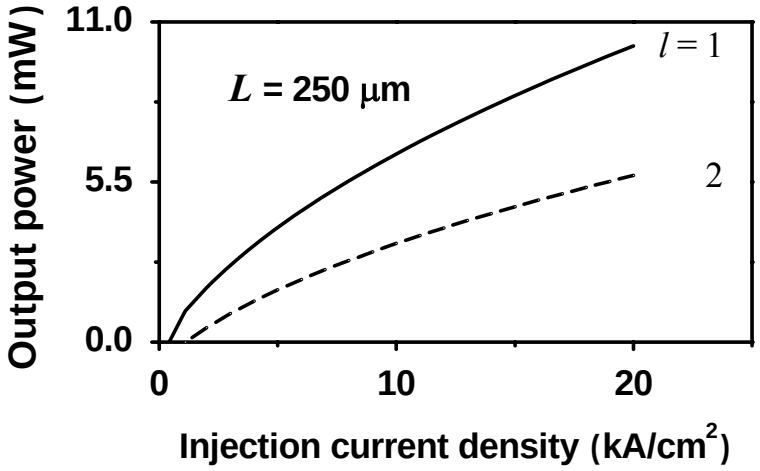

(a)

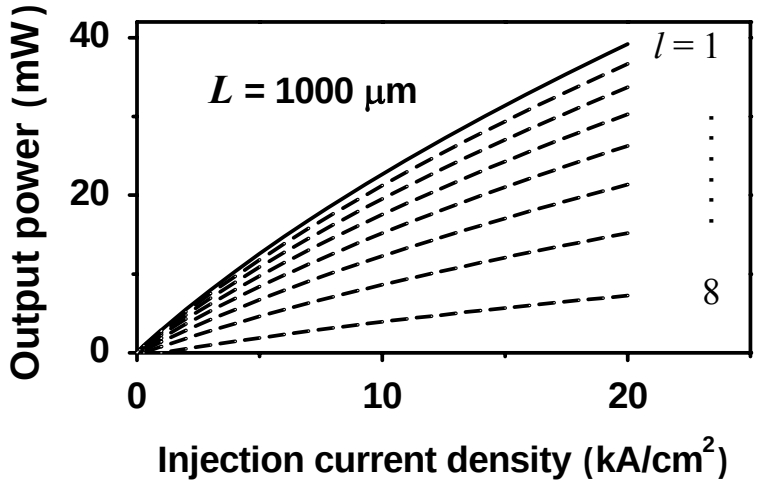

(b)

Fig. 4.11. Optical power of the main (solid curve) and higher-order longitudinal modes (dashed curves) against injection current density at different values of the cavity length *L*. (Fig. 6 of ref. [A1], reprinted with permission of IOP Publishing Ltd.)

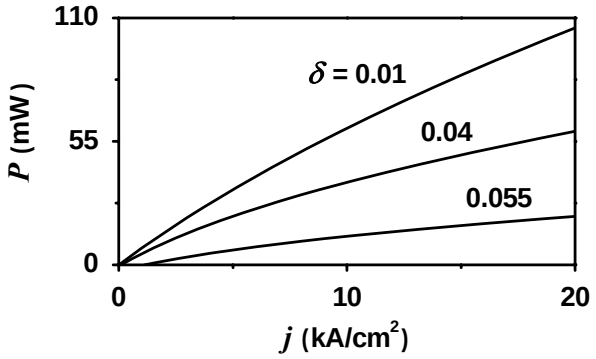

(a)

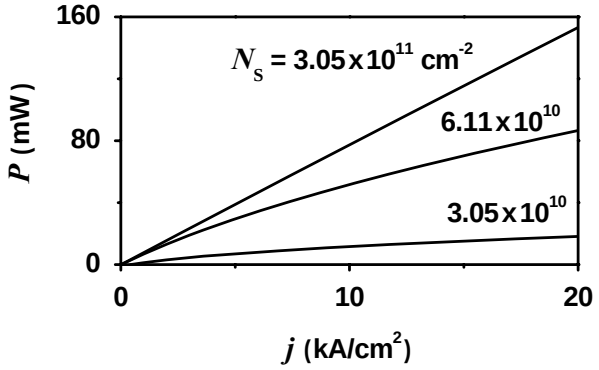

(b)

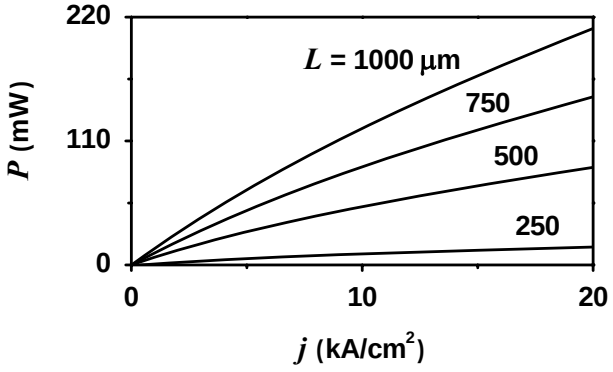

(c)

Fig. 4.12. Total optical power against injection current density at different values of the RMS of QD-size fluctuations δ (a), surface density of QDs N_S (b), and cavity length L (c). (Fig. 7 of ref. [A1], reprinted with permission of IOP Publishing Ltd.)

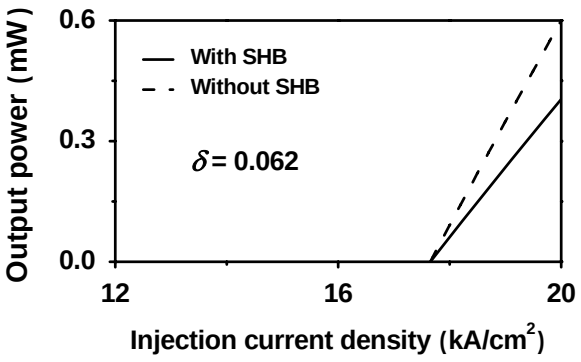

(a)

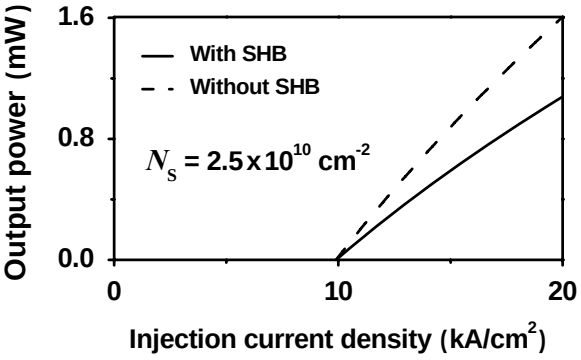

(b)

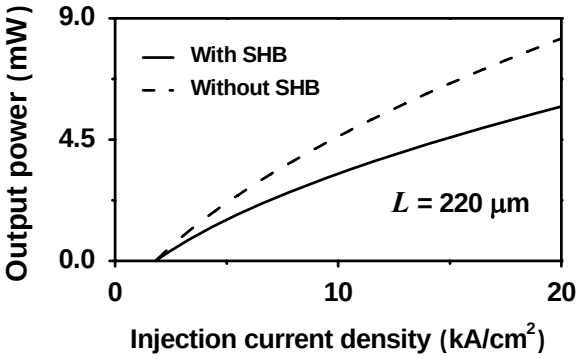

(c)

Fig. 4.13. Optical power of the main (and the only lasing) mode against injection current density calculated including (solid curve) and neglecting (dashed curve) SHB. The structure parameter is close to its critical tolerable value [$\delta_1^{\max}$ in (a), $N_{S,1}^{\min}$ in (b), and $L_1^{\min}$ in (c)]. (Fig. 8 of ref. [A1], reprinted with permission of IOP Publishing Ltd.)

Fig. 4.12 shows the total output power of all lasing modes versus the injection current density at different values of the structure parameters. With decreasing δ, or increasing N_S or L, the output power (at a given injection current) increases, and the overall LCC becomes more linear. One way of increasing N_S is to use multiple layers with QDs.

SHB reduces the power of the main mode even if there is no multimode generation (Fig. 4.13). This is the situation when any of the structure parameters is so close to its critical value for lasing of the main mode that all higher-order modes are cut off. The reduction of the power in this case is entirely due to nonuniform carrier distribution in the presence of SHB. Owing to this nonuniformity, the fraction of the spontaneous recombination is increased, and consequently that of the stimulated recombination is decreased.

4.8. Number of lasing modes as a function of current density

Figs. 4.14 and 4.15 show how the number of lasing modes evolves with injection current density at different temperatures and cavity lengths. As the temperature rises, the threshold current densities for the main and higher-order modes increase. While the increase of the threshold current density for the main mode is unwanted, the increase of the threshold current densities for the higher-order modes is wanted since it leads to a reduced number of modes lasing at a given injection current density (Figs. 4.14 and 4.15). The mechanism behind these temperature-dependences is specific to QD lasers and related to thermal escape of carriers from QDs. With rising temperature, thermal escape becomes more intense. This leads, on the one hand, to increased electron and hole densities outside QDs and hence to an increased component of the threshold current density associated with recombination outside QDs. On the other hand, carrier exchange between neighbouring QDs and, consequently, smoothing out nonuniform population inversion become more efficient. As a result, SHB is less manifested and the number of lasing modes is reduced at a higher temperature.

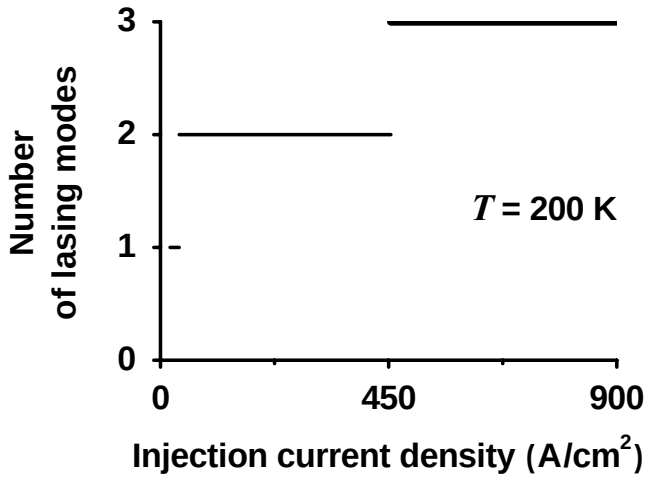

(a)

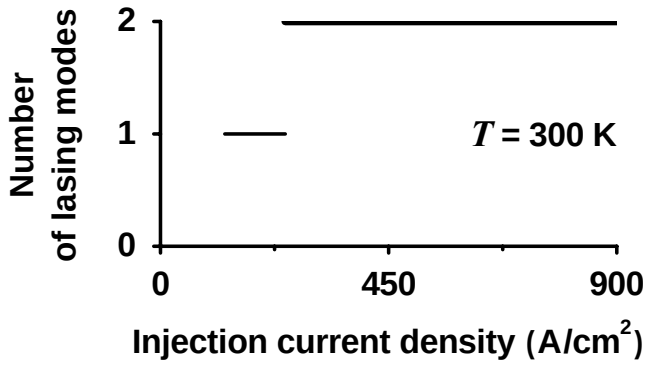

(b)

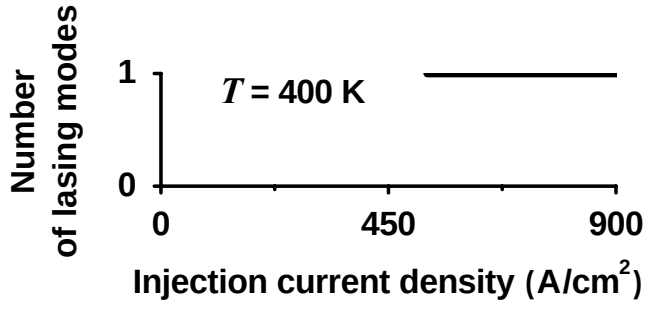

(c)

Fig. 4.14. Number of lasing modes against injection current density at different temperatures for the cavity length $L = 300$ μm. (Fig. 9(a) of ref. [A1], reprinted with permission of IOP Publishing Ltd.)

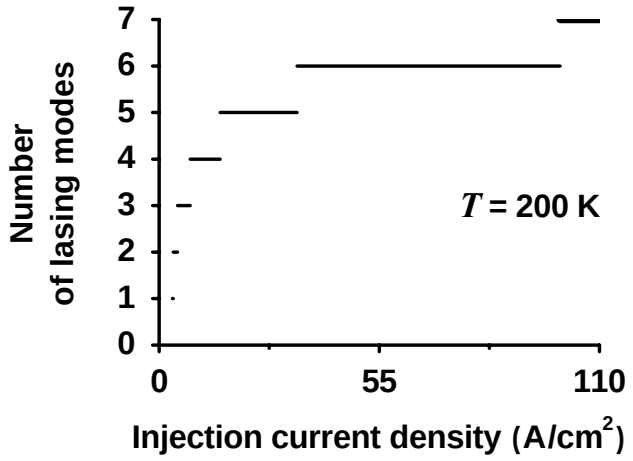

(a)

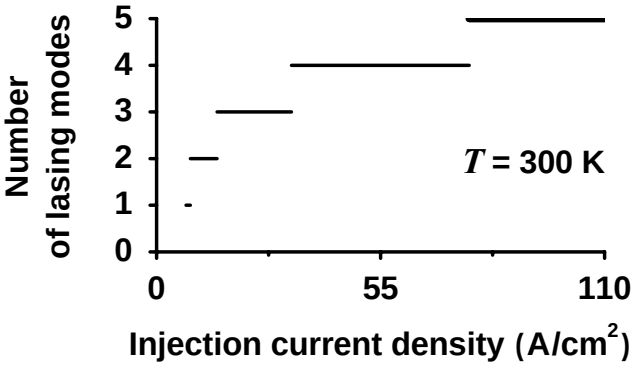

(b)

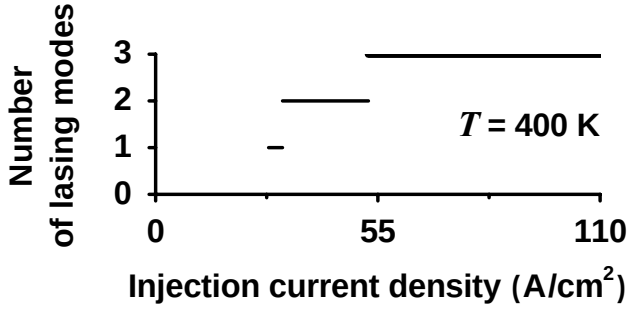

(c)

Fig. 4.15. Number of lasing modes against injection current density at different temperatures for the cavity length $L = 900$ μm. (Fig. 9(b) of ref. [A1], reprinted with permission of IOP Publishing Ltd.)

4.9. Conclusion

The QD laser operation at high injection currents (when spatial hole burning is strongly manifested) has been studied.

With increasing current, higher-order longitudinal modes start lasing in addition to the main mode. However, the number of modes remains limited. The maximum number of modes that can oscillate in a QD laser has been estimated analytically. This number increases with increasing surface density of QDs or cavity length, and remains limited with varying uniformity of the QD ensemble. The critical tolerable, cut-off values of the structure parameters for lasing of higher-order modes have been derived.

The threshold currents and optical powers of the modes have been calculated numerically. The power of the main mode is reduced due to lasing of higher-order modes and spatially nonuniform carrier distribution. As a new mode turns on, kinks appear in the LCCs of existing modes. SHB reduces the total optical power of a laser and contributes to nonlinearity of the overall LCC. The effect is more significant when any of the structure parameters is close to its critical tolerable value. The LCC becomes more linear with improving QD-size uniformity or increasing surface density of QDs or cavity length.

REFERENCES [*)]

[A1] L. Jiang and L. V. Asryan, "Multimode emission and optical power in a semiconductor quantum dot laser," *Nanotechnology*, vol. 19, no. 41, art. no. 415204 (8 pages), Oct. 2008.

[A2] L. Jiang and L. V. Asryan, "How many longitudinal modes can oscillate in a quantum dot laser: an analytical estimate," accepted for publication in *IEEE Photon. Technol. Lett.*, vol. 20, 2008.

[A3] L. Jiang and L. V. Asryan, "Maximum number of longitudinal modes oscillating in a quantum dot laser due to spatial hole burning," *International Semiconductor Device Research Symposium*. College Park, Maryland, Dec. 12–14, 2007. Paper no. WP9-18-07, 2 pages.

[1] Y. Arakawa and H. Sakaki, "Multidimensional quantum well laser and temperature dependence of its threshold current," *Appl. Phys. Lett.*, vol. 40, no. 11, pp. 939–941, June 1982.

[2] M. Asada, Y. Miyamoto, and Y. Suematsu, "Gain and the threshold of three-dimensional quantum-box lasers," *IEEE J. Quantum Electron.*, vol. QE-22, no. 9, pp. 1915–1921, Sept. 1986.

[3] D. Leonard, S. Fafard, K. Pond, Y. H. Zhang, J. L. Merz, and P. M. Petroff, "Structural and optical properties of self-assembled InGaAs quantum dots," *J. Vac. Sci. Technol. B*, vol. 12, no. 4, pp. 2516–2520, July/Aug. 1994.

[4] L. V. Asryan and R. A. Suris, "Inhomogeneous line broadening and the threshold current density of a semiconductor quantum dot laser," *Semicond. Sci. Technol.*, vol. 11, no. 4, pp. 554–567, Apr. 1996.

[5] A. Gubenko, I. Krestnikov, D. Livshtis, S. Mikhrin, A. Kovsh, L. West, C. Bomholdt, N. Grote, and A. Zhukov, "Error-free 10 Gbit/s transmission using individual Fabry-Perot

[*)] "A" in the reference number indicates the publications of the author of this dissertation.

modes of low-noise quantum-dot laser," *Electron. Lett.*, vol. 43, no. 25, pp. 1430–1431, Dec. 2007.

[6] V. P. Evtikhiev, I. V. Kudryashov, E. Yu. Kotel'nikov, V. E. Tokranov, A. N. Titkov, I. S. Tarasov, and Zh. I. Alferov, "Continuous stimulated emission at $T = 293$ K from separate-confinement heterostructure diode lasers with one layer of InAs quantum dots grown on vicinal GaAs(001) surfaces misoriented in the (010) direction in the active region," *Semiconductors*, vol. 32, no. 12, pp. 1323–1327, Dec. 1998.

[7] H. Statz, C. L. Tang, and J. M. Lavine, "Spectral output of semiconductor lasers," *J. Appl. Phys.*, vol. 35, no. 9, pp. 2581–2585, Sept. 1964.

[8] W. Streifer, R. D. Burnham, and D. R. Scifres, "Dependence of longitudinal mode structure on injected carrier diffusion in diode lasers," *IEEE J. Quantum Electron.*, vol. 13, no. 6, pp. 403–404, June 1977.

[9] T. P. Lee, C. A. Burrus, J. A. Copeland, A. G. Dentai, and D. Marcuse, "Short-cavity InGaAsP injection lasers: dependence of mode spectra and single-longitudinal-mode power on cavity length," *IEEE J. Quantum Electron.*, vol. QE-18, no. 7, pp. 1101–1113, July 1982.

[10] W. B. Joyce, "Role of the conductivity of the confining layers in DH-laser spatial hole burning effects," *IEEE J. Quantum Electron.*, vol. QE-18, no. 12, pp. 2005–2009, Dec. 1982.

[11] R. A. Suris and S. V. Shtofich, "Multifrequency stimulated emission from injection semiconductor lasers," *Sov. Phys. Semicond.*, vol. 16, no. 7, pp. 851–853, July 1982.

[12] R. A. Suris and S. V. Shtofich, "Role of impurities in the appearance of multifrequency emission from injection semiconductor lasers," *Sov. Phys. Semicond.*, vol. 17, no. 7, pp. 859–861, July 1983.

[13] H. Haken, *Light*, vol. 2 of *Laser Light Dynamics*. Amsterdam: North-Holland, 1985, p. 336.

[14] G. P. Agrawal and N. K. Dutta, *Long-Wavelength Semiconductor Lasers*. New York: Van Nostrand Reinhold, 1986, p. 473.

[15] H. Fu and H. Haken, "Multifrequency operations in a short-cavity standing-wave laser," *Phys. Rev. A*, vol. 43, no. 5, pp. 2446–2454, Mar. 1991.

[16] R. Schatz, "Longitudinal spatial instability in symmetric semiconductor lasers due to spatial hole burning," *IEEE J. Quantum Electron.*, vol. 28, no. 6, pp. 1443–1449, June 1992.

[17] M. A. Alam, "Effects of carrier transport on *L-I* characteristics of QW lasers in the presence of spatial hole burning," *IEEE J. Quantum Electron.*, vol. 33, no. 6, pp. 1018–1024, June 1997.

[18] L. V. Asryan and R. A. Suris, "Spatial hole burning and multimode generation threshold in quantum-dot lasers," *Appl. Phys. Lett.*, vol. 74, no. 9, pp. 1215–1217, Mar. 1999.

[19] L. V. Asryan and R. A. Suris, "Longitudinal spatial hole burning in a quantum-dot laser," *IEEE J. Quantum Electron.*, vol. 36, no. 10, pp. 1151–1160, Oct. 2000.

[20] L. V. Asryan, S. Luryi, and R. A. Suris, "Internal efficiency of semiconductor lasers with a quantum-confined active region," *IEEE J. Quantum Electron.*, vol. 39, no. 3, pp. 404–418, Mar. 2003.

[21] L. V. Asryan, "Maximum power of quantum dot laser versus internal loss," *Appl. Phys. Lett.*, vol. 88, no. 3, p. 073107, Feb. 2006.

[22] L. V. Asryan and S. Luryi, "Effect of internal optical loss on threshold characteristics of semiconductor lasers with a quantum-confined active region," *IEEE J. Quantum Electron.*, vol. 40, no. 7, pp. 833–843, July 2004.

[23] S. Selberherr, *Analysis and simulation of semiconductor devices*. New York: Springer-Verlag, 1984.

[24] J. Piprek, Ed., *Optoelectronic devices: advanced simulation and analysis*. New York: Springer, 2005.

[25] G. D. Byrne and C. A. Hall, Ed., *Numerical solution of systems of nonlinear algebraic equations*. New York: Academic Press, 1972.